SEXAFS and NISXW Studies of Adsorbates on Transition Metal Surfaces

by

N.P. Prince

P. H. D.

Declaration

The work presented in this thesis is my own except where stated otherwise was performed in the Physics Department, University of Warwick and the SERC Laboratory at Daresbury during the period from April 1986 to January 1989. No part of this material has been previously submitted to this or any other University.

Details of the work performed on Cu(111)-CH_3S (Chapter 4) have been published in Surface Science 215 p556-p575.

The work on the Ni(100)H_gC(2x2) (Chapter 6) Structure has been accepted for publication in the J. Phys. C and it is intended to submit the work on the ($\sqrt{7}$x$\sqrt{7}$)R19.1°-S to Surface Science (Chapter 5).

N.P. Prince

0.1 Abstract

The synchrotron radiation based techniques of Surface Extended X Ray Absorption Fine Structure (SEXAFS) and Normal Incidence Standing X Ray Waves (NISXW) have been applied to Four adsorption systems. These involved atomic and molecular chemisorption on the low index planes of single crystal Cu and Ni surfaces.

For the Cu(111)($\sqrt{3}$ X $\sqrt{3}$) R30 system the NISXW technique has found a layer spacing of 1.81 $\pm$ 0.05Å, this was consistent with an earlier result found by SEXAFS.

For the Ni(100)c(2 X 2)Hg system the combined use of NISXW and SEXAFS was attempted. The SEXAFS study, however, was unsuccessful due to the difficulties of obtaining SEXAFS from core states of high angular momentum. These difficulties were attributed to delayed onset of photoemission from the mercury M_V edge and strong variations of the pure atomic X ray absorption coefficient in the EXAFS energy range. NISXW studies were more successful and yielded an adsorbate - substrate layer spacing of 0.60 $\pm$ 0.1Å. This layer spacing is consistent with adsorption into the two fold bridge site at the Ni(100) surface rather than the more highly co-ordinated four fold site which might have been expected for a metallic bond. There are, however, some ambiguities in this assignment due to the lack of corroboration of this result by SEXAFS.

For the remaining two systems the combined use of SEXAFS and NISXW was successful. The Cu(111) CH_3S system was typical of most molecular chemisorption systems in that it possessed no long range order. For this system both the NISXW and SEXAFS techniques gave results indicative of reconstructive chemisorption. A corroborative interpretation of results for both techniques inv olved the adsorption of the CH_3S group's sulphur atom into distorted three fold hollow sites at the Cu(111) surface.Intra-molecular scattering was also observed in this system. This scattering was between the carbon and sulphur atoms in the mercaptide (CH_3S) group, and SEXAFS analysis found a C-S bondlength of 1.88Å. This appears to be the first recorded case of intra- molecular scattering in SEXAFS data.

Simple chemisorption is also ruled out for the ($\sqrt{7}$ X $\sqrt{7}$) R19.1°-S on Cu(111) surface. SEXAFS data for this system, like that for mercaptide, was dominated by a single shell and analysis of the polarization dependence of the SEXAFS amplitude for this shell gave an adsorbate-substrate bond angle, β, of 67 $\pm$ 5°. This value is well outside the range expected for simple non reconstructive chemisorption of S into the high or low symmetry adsorption sites of the Cu(111) surface. The NISXW data for this system was suggestive of a mixture of at least two distinct adsorbate-substrate layer spacings. One of which was well outside the range of values expected for simple chemisorption.

The data from both experimental techniques can only be explained in terms of reconstructive chemisorption which forms a surface sulphide involving a mixed layer of Cu and S. This sulphide is believed to be of distorted tetrahedral co-ordination. This model can explain the two distinct adsorbate-substrate for S as well as the observed polarization dependence of the Cu-S bondlength.

0.2 Acknowledgements

It was in Northwich in January 1988, curtains of hailstones came down in blinding slate like sheets, myself and my post-doctoral colleague were seated, as best we could be, on some litter bolstered cardboard boxes in the corner of a desolate wind swept shopping precinct. We were wading our weary ways upstream in vinegar sodden bags of particularly greasy chips, low expectations are not at a premium on the industrial waste heap of the research world. Dave wiped his greasy hands vigourously on his anorak, the cheap man made fibres crumpled easily in his grasp. He pointed over to a dilapidated adventure playground, long deserted by gleeful summer's play, and said 'Hey Nick why not go and play on the swings. I'll come and get you when you're Phd's finished'

Now it is finished. Thanks Dave.

At the beginning of this undertaking my supervisor, Dr D.P. Woodruff, said that the doctoral thesis should achieve two aims, one, it should be succinct, two, it should make adequate provision for the inexpressible advancement of humanity. The first objective has been satisfied and as everyone knows, brevity is the soul of personal linen. The second objective lies well beyond the scope of this work and possibly this worker, nevertheless, this shortcoming is not the fault of D.P. Woodruff.

Thanks to D.P. Woodruff and also Dr R.G. Jones who played a very important supporting role in the supervision on site at Daresbury, undoubtedly where it was most needed. This man will go down in history as the Bill Shankly of synchrotron radiation.

No experimental work can be undertaken without technical support. The dexterity, skill, humour and commitment of Robert Ian Johnston are therefore gratefully acknowledged. Paul Thompson's photography was much appreciated as well as that of Mel Davies, the Daresbury photographer. Thanks to Gerry Smith and Roger Buckle are offered for their manifold, and often dangerous, plumbing assignments.

The various administrative contributions of Dr Helmut Mykura have rid the last three years of many financial worries which may have otherwise blighted this work.

Thanks are also due to my sponsors BP, without whose money I could never have afforded the bicycles. Also, I would like to thank my industrial supervisor Dr Jack Frost for organising such a lovely meal at Sunbury on Thames.

I am also grateful to the staff of Daresbury Laboratory, in particular, Frances Quinn, Daniel Law, Paul Bailey, Dancing Don, Ron Hearsey, Roger Lowery and his assistant Arthur Rose as well as all the support scientists.

The staff of Hinstock hostel were also at great pains to make my stays enjoyable, the contribution of Miss Sheila Conwell was particularly noteworthy, especially after my cycling accident on Keckwick lane which caused such severe damage to my anorak. Anne Fances' sensitive hoovering of the hostel corridors after the night shift is also worthy of comment and her speedy introduction of the new style Laura Ashley curtains just after my arrival for another experimental run was, I am sure, no coincidence.

Some superb secretarial support was supplied by Pearl Kirby, Sandra Beaufoy, Hayley Gilder and Sue Thompson.

Greg McShane was indispensible as was Malcolm Black as they helped lay the quarrelsome spirit of the pop-eyed gremlin of beamline six.

Dave Tehan and Glyn 'Donkey' Derby gave advice on grammar and punctuation, thanks are also due to Prince Charles for his efforts in this field.

Tony Begley, Steve Barret, the chaps from King's College London, Chris 'Chuckles the Bunny' Muryn, Peter Hardman, Prakash, Ganesh, Allen Johnson, Carl Robertus, Nick Barret and Nagindar Singh provided excellent company during the work, which as every beamline jockey knows, makes all the difference to a sightless drudge at the tiller.

The financial support of the SERC and my Parents, in more or less equal measure is acknowledged.

Lastly I'd like to pay earnest and frank tribute to myself for my patient typing of this thesis, it was very good of me to make such a selfless commitment to the advancement of mankind.

0.3 Table of Figures

Contents

Chapter 1

Introduction

Much of what we understand about solids is based on our assumption of perfect three dimensional periodicity. The presence of defects in a solid will produce deviations from this periodicity and thus present a challenge to our theoretical understanding of solids. This in itself is a powerful motivation for their study, but another more practical goal is the full understanding of the technological importance of defects. For instance, it is known that the existence of defects in solids results in the fact that engineering materials rarely even approach their theoretical strengths.

Defects come in one, two and three dimensional forms. For example, vacancies and interstitials, grain boundaries and dislocations.

Of the two dimensional defects surfaces are the most extreme form, representing the complete loss of periodicity in one dimension. This loss of periodicity gives surfaces a range of novel properties, involving, for example, electronic and vibrational states not found in the bulk and surface chemical bonds and compounds possessing no bulk analogues. Thus the study of surfaces represents a logical continuation of solid state science.

The interest in surface science, however, is not purely academic as the importance of surface phonomena is apparent in a variety of areas. For example,

in the field of semiconductor physics it is known that charged layers in the vicinity of the surface cause an effect called Fermi level pinning, this prevents the sweeping of the Fermi level through the band gap of a semiconductor which is crucial to device operation. Another technologically important property of surfaces arises from the necessary presence thereon of unsatisfied ('dangling') bonds which make surfaces very reactive chemically. Couple this with the fact that a surface will provide a way of concentrating reactants in a small volume and it is easy to understand why some surfaces stimulate chemical reactions thus making them effective catalysts. In the broader area of surface chemical reactions surface science plays a role, both experimentally and theoretically, in the areas of molecular beam epitaxy, etching, corrosion and crystal growth. All of these areas are currently of major and expanding technological and financial interest (In the mid nineteen eighties corrosion represented a loss of approximately three billion pounds to industry [1]) but, the full microscopic description of these processes would be a very complicated exercise as they typically all occur under conditions that are difficult to characterize. For instance, the process of heterogeneous catalysis generally proceeds on poly-crystalline surfaces at elevated temperatures and pressures. Similar problems of environmental characterization will also occur in describing the turbulent conditions producing corrosion on oil rig legs, motor transport and, of course, bicycles. For this reason the kind of surface science pursued here involves the study of single crystal surfaces in the better characterized environment of ultra high vacuum. Despite the obvious abstraction from the 'real world' there have been cases when insights gained from U.H.V. surface science have been successfully applied in industrial environments.

All the surface chemical reactions listed above possess one broad common feature which persists intact in it s transition from the 'real world', they all involve the adsorption of atomic or molecular species at surfaces and it is the study of the structure of stable chemisorbed atomic and molecular overlayers on single crystal transition metal surfaces that are the subject of this thesis. The practical relevance of such studies is most apparent in the field of heterogenous catalysis where the concepts of'active sites' and structure sensitive reactions are now accepted.

In the mid nineteen seventies the only surface structural technique of any note was low energy electron diffraction (LEED). This technique readily provides information on the periodicity of chemisorbed overlayers but complete surface structural determination is complicated due to the strong scattering cross section of low energy electrons which gives rise to a high probability of multiple scattering. The presence of multiple scattering means that simple Fourier methods of inverting the LEED pattern to obtain the structure do not avail and the analysis of LEED data has to make recourse to trial and error methods. These methods are computationally time consuming and expensive. This inadequacy of the LEED technique led to a search for other techniques of surface structure determination with more routine forms of analysis.

Despite the disadvantage of it s requirement of a continuously tunable, high intensity source of X rays (synchrotron radiation) surface extended x ray absorption fine structure (SEXAFS) is just such a technique.

Although the EXAFS effect was first observed as early as 1930 it was not until 1975 that it was correctly understood in terms of short range order (previous theories had used long range order to explain the effect), and EXAFS

experiments were practically feasible. The fact that the EXAFS technique is applicable to systems not possessing long range order is a considerable advantage over LEED, in that we may now study the structure of molecular overlayers on surfaces which generally do not show long range order. The phonomenon of EXAFS may be described as follows.

If we expose an atom in a solid state environment to a source of X rays and then continuously tune this source, in energy, from before a characteristic X ray absorption edge of the atom to several hundred electron volts beyond the X ray absorption edge, we will observe a sharp rise in the X ray absorption cross section followed by a series of oscillations in the cross section which would not be present if we performed the experiment on an isolated atom. (see Figure 1). These EXAFS oscillations are caused by the coherent interference of emitted and backscattered fluxes which arise due to photoemission and back scattering directly onto the emitter respectively. As we tune past the absorption edge the wavelength of the emitted and backscattered photoelectron waves will decrease continuously. Thus these photoelectron waves will pass through points of constructive and destructive interference. At points in the spectrum where the interference is constructive the probability of absorption is greater than at points where the interference is destructive. Hence, the EXAFS oscillations. The periodicity of these oscillations contains local structural information as they are dependent on the scattering path lengths of the photoelectrons.

In the EXAFS process the emitter atom is effectively used as a detector and due to this fact a multiply scattered photoelectron must scatter through a succession of large angles if is to contribute to the EXAFS. This is highly improbable in the EXAFS energy range which is usually from fifty electron

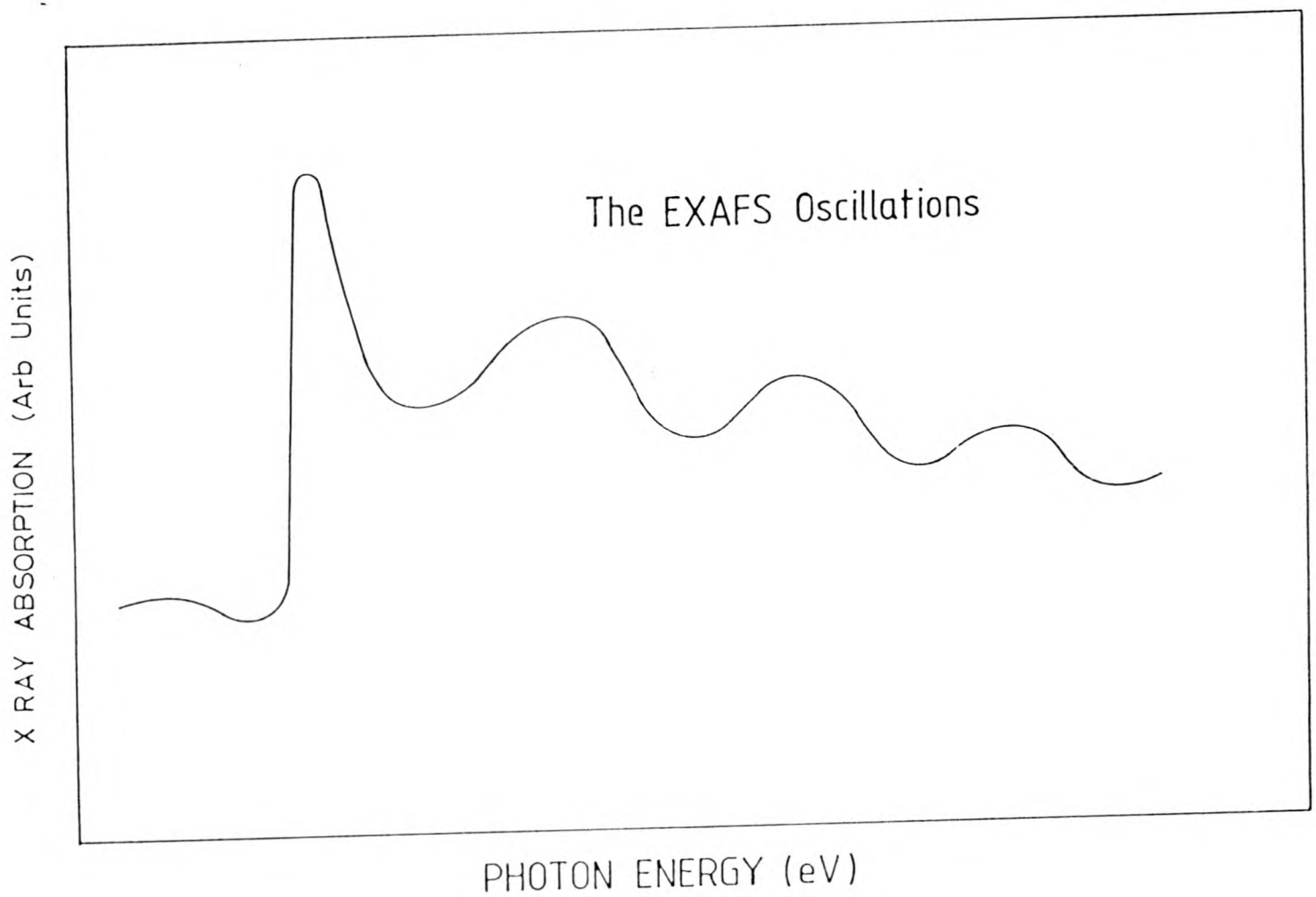

Figure 1.1 A schematic illustration of an EXAFS spectrum

volts above the absorption edge to several hundred electron volts beyond. (The exceptions are those multiple scattering events which occur along a string of collinear atoms but this gives rise to a long scattering path length which is easily distinguishable from the nearest neighbour path length during Fourier analysis.) This makes analysis by simple Fourier methods possible and allows the deduction of local structures in a model independent fashion, in direct contrast to the trial and error methods of LEED data analysis.

Ideally, SEXAFS data analysis consists of background subtraction and a Fourier transform and after allowing for the presence of scattering phase shifts in the photoelectron waves (caused by the passage of the photoelectron in and out of the atomic potentials) a radial distribution function of the local structure under study should be obtained.

However, for surface structures in which adsorption occurs in more than one distinct site then SEXAFS will average the structural information for these sites and hence limit the efficiency and accuracy of the structure determination . Also if two bondlengths in the structure are close together it may not be possible to resolve them using simple Fourier methods of SEXAFS analysis and recourse to modelling is necessary, thus regressing in partial measure (this modelling of SEXAFS data will not be as computationally demanding as LEED data modelling) to the trial and error methods associated with LEED data analysis. SEXAFS measurements are also subject to poor signal to noise characteristics and limited data ranges.

Of course all surface science techniques have their limitations and so the argument for using a range of techniques which provide complementary information on surface structure is compelling. For this reason these surface studies

have also employed normal incidence standing X ray waves. (NISXW). The physical basis of this technique is simple to explain in terms of Bragg diffraction.

In the vicinity of a Bragg reflection from a particular crystal plane, a standing X ray wave field with the same periodicity of the crystal planes is set up in a shallow region on either side of the surface. Over the range of total reflection, the phase of the standing X ray wave field behaves in the following manner. At the onset of the Bragg reflection the antinode of the wavefield is positioned half way between the atomic planes and as we tune in energy across the range of total reflection this antinode moves continuously to a position coincident with the atomic planes. Thus if we measure a characteristic X ray excited yield of an adsorbate throughout the range of total reflection then we will observe a maximum in this yield at the point where the SXW antinode is positioned over the centre of the adlayer and a minimum when the SXW node is in this position. Therefore we observe a strong modulation in the excited atom's yield. By analysing the exact shape and energy location of this modulation we can find the spacing between an adlayer and the crystal surface which may be compared to a SEXAFS derived result for the same adsorbate system. Thus if the SEXAFS and NISXW experiments are performed together on the same system then the information gained can be used in a complementary fashion in order to gain a more convincing structure determination than would have been obtained by the sole use of either technique. A good example of a mutually supportive interpretation of the two techniques in tandem is provided by studies of chlorine adsorption on Cu(111).[2,3]

The chlorine overlayer forms a ($\sqrt{3}$ x $\sqrt{3}$) R-30 LEED pattern. This taken

together with SEXAFS and photoelectron diffraction results [2] (see Figures 2a and 2b) reveal that adsorption occurs in the three fold hollow site corresponding to the position that a copper atom would occupy in the next layer of an f.c.c. structure. The copper-chlorine nearest neighbour bondlength was determined by SEXAFS to be 2.39Å $\pm$ 0.02 Å. From all this information the height of the chlorine adlayer above the copper surface would be expected to be 1.88 Å $\pm$ 0.03 Å. The value given by NISXW [3] for this overlayer is 1.81 Å $\pm$ 0.05 Å. The difference in these results are within the combined error bars of the two techniques but any slight actual differences may be due to contraction in the top copper atom layer spacing. To explain how this conclusion is reached it is useful to point out an essential difference between the types of information given by SEXAFS and NISXW. Due to the fact that the periodicity of the SXW wavefield is determined by the bulk, any adlayer spacing will be given relative to the continuation of the bulk periodicity. Thus the NISXW technique is blind to any distortions in the top few layer spacings of the substrate. Hence if a contraction occurs between the surface atomic layer and the layer below what effectively happens is that the adsorbate layer has moved closer toward the bulk substrate layers deeper in the solid and as the NISXW field periodicity is determined by the bulk periodicity the value of the adsorbate-substrate layer spacing given by NISXW will be reduced by an amount corresponding to the exact size of this contraction. If an expansion occurs between the top two layers of the substrate then the opposite effect occurs and the NISXW technique overestimates the true local value of the layer spacing by an amount corresponding to the exact size of the expansion whereas, SEXAFS being a highly local probe would give the actual local layer

Figure 1.2b NISXW data for the ($\sqrt{3} \times \sqrt{3}$)R-30°-Cl system

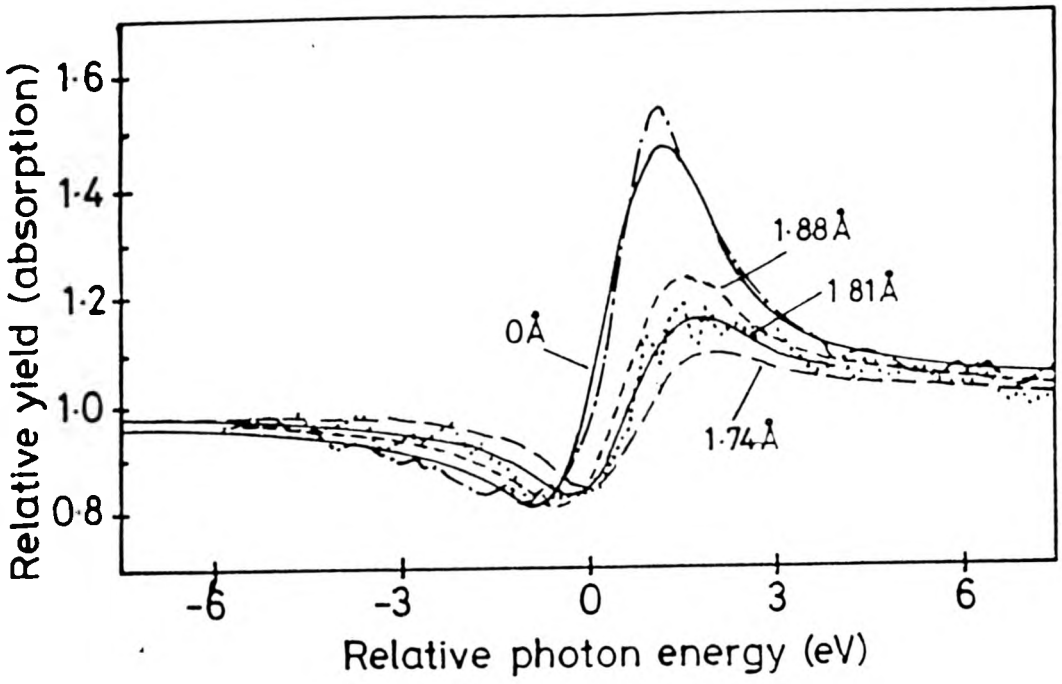

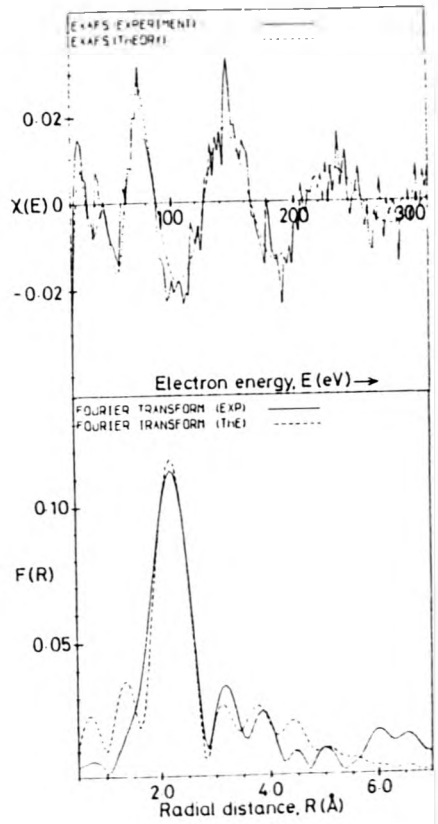

Figure 1.2a SEXAFS data for the ($\sqrt{3} \times \sqrt{3}$)R-30°-Cl system

spacing. Thus the two results taken together might suggest a slight contraction of the top layer spacing. Two previous LEED studies have in fact indicated that the clean Cu(111) is relaxed in this way and contractions of the top layer spacing of 0.08Å and 0.006Å have been reported [4,5] . This argument aside the two results are inside the error bars and the overall conclusion is that the structural determinations from both techniques are mutually supportive.

The remainder of the work presented here involves the application of SEXAFS and NISXW to widely different adsorption systems comprising molecular and atomic adsorbates. The outline of the thesis is as follows; Chapter 2 will present a more detailed introduction to the experimental techniques employed in these studies, Chapter 3 concerns itself with experimental details, Chapters 4, 5 and 6 will present results for structure studies of atomic and molecular adsorption and finally, Chapter 7 will draw conclusions on the entirety of the work.

1.1 References

1. U.M.I.S.T. Corrosion and Protection Centre Graduate Prospectus 1985

2. M D Crapper, C E Riley, P J J Sweeney, C F McConville, D P Woodruff and R G Jones Europhys. Letts. 2, 857 (1986)

3. D P Woodruff, D L Seymour, C F McConville, C E Riley, M D Crapper, N P Prince, and R G Jones Phys. Rev. Letts. Vol 58 No 14 (1987) p1460

4. P R Watson, F R Shephard, D C Frost, and K A R Mitchell Surf. Sci. 72 562 (1978)

5. S P Tear, K Röll and, M Prutton J. Phys. C. 14, 3297 (1981)

Chapter 2

Basic Experimental Principles

2.1 Introduction

This chapter is intended to serve as an introduction to the principles of the experimental techniques used in these studies and their general areas of application in surface science.

2.2 Low Energy Electron Diffraction

The process of LEED involves the normal incidence of an electron beam at a surface and the subsequent mutual interference of the secondary wavelets elastically scattered from atoms in the surface.

This produces electron beams emerging from the surface with angular separation, definition and intensity characteristic of the periodicity, order and structure of the surface under study. In order to separate the elastically scattered electrons from the lower energy inelastic tail the experimental arrangement illustrated schematically in Figure 1 is used.

The grid G_1 is earthed to ensure that electrons travel through a field free region between the electron gun and the sample, the grids G_2 and G_3 are biased a few volts positive with respect to the primary energy of the electron beam

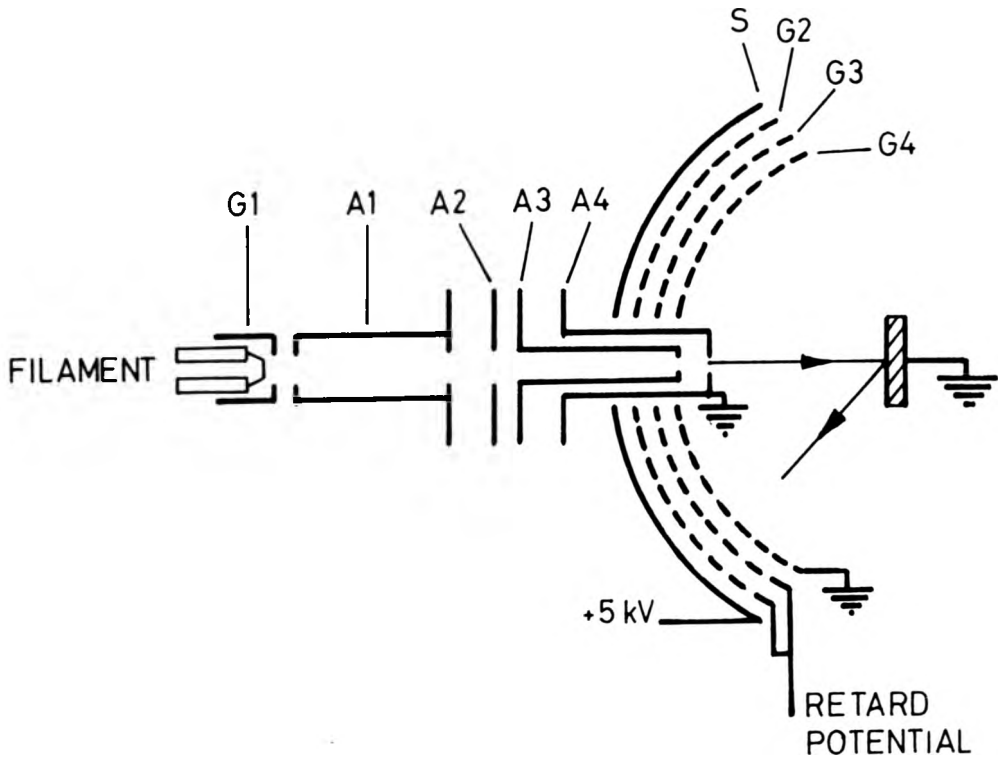

Figure 2.1 A schematic illustration of a LEED optics

hence allowing only elastically scattered to pass to the fluorescent viewing screen. The screen is biased 5kV positive in order to accelerate the electrons onto the screen thus providing the LEED pattern.

Although complete surface structural determinations are experimentally and analytically complicated it is possible to extract information on the periodicity and order of the surface with ease. This makes LEED an attractive technique for the in situ characterization of surfaces prior to the application of SEXAFS and NISXW; also LEED data on the periodicity of a surface structure makes a useful input in corroborating surface structure determinations provided by SEXAFS and NISXW.

Another attraction is that LEED involves the collection of only elastically scattered electrons which ensures the surface sensitivity of the technique. The reason for this is that the mean free path for electrons in the LEED energy range (100eV) is of the order of 5 Å and thus elastically scattered electrons emerging from the surface must originate from within the top few layers of the sample.(see Figure 2)

Yet another advantage is that the advanced state of electron beam technology allows the very routine application of LEED to the study of surfaces in ultra high vacuum.

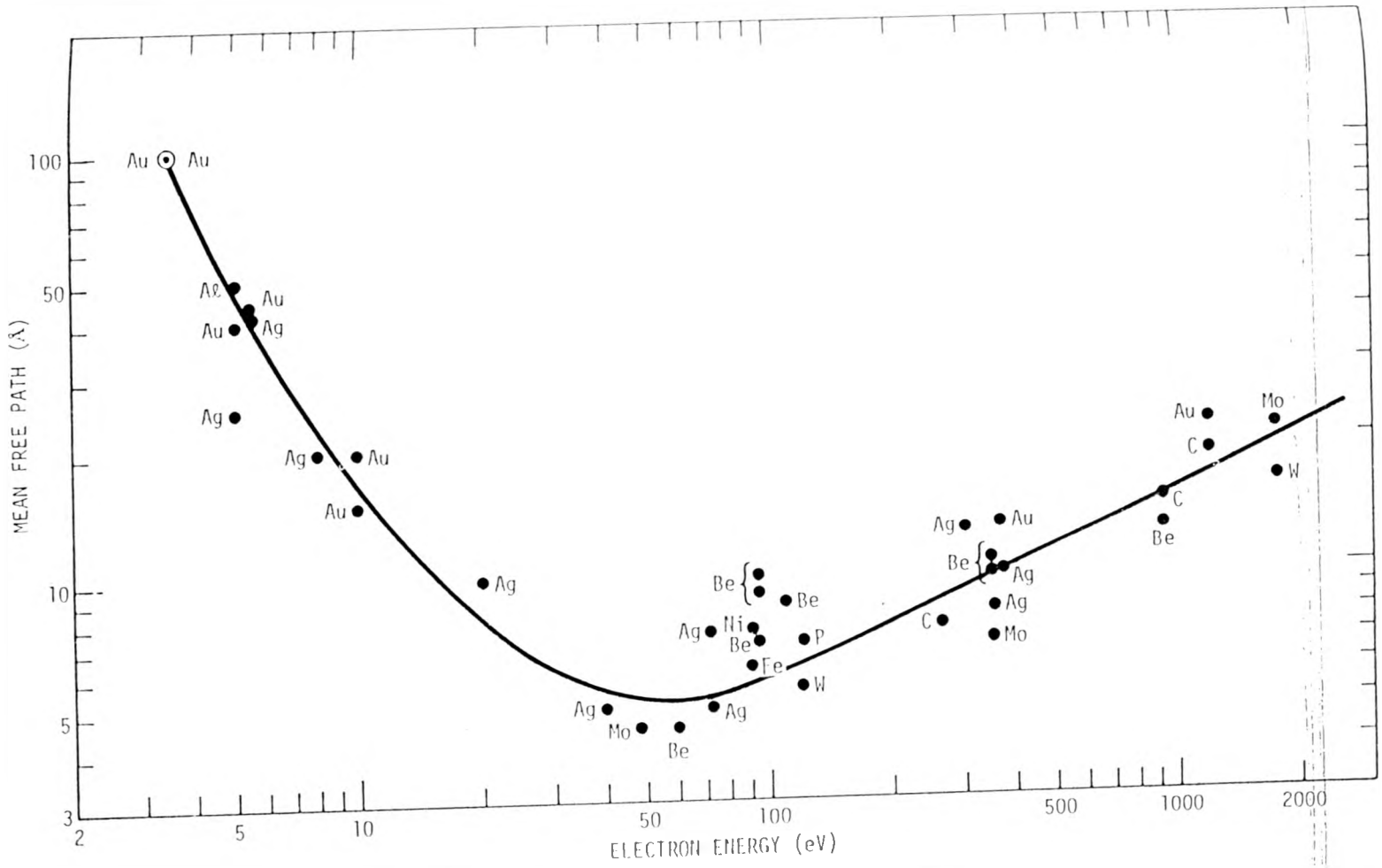

Figure 2.2 Mean free path curves as a function of energy [1]

2.3 Auger Electron Spectroscopy

The Auger effect can be observed as a result of either electron or photon impact ionisation of an atom with Z = 3 or greater. The phenomenon is described schematically in Figure 3.

After the creation of a core hole by the removal of an electron of binding energy E_K, an electron relaxes into the core hole from a less tightly bound state of energy E_L. This releases energy ($E_K - E_L$) which can then be taken up by another more shallowly bound electron of energy E_M. If ($E_K - E_L$) is greater than E_M then an electron of ($E_K - E_L - E_M$) is emitted from the sample. This energy E_{KLM} is a function of three discrete atomic energy levels and thus Auger electrons are highly characteristic of the atoms from which they are emitted. Hence AES is a good source of information on the chemical environment of the sample under study.

The Auger electrons will be emitted from the sample without energy loss with one proviso, that is, that they were created a distance from the surface which is comparable with the Auger electron's mean free path. The Auger electrons collected in this work ranged in energy from 50eV to 2106eV corresponding to a range of mean free paths between 6 Å and 10 Å, (Fig 2) thus their collection, without energy loss, outside the surface is a surface sensitive probe of chemical environment. This makes AES an attractive technique for providing a check on the contamination levels of surfaces studied by SEXAFS and NISXW, and, it is capable of detecting levels of contamination consistent with the adsorption of a few % of a monolayer of contaminants.

Because AES uses the same well developed electron beam technology as LEED it is a readily applicable surface science analytical tool in vacuum. An-

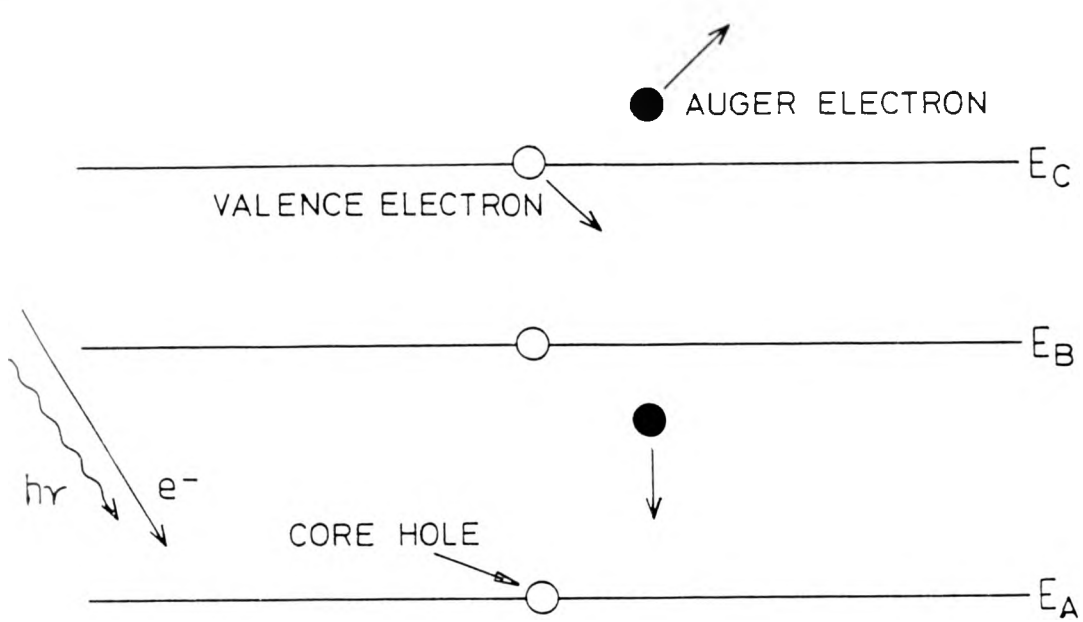

Schematic Diagram of the Auger Process
When the core hole is created an electron of binding energy E_B relaxes into this core hole releasing energy $E_A - E_B$ which is then taken up by an electron of binding energy E_C
This gives rise to an Auger electron of energy $E_A - E_B - E_C$

Figure 2.3 A schematic diagram of the Auger effect

other advantage is that the standard three grid LEED system can be used as an energy dispersive detector for Auger electrons, nevertheless in this work another type of analyser is used, namely the cylindrical mirror analyser (CMA). This is described in detail elsewhere [35].

2.4 Extended X-Ray Absorption Fine Structure (EXAFS)

The oscillations in a solid state or molecular atom's X ray absorption coefficient on the high energy side of an absorption edge have been known since 1920 [1,2]. The first theoretical interpretation was of the near edge structure [3,4], and it was not until the 1930's that Krönig attempted to explain the extended structure of the order of 50eV beyond the absorption edge using the newly developed quantum mechanics [5,6]. This theory was based on the assumption of long range order (LRO) but the fact that the effect was also apparent in molecular systems led Krönig to develop a short range order theory also.

It is interesting to note that it was not apparent at this stage that the physics of EXAFS was the same for both molecular and solid state environments and could be explained purely in terms of short range order (SRO).

It was only after the contributions of many workers that the modern accepted, SRO, form of the EXAFS equation was arrived at by which time it was agreed that the EXAFS oscillations were caused by coherent interference between an outgoing photoelectron wave and it's backscattered counterpart (see Figure 4) and that EXAFS was a short range effect.

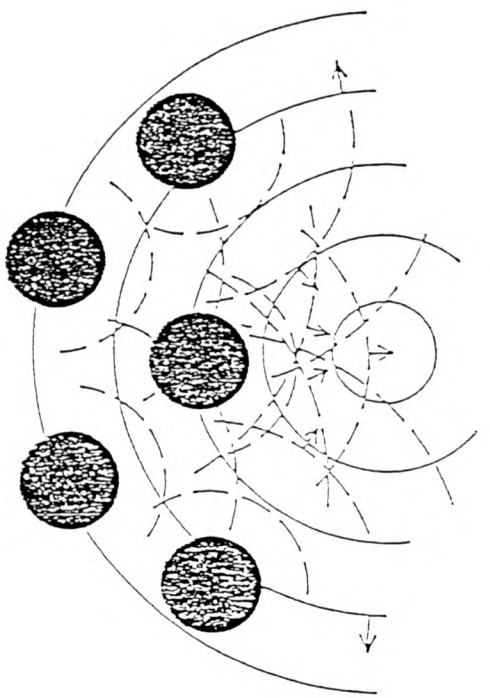

Figure 2.4 A schematic illustration of the EXAFS process

This interference between outgoing and backscattered directly modifies the final state thus producing the modulations in the absorption coefficient σ where

$$\sigma \sim \langle f|H|i \rangle^2$$

which is the dipole transition matrix element. These oscillations are represented by the equation

$$\chi(k) = \frac{\Delta\sigma}{\sigma} = -\sum_j \frac{N_j^*}{kr_j^2} F_j(k)\ sin(2kr_j + \phi_j(k))exp(-2(u_j)^2k^2)exp(\frac{2r_j}{\lambda_k})$$

$\Delta\sigma$ = The pure oscillatory part of the absorption coeffficient, in the expression above this is normalised to the total absorption coefficient.

The EXAFS equation is basically a sum of damped sine waves with periodicity determined by the scattering path length $2r_j$ between the central excited atom and the neighbouring atomic shell at r_j, and the photoelectron phase shift term ϕ_j which is caused by the atomic potentials of both the excited central atom and the backscattering neighbours.

Thus a Fourier transform of the EXAFS equation, with respect to photoelectron wavenumber k, should peak at distances characteristic of neighbouring shells. This Fourier transform method of analysis was first done in 1971 [7] and the transform produced only the first few shells in the 'radial distribution function' thus demonstrating the correctness of the short range order (SRO) theory and turning EXAFS into a useful experimental tool.

In 1975 the full SRO theory of EXAFS was published [8]. This formalism expressed the EXAFS as a sum of damped sine waves (as shown above). These sine waves are damped by the two terms on the left hand side of the equation, the first of these $exp(-2(u_j)^2k^2)$ is a Debye - Waller type factor which takes account of the smearing of co-ordination shells caused by lattice vibrations.

($(u_j)^2$) is the mean square relative amplitude of vibration of neighbouring shells.

The second term $\exp(\frac{-2r_j}{\lambda(k)})$ allows for the inelastic scattering that the photoelectron may suffer which will prevent it's contribution to the EXAFS effect.

Other factors influencing the amplitude are $F_j(k)$, the backscattering power, which is energy dependent and characteristic of the scattering atom and N_j^* the effective number of near neighbours. This number is not always equal to N_j, the actual number of neighbours, due to the strong directionality of photoelectron emission along the E vector of the X radiation used to excite the photoelectron. This effect can produce strong SEXAFS amplitude variations in data collected at various angles of incidence. These variations are of great utility in structure determinations and represent a great advantage of the SEXAFS technique.

The approximations involved in this equation are (i) the assumption of single scattering, this is generally valid in the EXAFS data range, which is fifty eV above the edge and beyond, because here the probability of multiple scattering through large angles is small. Thus we can infer that the EXAFS process which itself involves 180^o scattering has a low probability of occurrence but it is, of course, a single scattering process and hence has a much higher probability of occurrence than an event involving scattering through a succession of large angles which is generally necessary in an EXAFS multiple scattering process. One instance where multiple scattering events are significant in the EXAFS data range occurs for the case where three atoms are collinear along the incident X ray beam, here strong forward scattering through 0^0, which of course has a high probability of occurrence in the EXAFS data range, may

focus emitter electrons via the second atom onto the third which will lead to false conclusions about the third atoms bondlength in the analysis [8]. These events do, of course, give longer bondlengths which are easily separable from the nearest neighbour information in the Fourier transform. This means that the most valuable information given in SEXAFS analysis is unaffected by these collinear scattering events. Below fifty eV from the edge, the assumption of single scattering is not valid as here electron mean free paths are long and scattering cross sections are high and so scattering through large angles and long path lengths are plausible.

(ii) The second assumption is that the size of the backscattering atom is small with respect to the emitter-scatterer distance, this allows the impinging photoelectron to be approximated as a plane wave. This assumption is also more valid at higher energies where the effective scattering radius of the neighbouring atom is smaller than it is at low k. The assumption is obviously less valid for near neighbours than more distant ones.

(iii) It is also assumed that EXAFS is a one electron process, however, in certain cases many body effects occur, in these cases energy from the incident photon may be imparted to electrons other than the one emitted causing it to lose coherence and preventing it taking part in the EXAFS. Other multi-electron effects are taken under the wing of the mean free path term which allows for the finite life time of the core-hole [9].

(iv) The final assumption is that a symmetric distribution (Gaussian) function is assumed to account for the thermal averaging of the radial distribution function. This is not appropriate in systems possessing vibrational disorder where the harmonic approximation is not valid and an assymmetric distribu-

tion function must be used. The effect of these anharmonic vibrations is to add an extra term in the EXAFS phase and thus a failure to allow for it can produce very significant errors in distance determinations [10].

2.5 SEXAFS Detection Schemes

In order to perform an EXAFS experiment it is necessary to monitor the oscillations in the x ray absorption coefficient on the high energy side of an absorption edge. In achieving this, EXAFS experimenters have resorted to various detection schemes, each involving its strengths and weaknesses.

The first EXAFS experiments measured the absorption by taking the ratio of the incident and the transmitted flux passing through the sample, clearly this method will provide information on bulk structure only and therefore is not generally applicable to surfaces. In order to make EXAFS surface sensitive it is necessary to monitor the absorption by some other means . One obvious method would be to measure the yield of the directly emitted elastic photoelectrons , as this signal is expected to be proportional to the EXAFS oscillations, however due to the fact that the photoelectron energy is changing throughout the experiment, the yield is modulated by photoelectron diffraction. These modulations are typically ten times the size of the EXAFS oscillations for an angle resolving detector and hence would drown the EXAFS [11]. Due to this effect, the direct photoyield signal is not proportional to the rate of creation of core holes and hence does not contain pure EXAFS information.

Thus it is necessary to monitor the EXAFS by a less direct means. Another way of performing the experiment is to measure the rate of decay of the core holes created in the EXAFS process. This decay may occur by either one of two

processes, fluorescence or Auger electron emission, the competition between these two mechanisms is represented by a Z dependent branching ratio. If Z is less than 31 then the Auger process dominates (for K shell holes) therefore if we measure an Auger yield from a low Z atom as a function of energy beyond one of its characteristic x ray absorption edges and we detect these electrons outside the surface without energy loss then we have a surface sensitive probe of the local atomic structure around this atom. Hence the term surface EXAFS. The Auger energy is of course independent of the incident beam energy and hence this signal is not modulated by Auger electron diffraction

This form of detection was first employed in 1978 by Citrin et al [12] after the suggestion of Lee, and Landman and Adams [13,14] that the Auger electron intensity should be directly proportional to the x ray absorption coefficient. This detection scheme has good signal to background characteristics at the expense of a weak signal. A larger signal is provided by monitoring the total electron yield from the surface during absorption, which is in principle also proportional to the absorption coefficient. Nevertheless this scheme has its drawbacks. This signal comprises elastic and inelastic photo and Auger electrons plus a cascade of low energy secondary electrons some of which have long mean free paths and therefore the surface specificity of this scheme is highly questionable. In the case of Auger yield however it is possible to select Auger electrons with a short mean free path and thus ensure surface sensitivity. This scheme has added versatility in that it is possible to select from a range of Auger electron transitions each with different energies thus the surface sensitivity can be varied to provide information on the structure of various near surface regions [15]. Another problem with total yield is that de-

spite its high signal it suffers from poor signal to background characteristics, this means that any slight variations in the background can intrude strongly in the EXAFS. The strongly curved shape of this background also causes problems in the background subtraction part of the analysis and so the Auger yield is generally the preferred electron detection scheme excepting the case when a photoelectron peak sweeps through the Auger electron energy. Nevertheless, the decision as to which scheme to use can never be made in advance before an experiment as the behaviour of signals, noise and backgrounds are dependent on the sample system and the experimental equipment, factors which always vary from experiment to experiment. Therefore it is necessary to perform preliminary experiments on each individual system in order to decide upon which detection scheme to use.

If Z is greater than 31 then the fluorescence yield dominates (for K edges), monitoring this signal requires the detection of photons emerging from the surface, these have a very long escape depth and hence this scheme is not inherently surface specific. However by selecting an angle of incidence well below a certain well defined critical angle where the angle of refraction is zero, then total external reflection occurs and the penetration depth of the x rays is limited to between 20 and 200 Angstroms, thus in this case the fluorescence yield is surface specific. Also if a fluorescence yield is measured from an adsorbate bonded to a surface and this adsorbate does not diffuse into the bulk, then surface sensitivity avails without the need for glancing incidence. The disadvantages of this technique are that the signal is very low, for low Z adsorbates, and also the fact that fluorescence detectors are generally less efficient than electron detectors. A considerable advantage however is that

fluorescence signals have a very good signal to background ratio, (especially in the case of high Z adsorbates on low Z substrates as here there is no significant background [16].) which means that fluorescence is a highly sensitive monitor of X ray absorption, hence SEXAFS can be studied on very dilute systems [17]. Notice also that the fluorescence yield will not be troubled by the intrusion of photoelectron peaks in the signal.

Another major advantage is that due to the penetrating nature of fluorescent photons a vacuum environment is not necessary and in future it may be possible, using suitable high pressure cells with Be or PTFE windows, to perform SEXAFS experiments on working catalytic systems.

Another detection scheme involves measuring the reflectivity of x rays from the surface, thus we can measure the complex component of the refractive index and hence the absorption. Unfortunately this method also measures the real part of the refractive index which, although it contains the EXAFS information it does so at a phase shifted with respect to the complex part. This greatly complicates the EXAFS analysis, however, this contribution can be rendered insignificant by performing the experiment at extreme grazing incidence below which total external reflection occurs. Thus analysis is simplified, however this need for glancing incidence engenders several experimental difficulties, firstly it requires very large samples the homogeneity of which may be difficult to ensure secondly, it prevents the performance of polarization dependent SEXAFS measurements and, lastly this experiment requires precise sample alignment. Another problem which relates to the EXAFS analysis is that the optical constants of the sample must be accurately known which is unlikely to be the case especially for adsorbates on surfaces.

One further method for the detection of surface EXAFS oscillations involves photon stimulated ion desorption. This process occurs for an important class of maximally co-ordinated metal oxides in which a substrate metal atom is stripped of all its valence electrons by an adsorbed oxygen atom. Thus, if the highest metal substrate atom core hole is created by photon impact then, the main relaxation channel for this hole will be via an inter-atomic Auger process. A transition that may remove two or three electrons from the oxygen atom which will leave it in a strongly repulsive state with respect to the surface and therefore the ion will desorb. If we detect this ion yield using a time of flight mass spectrometer we will be monitoring the decay of core holes in the substrate. Hence we will be measuring SEXAFS using a substrate X ray absorption edge. This allows surface structural studies of adsorbates like hydrogen which would be impossible by any other means. Other advantages include high surface sensitivity and high sensitivity to valence information, for instance, if the metal oxide is not maximally co-ordinated there will still be valence electrons residing on the metal atom and hence any metal core hole will decay via a normal intra-atomic Auger transition and no ion yield will be expected. Amongst the disadvantages of this scheme are its low yield of ions per incident photon (10^{-7} as compared with 10^{-2} for electrons) and the possibility of electron rather than photon stimulated ion desorption. If the desorption is stimulated by inelastically scattered electrons then we will just be measuring the same sort of signal as that given by the total yield which , if we are using a substrate x ray absorption edge will provide bulk information only. Despite these difficulties this technique has been successfully applied to some chemisorption systems [18,19]

2.6 Analysis

The analysis of SEXAFS data may proceed by two distinct approaches, one is a truly model independent method which requires no preconcieved ideas about the structure, the other scheme involves fitting to experimental data which does require a guess to be made at the structure which is then refined by iteration. This trial input, however, is minimal compared to that required for LEED calculations. These approaches are the single shell and multi shell methods respectively. The single shell package was developed at Warwick and the data simulation program was developed at Daresbury laboratory [20].

Before any of these analyses are possible it is first necessary to subtract the background from the experimental data. For single shell analyses, this procedure involves the subtraction of a linear background followed by the subtraction of a cubic spline approximation to the pure atomic absorption. This spline is a cubic curve constructed of a series of polynomials, the function value and first derivative of these are matched at the link points. Then after normalization to the edge jump (the large rise in photoabsorption at the absorption edge) we arrive at

$$\chi(h\nu) = \frac{\sigma - \sigma_0}{\sigma_0 - \sigma^*}$$

(for definitions of these σs see figure five)

Thus we now have only the oscillatory part of the absorption spectrum (EXAFS). The next step is to obtain the oscillations as a function of k, the photoelectron wavenumber. This is done by the following change of variable.

$$k = \sqrt{\frac{2m}{\hbar^2}(h\nu - E_0)}$$

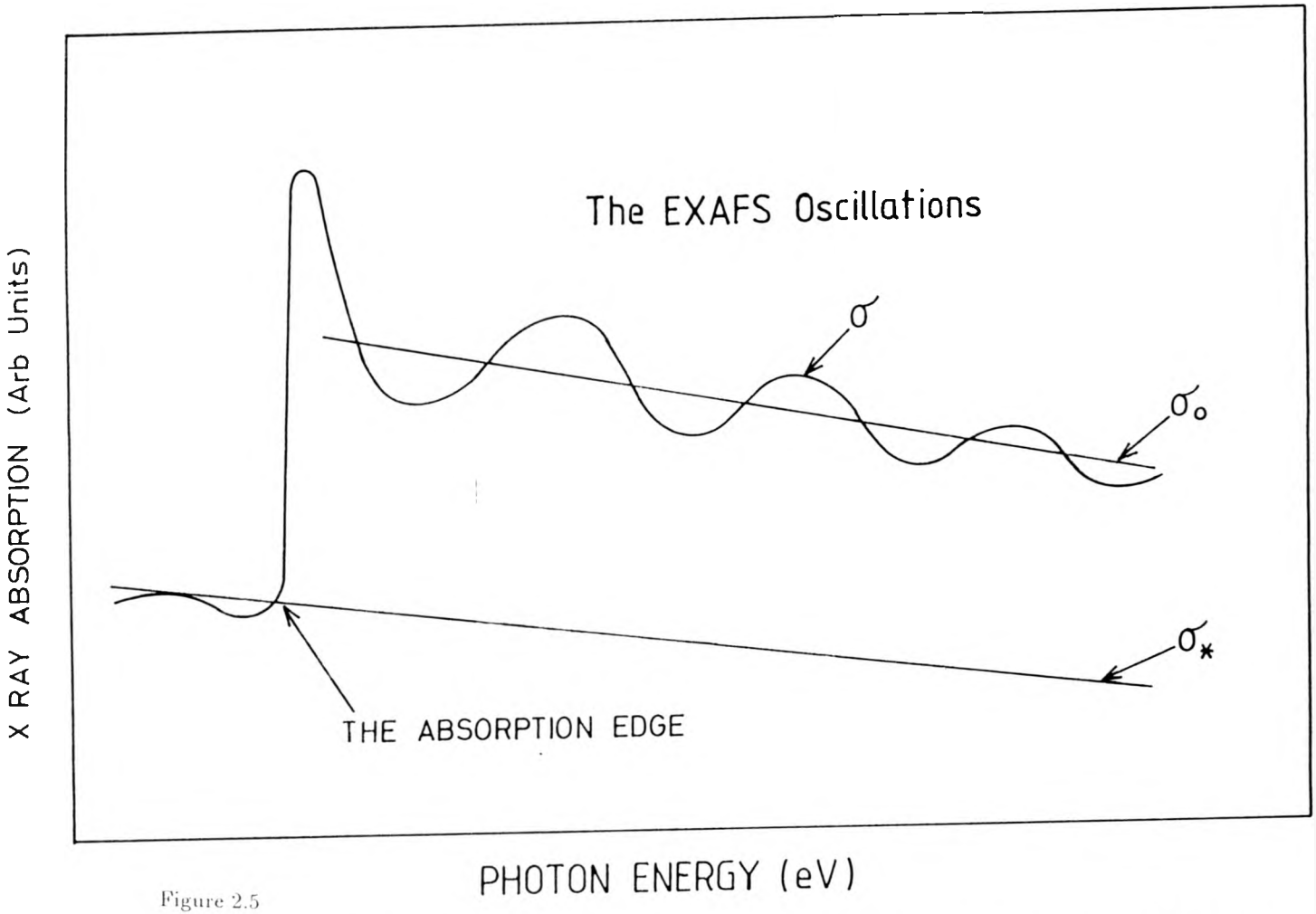

Figure 2.5

A schematic EXAFS spectrum illustrating the background subtraction

where E_0 is the zero of the photoelectron kinetic energy scale which is arbitrarily selected at the outset of analysis to be the point of inflection on an absorption edge. It's absolute value is fixed later in the analysis (see later).

Thus we now have the EXAFS equation or the fine structure function as it is sometimes called

$$\chi(k) = -\sum_j \frac{N_j^*}{kr_j^2} F_j(k) sin(2kr_j + \phi_j(k)) exp(-2(u_j)^2 k^2) exp\frac{2r_j}{\lambda_k}$$

where all the terms are as previously defined. The fine structure function is now weighted by a factor k^n, where n = 1,2,3. This is to allow for the k dependent attenuations in the various parts of the fine structure function. The number n is selected such that all the SEXAFS oscillations in the data have equal prominence.

We are now ready to Fourier transform the data, first we select appropriate limits in k space to determine the data range to be transformed. These limits should be chosen such that the average value of the fine structure function is zero over the data range and that the truncation is at a smooth part of the spectrum. This is to avoid getting poles at the origin of the transform and truncation ripples throughout it's range. The Fourier transform produces a modified radial distribution function characterized by the scattering phase shifts and path lengths. In single shell analyses all but the largest peak, which corresponds to a nearest neighbour are discarded and the main peak is multiplied by a smooth window function (see figures 5,6,7). This isolates the first shell contribution prior to a Fourier back transform. It is now possible to separate the amplitude and phase parts of the Fourier transform which are the modulus and the ratio of the real and imaginary parts of the back transform respectively.

Figure 2.6 RAW DATA SETS CH_3S on Cu(111)

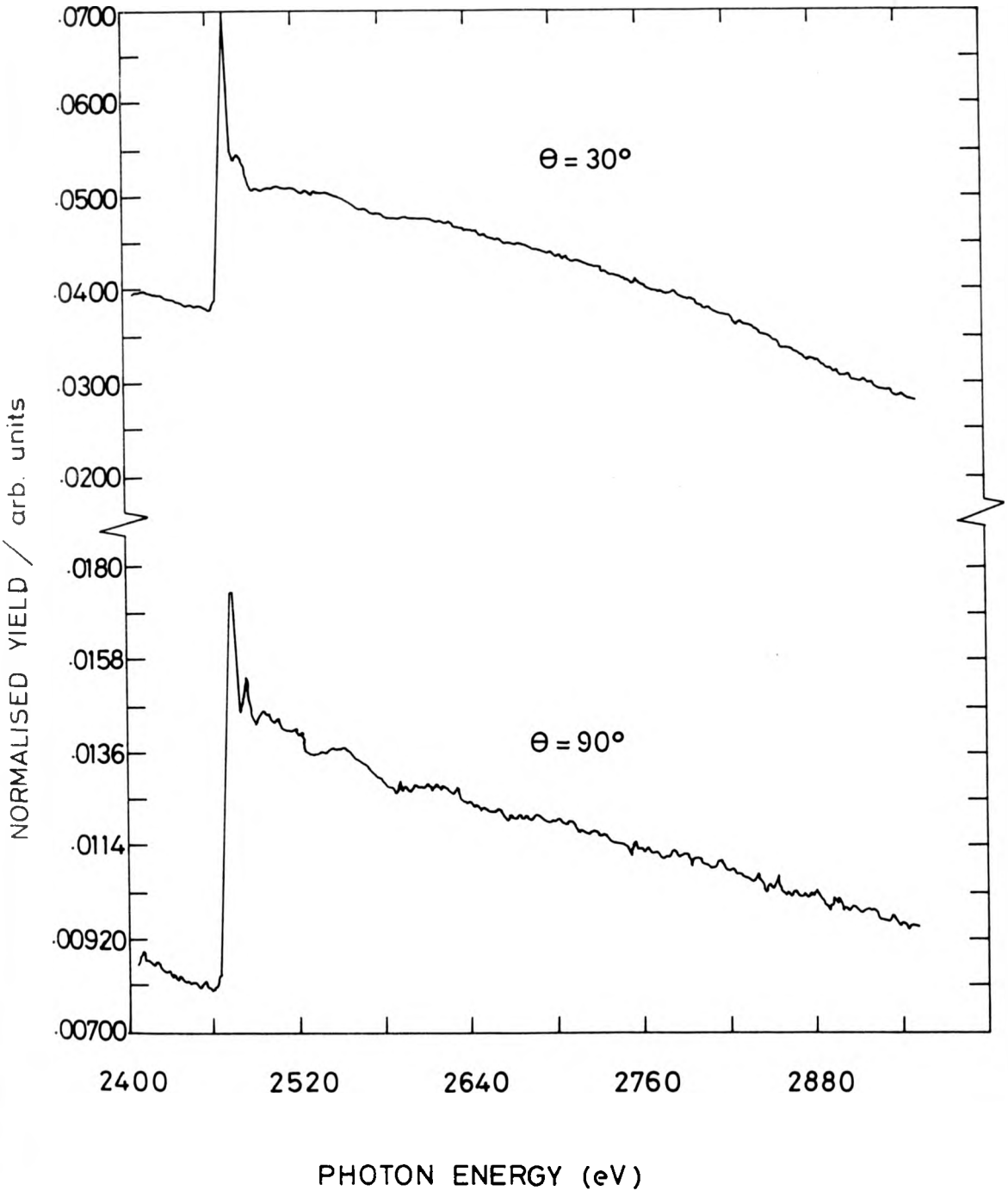

Figure 2.7 FINE STRUCTURE FUNCTIONS SUPERIMPOSED ON FOURIER BACKTRANSFORM

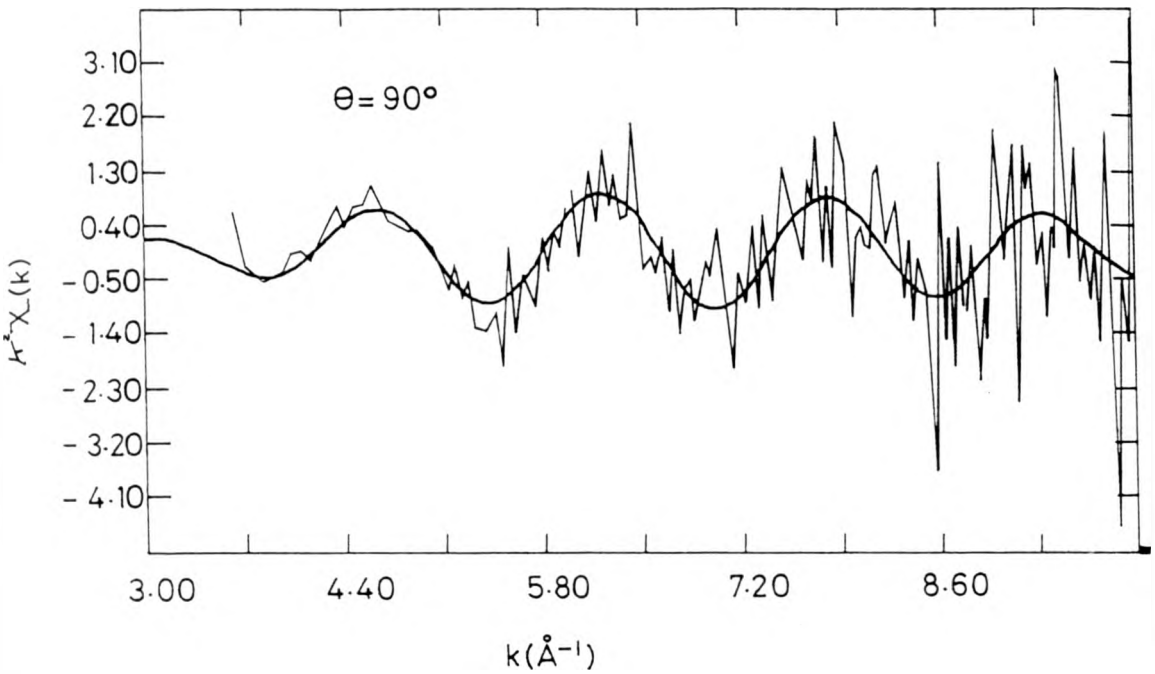

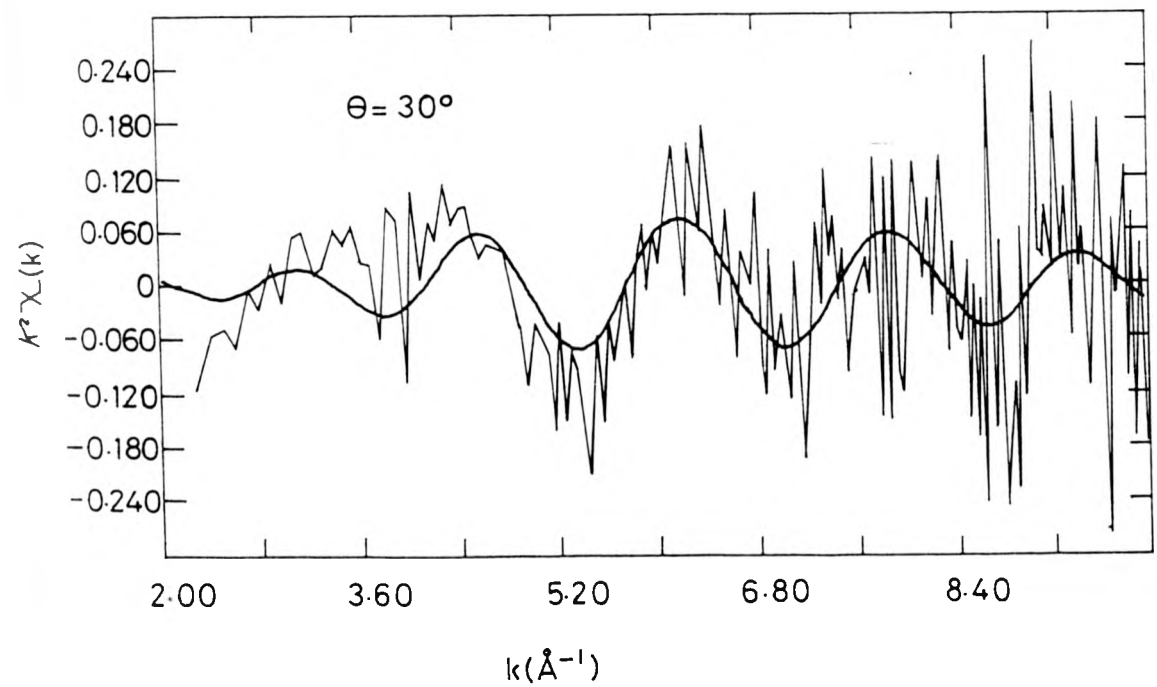

Figure 2.8 Fourier Transform for the mercaptide on Cu(111) data

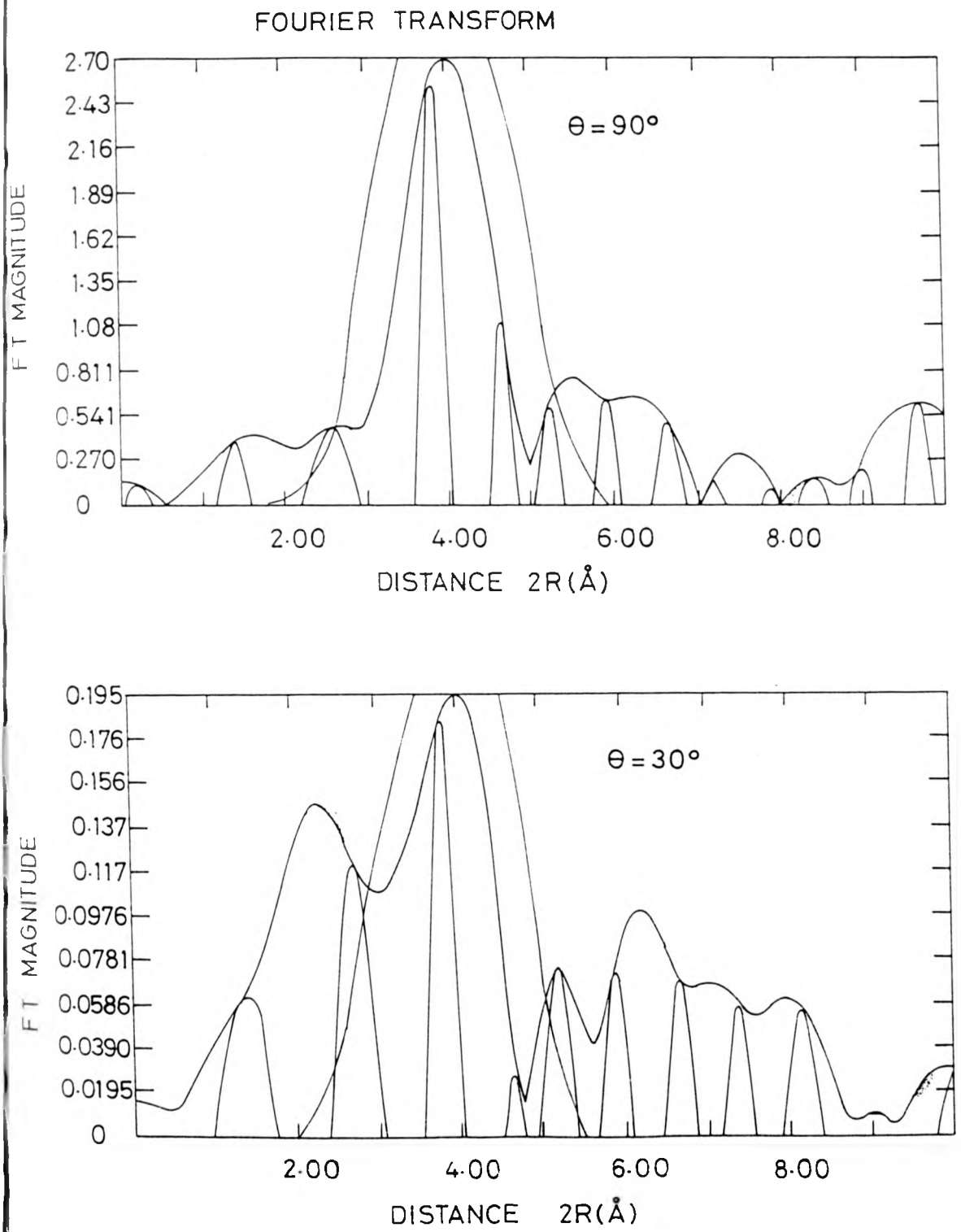

Figure 2.9 SUBTRACTION OF PHASE FUNCTIONS OF MODEL COMPOUND AND SURFACE STRUCTURE CH_3S on Cu(111)

Note that the difference passes through the origin.
The gradient of this line = the difference in model and surface compound bondlength × 2

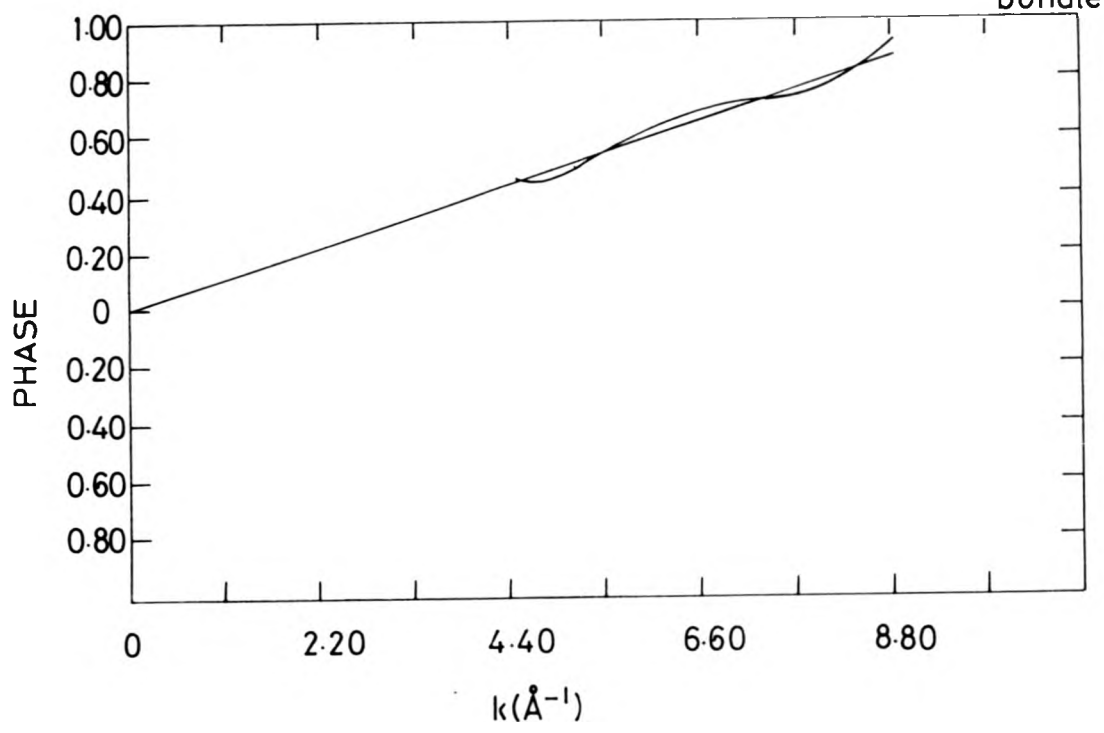

Thus we have the phase term, which is

$$(2k.r_j + \phi_j)$$

The removal of ϕ_j is the last part of the analysis on the way to r_j. In order to remove the ϕ_j term it is necessary to extract the phase function from bulk EXAFS data from a 'model compound' containing the same emitter-scatterer pair.

Subtracting these two phase function should give

$$(2k.r_j - 2k.r_{model})$$

the phase term having cancelled. However, due to differences in chemical environments that exist between the bulk and surface compounds the cancellation may not be perfect. This chemical effect may be allowed for by varying the E_0 value (chosen arbitrarily at the outset of the analysis), this variation of E_0 is performed such that the difference of the phase functions, as a function of k, passes through the origin, this should give a straight line of gradient

$$2(r_{exp} - r_{model})$$

Thus measuring this gradient gives the surface bondlength provided that the model compound bondlength is accurately known (see fig 8). This part of the analysis relies on the idea of phase shift transferability between surface and model compounds. This concept has been tested and proven elsewhere [34]

2.7 Multishell Analysis

If two shells in a given structure are rather close and the data range is short then they may both contribute significantly to a single peak in the Fourier

transform and spectral isolation of these by Fourier filtering will not be possible and any results obtained by this method may be largely in error. In these cases it is therefore necessary to analyse more than one shell at a time and adopt a curve fitting approach to the analysis of the EXAFS oscillations. This is called multishell analysis. All simulations of this type were performed using the EXCURVE program which is described in detail elsewhere [20].

Analysing data this way requires a small amount of modelling of the surface structure, ie values of N_i and R_i for each shell must be input into the program as well as details of atom types and their respective phaseshifts. After this trial structure has been input it may be refined iteratively such that the best least mean squares fit of theory to experiment is obtained. The parameters that may be iterated include;

r_j - the bondlength from the central atom to the atoms in the j^{th} shell

E_0^j - the energy of the emitted photoelectrons at the edge which was chosen arbitrarily at the outset of the analysis as the zero of the photoelectron kinetic energy scale, this may be different for each shell as the chemical environment for each shell is different.

N_j^* - the effective co-ordination number of the shell which differs from the actual co-ordination number N due to the strong directionality of photoemission.

A_j - Debye-Waller type factor ($2\sigma_j^2$) - the mean square relative displacement of the shells rather than an actual Debye-Waller factor.

VPI - An imaginary part of the inner potential which produces a decaying wave amplitude - this allows for a finite mean free path.

AFAC - This allows for losses in coherence of the photoelectrons due to

many body effects and effects caused by the finite lifetime of the core-hole.

During these iterations it is important to ensure that all the above parameters remain physically reasonable.

The phaseshifts employed in the multishell analysis are arrived at in a different way than is the case for single shell analysis but, a model compound is still required. It is assumed that the structure of this compound is well known - so that all the relevant co-ordination lengths and numbers, Debye-Waller type factors and atom types are fed into the program - then theoretically calculated phase shifts may be iteratively modified to least squares fit the 'model compound' data.

Assuming phase shift transferability we may now fit surface data using this refined phase shift. Of course E_0 may be varied in the usual way to allow for differences in the chemical environment in the same way as for the single shell analysis.

The EXCURVE program may also be used to analyse the amplitude of the SEXAFS oscillations. Thus it is possible to analyse the polarization dependences of the SEXAFS. It is one of the more prominent advantages of the SEXAFS technique that these dependences of amplitude on the angle of incidence may be simply analysed. These polarization dependences arise due to the well defined state of polarization of the electric vector of the synchrotron radiation which gives rise to strongly directional photoelectron emission leading to some shells being 'seen' to a greater extent than others for a given angle of incidence. Thus by varying the angle of incidence and noting the corresponding amplitude variations of a given shell and comparing these with the following expression we may obtain information on bonding angles between

adsorbate and substrate which can lead to incisive structure determinations

$$N_j^* = 3N_j(cos^2\theta\ cos^2\beta + sin^2\theta\ cos^2\beta\ cos^2\phi)$$

where θ = the angle between the normal to the surface and the polarization vector of the incident radiation

and β = the angle between the surface normal and the bond between the adsorbate and the scatterer

and ϕ = the azimuthal angle between the electric vector and the bond - variations due to this term disappear for surfaces possessing greater than 2 fold symmetry as $cos^2\phi$ simply averages to 0.5

and N_j = the co-ordination number of the shell

The polarization dependence of the SEXAFS amplitudes can be quite strong for photoelectrons excited from a K shell as the p wave dumb bell shape is peaked strongly in the emission direction. In the case of L_2 or L_3 photoelectrons, however, photoexcitation is permitted into two channels and either s waves or d waves may be produced, these do not have such strongly preferred emission directions and hence polarization dependences are not as strong and hence they are not as useful for site determination. Here

$$N_j^* = 0.7N_j + 0.9\sum_{i}^{N_j} cos^2\theta_{ij}$$

where θ_{ij} is the angle between the **E** vector and the vector joining the absorbing atom to the i^{th} atom in the j^{th} shell.

2.8 Standing X Ray Waves

The technique of standing X ray waves owe s it s existence to a dynamical interaction of the incident and reflected X ray beams which occur during a

Bragg reflection. For this dynamical interplay to occur it is necessary that the reflected and incident beams are of comparable intensity, thus the reflection has to build up over many lattice planes and a kinematical approach to this diffraction problem is inappropriate. If the reflection is required to build up over many lattice planes then it is reasonable to assume that the effect will only occur in perfect crystals. For a long time since the first use of the standing X ray wave technique (it was first used as a probe of the electric fields in a crystal rather in order to test the dynamical theory of Ewald which was developed in 1913) in 1964 [21] this was thought to be the case. However, in 1986 the experiment was performed, successfully, for the first time, on a non perfect crystal of Cu(111) [22] which was prepared in the normal way for surface experiments. This experiment differed from many previous ones in that it exploited the fact that the angular width of the Bragg reflection at normal incidence is of the order of 1 or 2^0 and therefore any slight misalignment of the crystal planes (mosaicity) of the order of less than a degree will not prevent the build up of a Bragg reflection and thus the dynamical interaction may occur between primary and reflected beams of comparable intensity. Previous experiments had worked at more grazing incidence where the angular width of the Bragg reflection was much smaller than it is at normal incidence (the order of microrads) and hence these experiments required samples of high crystalline perfection, such perfection was normally only attainable for semiconductor crystals [23,24,25,26,27].In the later version of the experiment the sample was fixed at normal incidence and the region of total reflection was scanned in energy, all previous experiments had scanned the Bragg condition in angle, which due to the narrowness of the Bragg condition in angle, required high

precision sample goniometers which are unnecessary in the NISXW experiment [22]. One group of experimenters had already recognised the possibility of performing near normal incidence SXW experiments on a SEXAFS beamline but these authors had apparently not noticed the very special advantages of performing the experiment at normal incidence [28]. The normal incidence experiment also has the advantage of requiring much softer X rays thus giving improved monochromator resolution.

In the range of total reflection the dynamical interaction between the reflected and incident beams leads to the formation of a standing X ray wave field in a region 1000's of Å deep on either side of the crystal surface. This wave field has the same periodicity as the Bragg reflecting planes . As we scan in energy throughout the region of total reflection the phase relationship between the incident and reflected waves varies such that the phase of the resultant standing X ray wave field is translated through a period of one half of the layer spacing of the Bragg reflecting planes.

Thus if we have an energy tunable source of photons (a synchrotron and a monochromator for instance) we have a means of carefully controlling the position of the antinodal plane of the standing X ray wavefield in the area of the lattice planes within several thousands of angströms of the crystal surface. Thus we may expect to see strong modulations of characteristic X ray induced electron emissions from either crystal or adsorbate atoms as the Bragg condition is scanned. The maxima of these modulations corresponds to points at which the SXW antinode coincides with the atom's position and the minima, of course, corresponds to the point at which the nodal planes of the SXW field are centred on the atom's position. As the wavefield is set up on either side

of the surface it is possible to study the geometry of adsorbates bonded to surfaces (as well as the distribution of bulk and near surface interstitial or substitutional impurities and crystal defects). This is achieved by measuring the energy dependence of the adsorbate's X ray absorption and subsequently analysing the shape position and size of the resultant modulation.

2.9 NISXW Detection Schemes

The NISXW modulations may be detected by monitoring Auger emission, Fluorescence , Ion yield, sample current, or any of the schemes suggested in section five, (sample current and total yield, of course, have no energy discrimination and so cannot be used to study adsorbate geometry). The decision as to which to use must refer to arguments presented in that section but the NISXW modulations are of course much larger than SEXAFS modulations (typically over an order of magnitude larger) and so signal to noise is not such a consideration here as it is for SEXAFS.

In all previous studies several methods of detection have been employed, namely fluorescence [29], Auger emissions [30] and photoelectron yields [31]. In studies which attempt to probe the distribution of bulk impurities fluorescence detection is preferred due to it's high sensitivity to low concentrations [32]. For studies of near surface regions, however, the more surface sensitive scheme of Auger detection may be preferred, but recent work employing both Fluorescence and Auger yield on the c(2 x 2)S - Ni(100) surface [T Yokoyama et al unpublished] has suggested that problems of background subtraction for the Auger detection scheme have resulted in erroneous results and that fluorescence is the indispensible detection scheme. It is possible, however,

that the discrepancy between the Auger and fluorescence yield values for the NISXW layer spacings, found by these authors, may also be accounted for by assuming that S diffuses into the bulk Ni or that S impurities already in the Ni crystal are contributing to the experimental signal, thus giving an inaccurate adsorbate-substrate layer spacing. Nevertheless the absolute reliability of either detection scheme is as yet undetermined.

2.10 Theory

The equations describing the NISXW technique are found by solving Maxwell's equations for the case of periodic dielectric constant, this procedure finds a Bragg band gap in the spectrum of the traveling wave solutions to these equations and only standing wave solutions are possible in this band gap which corresponds to the range of total reflection.The range of this region of total reflection is inversely proportional to the strength of the scattering from the Bragg planes. The reason for this is that a strong scatterer will reflect more X rays than a weak one thus limiting the penetration depth of the X rays and hence reducing the number of scatterers taking part in the reflection. This in turn leads to a widening of the energy width of the Bragg reflection. During this region of total reflection the standing X ray wave field is set up, the phase of this wave field moves as we tune in energy across the Bragg reflection (as described in the last section) and this gives rise to the modulation of the X ray excited yield of the adsorbate atom. The basic equation describing the SXW yield is,

$$I(A) = (1 + 2\frac{E_H}{E_0} f_i \cos(\nu - 2\pi \frac{d_z}{d_H}) + (\frac{E_H}{E_0})^2)$$

where

$$\frac{E_H}{E_0} = -\frac{F_H}{F_{-H}}^{\frac{1}{2}} (\eta \pm (\eta^2 - 1)^{\frac{1}{2}})$$

and

$$\eta = \frac{\Delta\theta \ sin2\theta_B + \Gamma \ F_0}{|P|\Gamma \ (F_H F_{-H})^{\frac{1}{2}}} \quad [33]$$

if we change variable, we have

$$\eta = \frac{(-2\frac{dE}{E} sin^2\theta_B + \Gamma \ F_0)}{|P|\Gamma \ (F_H F_{-H})^{\frac{1}{2}}}$$

where I(A) is the Auger yield

E_0 and E_H are the incident and reflected electric fields respectively.

d_z is the layer spacing of the X ray absorbing atom.

f_i is the coherent fraction of the absorbers ie the percentage that may be ascribed to a particular layer spacing d_z.

ν is the standing X ray wave phase angle.

d_H is the bulk lattice interlayer spacing for a given set of Bragg reflecting planes.

F_H and F_{-H} are the structure factors for the F_H and the F_{-H} reflections respectively.

η is a dimensionless parameter which describes the range of total reflection which occurs if $1 < \eta < 1$ and $\eta = 0$ corresponds to the centre of this range.

P is the polarization factor which equals $cos2\theta_B$, for $\theta_B = 90^0$ this is equal to unity.

and

$$\Gamma = (\frac{e^2}{4\pi \ \epsilon_0 mc^2})\frac{\lambda^2}{\pi \ V}$$

Where V is the volume of the unit cell, λ is the X-ray wavelength, e and m are the charge and mass of the electron, ϵ is the permittivity of free space and c is the velocity of light

So we can now describe the behaviour of the NISXW modulated Auger yield in terms of the incident photon energy throughout the range of total reflection. As the quantity $\frac{E_H}{E_0}$ is complex it is possible to define a phase for $\frac{E_H}{E_0}$

$$\nu = tan^{-1}\left(\frac{real\ part\ of\ E_H}{imaginary\ part\ of\ E_0}\right)$$

this phase angle varies from 0 to π in the range of total reflection (Note that ν = the standing wave phase angle referred to earlier) and a maximum in the Auger yield will occur if $\frac{\nu}{2\pi} = \frac{d_z}{d_H}$.

2.11 NISXW Analysis

The analysis of the NISXW data consists of modelling the experimental data using the equations detailed in section .10. This is achieved using a set of FORTRAN programs which were written by D P Woodruff. The first of these programs has the function of calibrating the energy scales of the NISXW data sets. This was necessary as the energy ranges of the raw data sets were found to be susceptible to slight drifts of the monochromator calibration. Even though these drifts were always less than a few eV they still posed a real problem as the analysis procedures depend upon the accurate determination of the energy differences between the peaks of the experimental signals in order that an accurate layer spacing may be obtained. These differences were usually never more than 2 to 4 eV, hence the need for calibration is apparent.

This calibration was obtained by the simultaneous measurement of total yield signals from the surface during all scans. The energy at the peaks of the total yield scans was assumed to be constant for all experimental scans. The alignment program then measured the difference in energy location between the peak of the total yield signal and the peak of the Auger signal whereupon it set the total yield peaks at a certain fixed point in a relative energy range and referenced the Auger signal to this point. This procedure was adopted for the referencing of both adsorbate and substrate signals.

Secondly, the data sets were background subtracted. This was done by simply subtracting experimental signals which were measured fifty eV above the Auger peak from the signals measured at the Auger peak energy. The signals measured 50eV above the Auger peak were deemed characteristic of the background due to their close resemblance to the total yield signals and substrate Auger signals which are derived from the substrate as is the main part of the background.

Thirdly, the substrate profile is modelled, this is assumed to fit to a d_z value of 0.0Å, which is a reasonable assumption as this signal is collected in appreciable measure from at least six substrate layers and it is expected that only the top few layers will be slightly, if at all, disturbed from their normal bulk equilibrium positions (ie 0.0Å, LEED and Ion scattering results usually find these disturbances to produce distortions of only a few % of the bulk interlayer spacing). At this stage the non structural parameters are varied in order to fit the 0.0Å profile, these are; the Debye-Waller factor, the coherent fraction and, the energy broadening of the monochromator output which is assumed to be Gaussian. The coherent fraction is defined the percentage of

X-ray absorbing atoms at the layer spacing being modelled. For the modelling of the 0.0Å layer the coherent fraction was usually found to be around 0.9, for adsorbate layers it was somewhat smaller, usually around 0.8 to 0.85.

Fourthly, assuming the values for the non structural parameters derived in the last process, the adsorbate profile is fitted by varying d_z in the first equation in section 2.10 In this procedure care is taken that the size and shape as well as the energy location of this profile is correctly fitted. These fits were monitored by visual assessment only. Single, aligned, background subtracted spectra were analysed singly in order to estimate experimental errors. Summations of data sets were also analysed so long as they were first deemed reproducible. Problems of reproducibility outside quoted error bars [see forthcoming results] were never experienced.

A further program was available in order that systems involving multiple adlayer occupation could be analysed. This program calculated NISXW profiles involving a range of relative occupancies of two distinct layer spacings. This procedure was found necessary for the analysis of data from Cu(111)+ S surface see Chapter 5.

2.12 References

1. H Fricke Phys. Rev 16 (1920) 202.
2. G Hertz Zeit. f. Physik 3 (1920) 19
3. W Kossel Zeit. f. Physik 1 (1920) 119
4. W Kossel Zeit. f. Physik 2 (1920) 470
5. R de L Krönig Z Physik 70 (1931) 317
6. R de L Krönig Zeit. f. Physik 75 (1932) 468
7. D E Sayers, E A Stern, and F W Lytle Phys. Rev. Letts. 27 1204 (1971)
8. P A Lee and J B Pendry Phys. Rev. B 11 2795 (1975)
9. E A Stern, B A Bunker, and S M Heald, Phys. Rev. B 21 No 12 p5521-5539
10. P Eisenberger and G S Brown Solid State Comm. Vol 29 p481-484
11. A L D Kilcoyne, C F McConville, N P Prince, D L Seymour, D P Woodruff, A M Bradshaw, T Lindner, J Somers, R G Jones, and W Walter p102 The Synchrotron Radiation Appendix to the Daresbury Annual Report 1987/1988
12. P H Citrin, P Eisenberger, and R C Hewitt Phys. Rev. Letts. 41 309 (1978)
13. P A Lee, Phys Rev B 13 p5621
14. U Landman and P L Adams, Proc. Natl. Acad. Sci. USA 73,2250
15. D Chandesris, P Roubin, G Rossi, and J Lecante, Surf. Sci. 169 (1986) p57-70

16. S M Heald, E Keller, and E A Stern Physics Letts. Vol. 103A No 3 (1984)

17. J Stöhr, E B Kollin, D A Fischer, J B Hastings, F Zaera, F Sette Phys. Rev. Letts. Vol 55 No 4 (1985) p1468-1471

18. R McGrath, I T McGovern, D R Warburton, G Thornton, D Norman, Surf. Sci. 178 (1986) p101-109

19. R Jaeger, J Feldhaus, J Haase, J Stöhr, Z Hussain, D Menzel, and D Norman Phys. Rev. Letts. 45 p1870-1873

20. S J Gurman, N Binsted, and I Ross J. Phys. C 17 p142 (1984)

21. B W Batterman Phys Rev 133 A759 (1964)

22. D P Woodruff, D L Seymour, C F McConville, C E Riley, M D Crapper, N P Prince, and R G Jones Phys. Rev. Letts. Vol 58 No 11 p 1460 (1987)

23. B N Dev, G Materlik, R L Johnson, W Kranz, and P Funke Surf. Sci. (1986) 1-9

24. M J Bedzyk and G Materlik DESY SR 85-07 July (1985)

25. N Hertel, G Materlik, and J Zegenhagen DESY SR 84-205 December (1984)

26. G Materlik and J Zegenhagen DESY SR 84-05 March (1984)

27. M J Bedzyk, G Materlik, and M V Kovalchuk, DESY SR 84-06 March (1984)

28. T Ohta, H Sekiyama, Y Kitajima, H Kuroda, T Takahashi, S Kikuta Japan. J. Appl. Physics 24 (1985) L475

29. P L Cowan, J A Golovchenko, and M F Robbins, Phys. Rev. Letts.44 p1680 (1980)

30. S M Durbin, L E Berman, B W Batterman, and J M Blakely Phys. Rev. Letts. 56 (1986) 236

31. S Kikuta, and T Takahashi Japan. J. Appl. Physics Vol 17 (1978) Suppl 17-2 p271-274

32. J A Golovchenko, B W Batterman, and W L Brown Phys. Rev B10, 4239 (1974)

33. R W James The Optical Principles of X Ray Diffraction Bell, London (1962)

34. P H Citrin, P Eisenberger, and B M Kincaid, Phys. Rev. Letts. Vol 36 No 22 p1346

35. P W Palmberg J. Vac. Sci. and Technol. Vol 12 No 1 (1975) p379-384

Chapter 3

Experimental Details

3.1 Introduction

This chapter describes the procedures and hardware involved in SEXAFS and NISXW data acquisition.

3.2 The Beam Line

All the experiments reported here, save for sample characterization studies performed at Warwick, were carried out at beamline six, station three of the Daresbury laboratory synchrotron radiation source (SRS).

The output of this machine forms a broad continuum of X ray energies, but the SEXAFS and NISXW experiments require a continuously tunable photon source and thus a scanning monochromator is required to select the X ray wavelengths needed for experimentation. Another requirement of the experiments is that a small X ray beam is incident on the sample - (to get as many photons as possible into the spot size sampled by the CMA) the ultra high vacuum (U.H.V.) layout used in order to meet these exacting criteria is shown schematically in Figure 1. The beam direct from the SRS is 2mm horizontal and 0.4mm vertical f.w.h.m.. A two to one demagnification of this

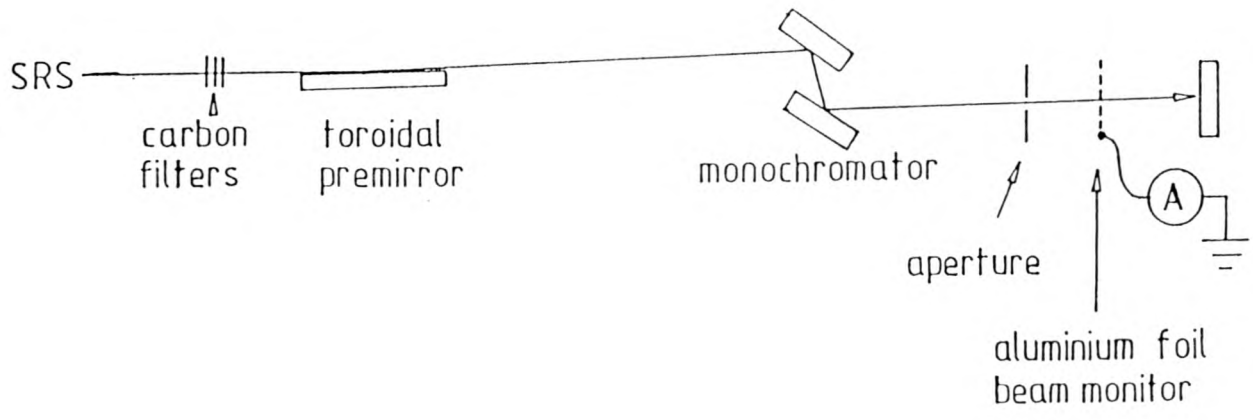

Figure 3.1 The U.H.V. beamline layout on station 6.3 [2]

beam size is achieved by a toroidal premirror (see Fig 1) .This premirror is made of quartz and is coated with a layer of gold such that it acts as a high energy X ray cut off filter. The reason for this is that for monochromatic X rays incident on a planar surface there exists a well defined angle of incidence below which the angle of refraction is zero and total external reflection occurs. This angle is dependent on energy in the following manner

$$\Psi_c \sim \frac{20\rho^{\frac{1}{2}}}{E}$$

where

Ψ_c(mrad) = the critical angle for total external reflection

and ρ (gcm^{-3}) = the density of the material

and E(KeV) = the energy of the X rays

Thus the critical angle becomes smaller the higher the incident X ray energy. The SRS beam impinges on the premirror at 0.5^0 grazing incidence, this gives a high energy cut off of 11.1KeV (ie any X ray of energy higher than 11.1KeV is absorbed by the premirror). A lower energy cut off is also required in order to remove the ultra violet component of the SRS beam which would otherwise transmit through the monochromator by specular reflection. This is achieved by a rack of ten carbon filters, each 2000Å thick, which absorb strongly in the u.v. region .

After the beam is demagnified and filtered it enters a U.H.V. compatible double crystal monochromator which operates using the phonomenon of Bragg reflection from a crystal (see figure 2). Scanning of the energy output of this monochromator is achieved by rotating the monochromator crystals in order to vary the angle of incidence of the X rays onto the crystals and thus vary the energy of Bragg reflection. This angle of incidence variation is achieved

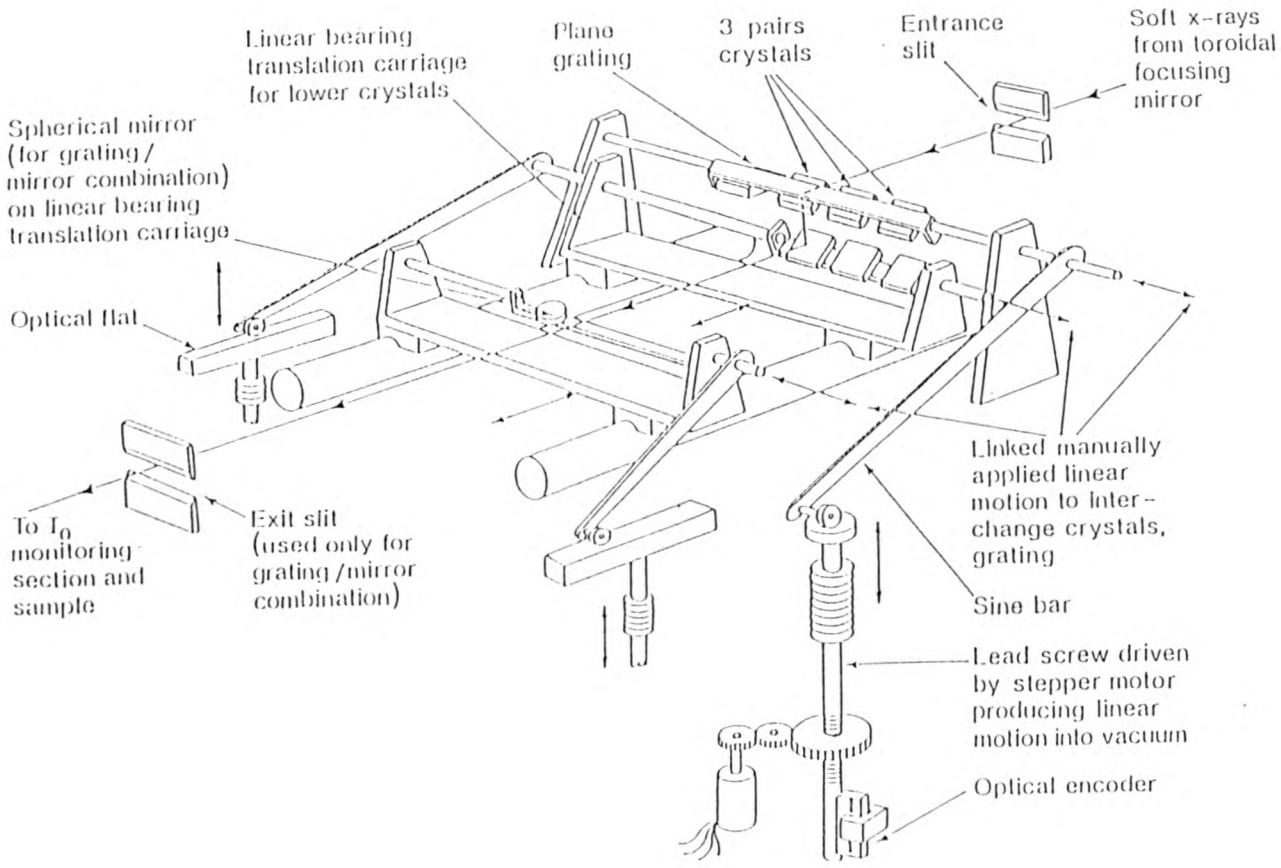

Figure 3.2 The 6.3 soft X ray monochromator [3]

by stepper motors outside the vacuum (see Fig 2 [1]) the movements of which are calibrated by optical interference encoders.

The crystals are in antiparallel arrangement and if both may rotate and the bottom translate then this arrangement allows for an exit beam from the monochromator which has a constant vertical deviation throughout the monochromator's energy range. Thus the beam is spatially fixed throughout an experimental scan, unless, of course, the beam moves in the synchrotron ring.

The crystals angular ranges are between 13^0 and 72^0 and by utilizing three pairs of crystals Ge(111), InSb(111) and, Ge(220) any energy range between 1745eV and 11100eV is obtainable.

After the experimenter selects an energy range the Bragg angles required are computer calculated from the trigonometry of the instrument and then the crystals are stepper motor driven to the calculated encoder values. This procedure alone usually results in no output from the monochromator. This is due to the fact that the first monochromator crystal receives the white light continuum from the SRS and is thus subject to a high thermal load, this load may produce a temperature differential between the two crystals of as much as 200 ^{0}C (this depends, of course, on the electron synchrotron beam current which is normally between 100 and 300mA). Therefore the 2d spacing of the first monochromator crystal may be appreciably different from that of the second and hence the simply calculated Bragg angle will not produce a beam onto the second crystal. This is the main reason why a computerized peak finding routine is necessary. Another reason for the peak finding routine is to allow for the removal of beam contamination which is caused by higher

order Bragg reflections from the monochromator crystals. The peak finding routine involves rotating the first crystal until an an X ray output is monitored coming out of the monochromator. This output signal is measured as a drain current from a photodiode (86% transmittance copper mesh) and this current is then used as a signal for a feedback loop into the computer and thus the peak of the monochromator's output for a given energy may be accurately tuned by the computer. This drain current is in the range of 10^{-9} to 10^{-11} amps and is measured by a Keithley picoammeter. This simple tuning to the peak of the monochromator's output for a given energy, however, will not remove contamination of the beam caused by higher order Bragg reflections from the monochromator crystals. Thus harmonic rejection is required . This harmonic rejection is achieved by exploiting the fact that higher order Bragg reflections have a narrower energy width than the lower order reflections, thus by detuning away from the peak of the monochramator output, it is possible to reject all the higher order contamination whilst still retaining most of the required Bragg reflection. Generally the detuning process rejects 20% of the maximum signal.

Another effect of the thermal loading is that it causes a deflection of the beam (see figure 3 [1]).

Before the beam arrives at the sample chamber it passes through beam defining apertures which may be required to match the beam size to sample size and therefore another signal monitor is required to measure the flux after this aperture as only this signal will be suitable for normalizing the experimental signal (this is necessary as it removes any spurious oscillations in the beam that may pass through the monochromator).The beam may also pass through

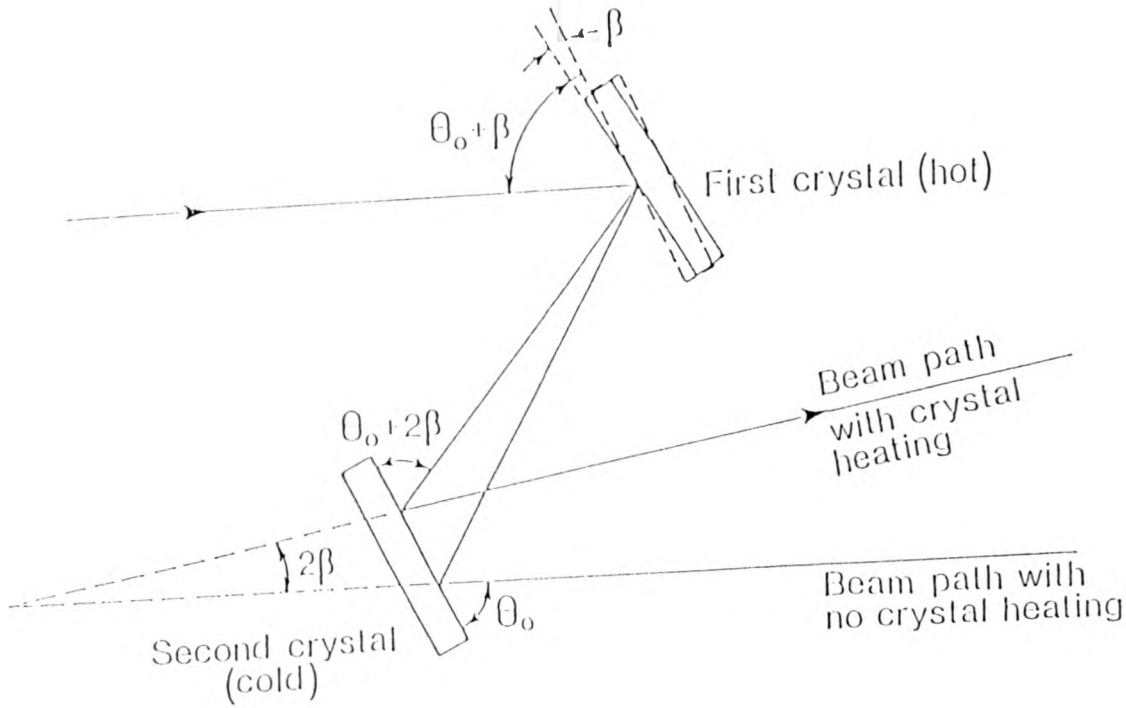

Figure 3.3 An illustration of thermally induced beam deflection for the 6.3 monochromator

a rack of calibration foils to provide energy calibration for the monochromator. This calibration is done by referencing monochromator output to absorption edges characteristic of the foil, these absorption edges can be seen in the drain current from the calibration foil. After calibration is complete the foils are removed.(This monochromator is discussed in greater detail elsewhere[1])

3.3 The Sample Chamber

The beam now arrives in the sample chamber which is illustrated schematically in figure 4. This chamber is pumped to below 10^{-9}mbar by a combination of rotary, sorption, and turbo pumping as well as cryopanel and titanium sublimation pumping. The total pressure is measured by a Bayerd-Alpert gauge and the partial pressures of the individual component gases of the vacuum are measured by a Vacuum Generators residual gas analyzer (a quadrupole mass spectrometer).

Prior to the formation of chemisorbed overlayers and synchrotron radiation experimentation, a clean well ordered surface must be obtained. All samples are initially prepared outside vacuum by spark machining from a single crystal bar. This resulted in elliptically shaped copper crystals of major axis 15mm and minor axis 12mm and 2mm thickness, some measurements were made on a Ni crystal, this was circular with a radius of 5mm. After spark erosion the crystallographic orientation of the sample is checked by Laue diffraction. All crystals were found to be within 1^0 of the manufacturer's specified orientation. The crystal is then polished by diamond paste down to a particle size of 1 micron. The resulting surface is inadequate for surface science experiments and some in vacuum sample preparation is required. The experimental surfaces are

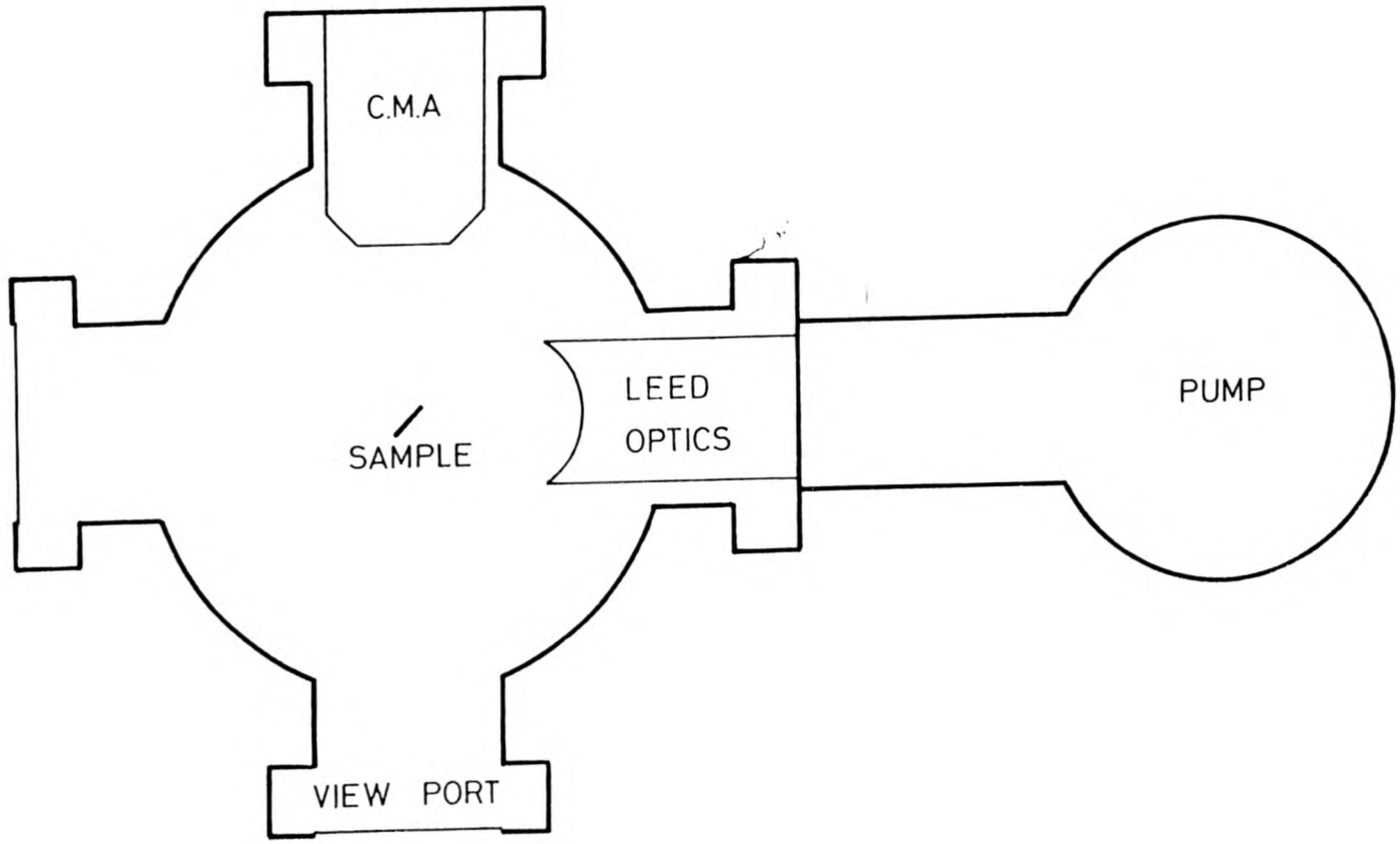

Figure 3.4 A schematic illustration of the 6.3 sample chamber

obtained by a combination of argon ion bombardment and thermal annealing. To this end the sample chamber was equipped with a Vacuum Generators argon ion gun and a sample manipulator capable of in vacuum electron beam heating. Typical argon ion energies were from 2 to 4kV and ion currents ranged from 20 to 50μA. Sample temperatures of five to six hundred ^{0}C were monitored by a chromel-alumel thermocouple which was spot welded to the sample holder. The sample holder is supported on a Vacuum Generators high precision long throw manipulator which is equipped with X,Y, and Z drives as well as polar and azimuthal rotations.

After several cycles of argon ion bombardment and annealing the surface order and cleanliness of the sample were checked by LEED and AES respectively. The number of cycles required depends on the sample's 'history'- more cycles being required for those crystals which have only recently been spark machined.

The LEED experiments were performed using a Vacuum Generators LEED optics (see chapter 2) and AES was measured by a Physical Electronics double pass precision cylindrical mirror analyser (CMA) which has already been described in detail elsewhere [2]. This dispersive electron energy analyzer was used for experiments involving both electron and photon impact ionization of the sample (ie for SEXAFS and NISXW as well as AES). Electrons were incident from an integral electron gun which was mounted on the axis of the CMA. In this electron impact mode the experimental signal is measured by phase sensitive detection - technique which enhances the signal variations caused by Auger emission the details of which are reported elsewhere [3]. For the case of photon impact ionization sample currents are much lower $\sim 10^{-9}$ to

10^{-11}amps rather than $\sim 10^{-6}$amps and electronic pulse counting techniques are required to collect the experimental signal. For both types of data acquisition the detector resolution is 0.6% of the measured energy [2]. (The detector was run inunretarded mode)

A total electron yield detector was also mounted in the sample chamber, this detector collected SEXAFS data simultaneously with the CMA, none of these total yield SEXAFS data, however, were analysed due to the fact that superior signal to noise relative to the edge jump was obtained by CMA detection.

Total yield signals did, however, provide useful information in the analysis of the NISXW data. These measurements provided energy calibration for the NISXW signals, this was necessary due to the experimental drift which was observed in the monochromator calibration. In order to obviate this difficulty simultaneous total yield measurements were collected during all NISXW scans. The total yield signal is dominated by electrons from the substrate and it s profile (modulation) should maximise at an energy location corresponding to that which would expected for an emission from a layer of atoms at 0.0 Å with respect to the substrate. It is safe to assume that this energy location of the maximum in the total yield signal will always be the same for all experimental scans. Thus referencing all the Auger detected signals from the CMA to the total yield detector's signal maximum provides suitable energy calibration for the NISXW scans. No other signal (save for sample current) can be used as a reference as it is necessary that this calibration signal is measured during all NISXW scans. Previous experiments have measured X ray reflectivity simultaneously with fluorescence yields in order to calibrate their energy scales.

This calibration is necessary because NISXW analysis relies on accurate measurements of the separation in energy of Auger emissions from adsorbate and substrate atoms, which must be measured, for obvious reasons, in separate experimental scans. These differences are rarely more than 4eV and the calibration drift of the monochromator has been found to be of the 1eV from scan to scan hence the need for calibration of all NISXW scans.

3.4 S on Cu(111)

The $(\sqrt{7}X\sqrt{7})$R-19.1°-S surface was formed by backfilling the U.H.V. chamber with H_2S from a base pressure of less than 10^{-9}mbar to a final steady state pressure of 1 x 10^{-8}mbar. Various exposures were obtained, these were between 5 and 50L (1L = 10^{-6}torr for 1 second). The H_2S gas was of research grade and was supplied by B.O.C., it's purity was quoted as 99.99%. The purity could be monitored in situ by the mass spectrometer trace (VG SX200)- (this was to check for contamination in the gas line). The rate of entry of H_2S to the sample chamber was controlled by a standard leak valve. All exposures, 5 to 50L , gave rise to the same LEED pattern $(\sqrt{7}\ X\ \sqrt{7})$R 19.1°-S, and the surfaces formed were shown to be contamination free by AES.

All SEXAFS measurements were recorded above the sulphur K edge at 2472eV. The energy range of these scans was from 2450eV to 2950eV . These scans were divided into 2eV increments and the counting time for each step was ten seconds. Total data acquisition times were typically of the order of one hour. To exploit the polarization dependence of the SEXAFS oscillations the experiments were performed at two different angles of incidence (36° and 90°) (ie the spectra were recorded with the X-ray beam normally incident on

the surface and with the beam 54° off normal). The SEXAFS oscillations in the X ray absorption cross section were monitored by detecting the KLL Auger electrons at 2106eV. No difficulties were experienced with substrate and adsorbate photopeaks traveling through the energy 'window' of the detector.

For the NISXW experiments the modulation of the X ray absorption coefficient were monitored by measuring the S KLL yield at 2106eV and the Cu LVV yield at 910eV, this time however the monochromator was set to scan through a range of 15eV on either side of the normal incidence Cu(111) Bragg reflection. This range was from 2960eV to 2990eV and contained 151 data acquisition points at 0.2eV intervals. Each increment had a counting time of three seconds giving a total data acquisition time of approximately 15 minutes. As well as detecting electrons in the Auger peak we also ran scans in which the detector 'window' was set to detect electrons fifty electron volts above the Auger peak energy. This signal was collected in order to perform background subtractions. This background is constituted of inelastically scattered photoelectrons which have a yield which also modulates in the Bragg reflection energy range, if these electrons were allowed to contribute to the analysed modulation then the modulation would be unrepresentative of the structure of the adsorbed overlayer (or the substrate structure if a substrate emission is measured). Care is taken to ensure that both the on and off peak NISXW scans are representative of the required signal. To this end various energy distribution curves were measured at several photon energies throughout the Bragg reflection range to check that no photopeak directly interfered with the experimental signals. Collecting these energy distribution curves (EDC's) involved setting the monochromator at a fixed photon energy and then scanning

the CMA detector window throughout the entire energy range of the electrons emitted from the surface.

3.5 CH_3S on Cu(111)

The CH_3S on Cu(111) surface was formed by backfilling the chamber to a pressure of 10^{-8} mbar with dimethyl disulphide $(CH_3S)_2$. This gas was admitted to the sample chamber in the same way as the H_2S. Exposures from 5 to 50L were experimented upon. These surfaces possessed no long range order and because exposure to an electron beam for a short time results in the decomposition of CH_3S to form $(\sqrt{7} X \sqrt{7})$ R 19.1^0-S. Thus AES was not possible and checks for contamination were performed using incident photons in an XPS experiment.

The SEXAFS measurements were recorded above the sulphur K edge at 2472eV . These were performed at 60^0 off normal and at normal incidence (ie at 90° and 30° incidence respectively) These scans were recorded over the same ranges as the H_2S experiments. The normal incidence standing X ray wave scans were monitored by detecting the sulphur KLL and the copper LVV Auger emissions, at 2106eV and 910eV respectively, in the range of the Cu(111) Bragg reflection. Once again on and off peak scans were collected in exactly the same way as for the case of atomic S adsorption (ie incident photons between 2960eV and 2990eV)

3.6 Hg on Ni(100)

This surface was formed by dosing a clean Ni(100) crystal for a few minutes with an SAES getter source. After dosage the surface exhibited a c(2 x 2)

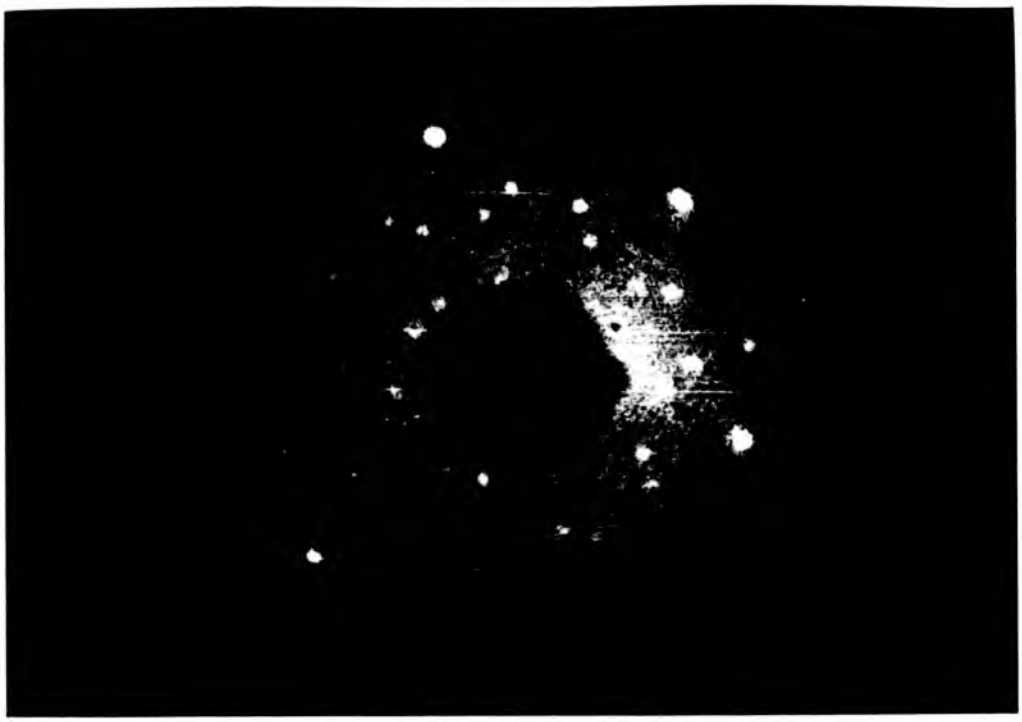

A LEED photograph of the ($\sqrt{7}$ X $\sqrt{7}$)R19.1°-S overlayer on Cu(111)

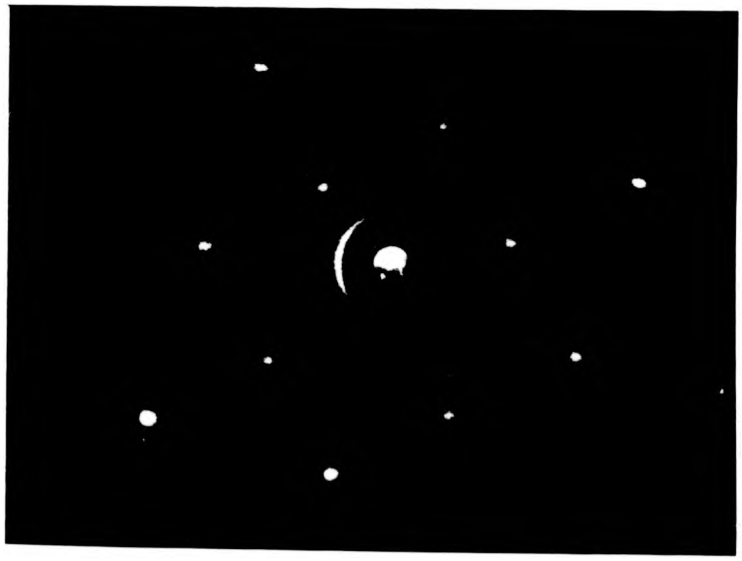

A LEED photograph of the Ni(100)c(2 X 2)-Hg overlayer

LEED pattern and was found to be contamination free by AES, some problems were encountered with carbon contamination but these were solved by annealing the crystal in an atmosphere of oxygen.

SEXAFS measurements were attempted above the Hg M_V edge at 2295eV. Data was collected from only one angle of incidence due to the poor quality of this SEXAFS data (only two runs were collected, see chapter 6).

NISXW measurements were performed by detecting Ni LVV (848eV) and Hg MNN (2072eV) Auger electrons in the vicinity of the normal incidence Ni(200) Bragg reflection at 3522eV. As in previous experiments these scans were collected on either side of the Bragg reflection in a range of 30 electron volts. This range was used for both on Auger peak and off Auger peak scans

3.7 References

1. A A McDowell, D Norman and J B West, Rev. Sci. Instruments. Vol 57 (1986) p2667

2. P W Palmberg J. Vac. Sci. and Technol. Vol 12 No 1 (1975) p379-384

3. N J Taylor, Rev. Sci. Instruments Vol 40 (1971) p792

Chapter 4

CH_3S on Cu(111)

4.1 Introduction

Until the mid nineteen seventies the study of the detailed structure of adsorbates on surfaces was dominated by the use of low energy electron diffraction. Amongst the limitations of this technique are the fact that it cannot be used to study adsorption systems which do not possess long range order and also that the usage of electrons as a structural probe may result in the alteration or damage of the system under study. These problems are rather severe in the case of molecular adsorption systems which frequently do not show long range order and often involve weak intramolecular or molecule to substrate bonding. (For the CH_3S Cu(111) system reported here it is known that the exposure of this system to an electron beam of the type used in LEED experiments $E_p \sim$ 100eV results in the scission of the C-S bond).

The SEXAFS technique is not subject to either of these limitations and hence it is expected to be highly applicable to the study of the structure of molecular adsorption. Despite this fact it appears that the technique has not yet been extensively applied in this area even though the need for structural information on molecular adsorption is crucial to the understanding of a range

of surface chemical reactions, ie MBE, MOMBE and some catalytic reactions, where the idea of an active molecular adsorption site is thought to be very important. Other surface analytic techniques like reflection absorption infra red spectroscopy (RAIRS) and electron energy loss spectroscopy (EELS) have been more widely applied to molecular adsorption at well characterized substrates. These techniques provide detailed information on the chemical nature of the adsorbate, the molecular orientation on the surface and also some information on the adsorption site is often indicated [1], but this is cosiderably less incisive than that which is readily obtained by SEXAFS. Certainly the data acquired to date on surface structure by vibrational spectroscopies could not be employed as an input to calculations of local surface electronic structure whereas SEXAFS data have been used for this purpose [2].

The technique of normal incidence standing X ray waves, because it involves incident photons, is also applicable to the study of molecular chemisorption structures and once again long range ordering is not required.

Some previous SEXAFS studies of molecular adsorption have involved the catalytically relevant interaction between the formate species HCOO and the Cu(100)[3] and Cu(110)[4] surfaces. One of these studies also produced results for CH_3O on Cu(100). All these experiments have the common features that the data are recorded above the K absorption edge of oxygen at 543eV and that all of these data are of poorer quality than that which was collected for mercaptide on Cu(111) which is the system studied here. The contrast is particularly stark when comparing CH_3S/Cu(111) data with that which was obtained for the mercaptide group's oxygen analogue, CH_3O, on Cu(100). The reason for the better quality of the mercaptide on copper SEXAFS data is due

to the fact that sulphur has a deeper lying K edge (2472eV) than oxygen, and hence it's EXAFS will attenuate less rapidly than for oxygen as EXAFS oscillations fall off with a rapidity in inverse proportion to the binding energy of the X ray absorption edge above which they are recorded. Also the fact that the Cu-S bondlength is expected to be longer than the Cu-O bondlength means that more oscillations are observed in a given data range for the Cu-S system than in the Cu-O system. This improves the accuracy of the data analysis. A very large bondlength, however, can lead to very small EXAFS oscillations due to the $\frac{1}{R_j^2}$ factor in the EXAFS equation. Nevertheless for the Cu(111)- CH_3S system studied here this factor is outweighed by the other favourable circumstances outlined above and it is hoped that systems like this with deep lying edges might help in gaining a better understanding of the chemistry of analogous molecules containing lower Z components which are harder to study by SEXAFS. Results of NISXW studies also gave rather good signal to noise characteristics and a corroborative interpretation of both SEXAFS and NISXW data has been found. These results suggest a structural rearrangement of the substrate which is the first reported case of adsorbate induced reconstruction caused by molecular adsorption

4.2 Results

The raw data sets were collected at 90^0 (normal) incidence and 30^0 (60^0 off normal) incidence of the X ray beam to the surface. These data sets were measured above the S K edge at 2472eV and are shown in figure 1. They were measured by collecting sulphur KLL electrons (2106eV) and this detection scheme gave acceptable signal to noise characteristics as well as very well

Figure 4.1 RAW DATA SETS CH_3S on Cu(111)

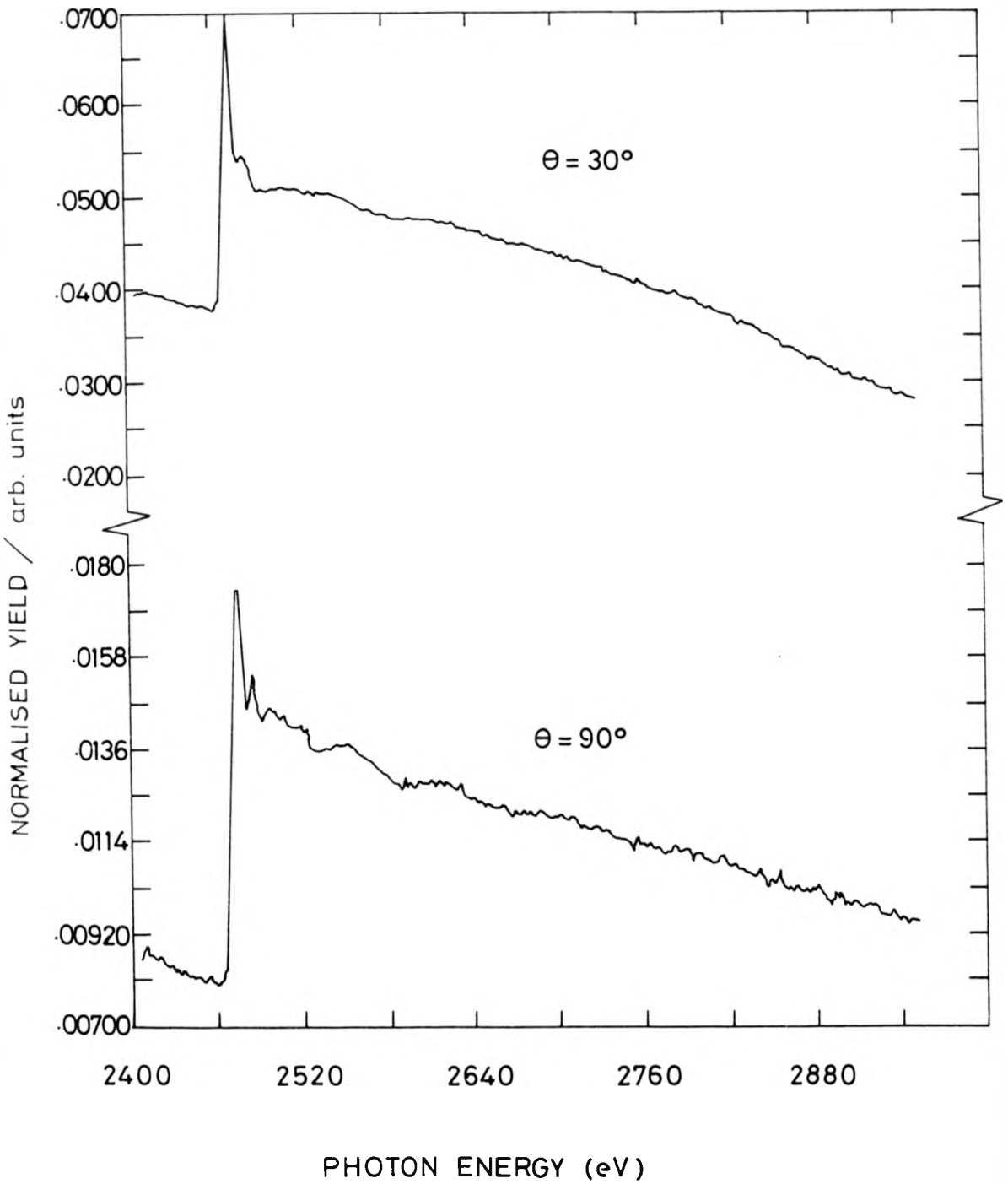

Figure 4.1a

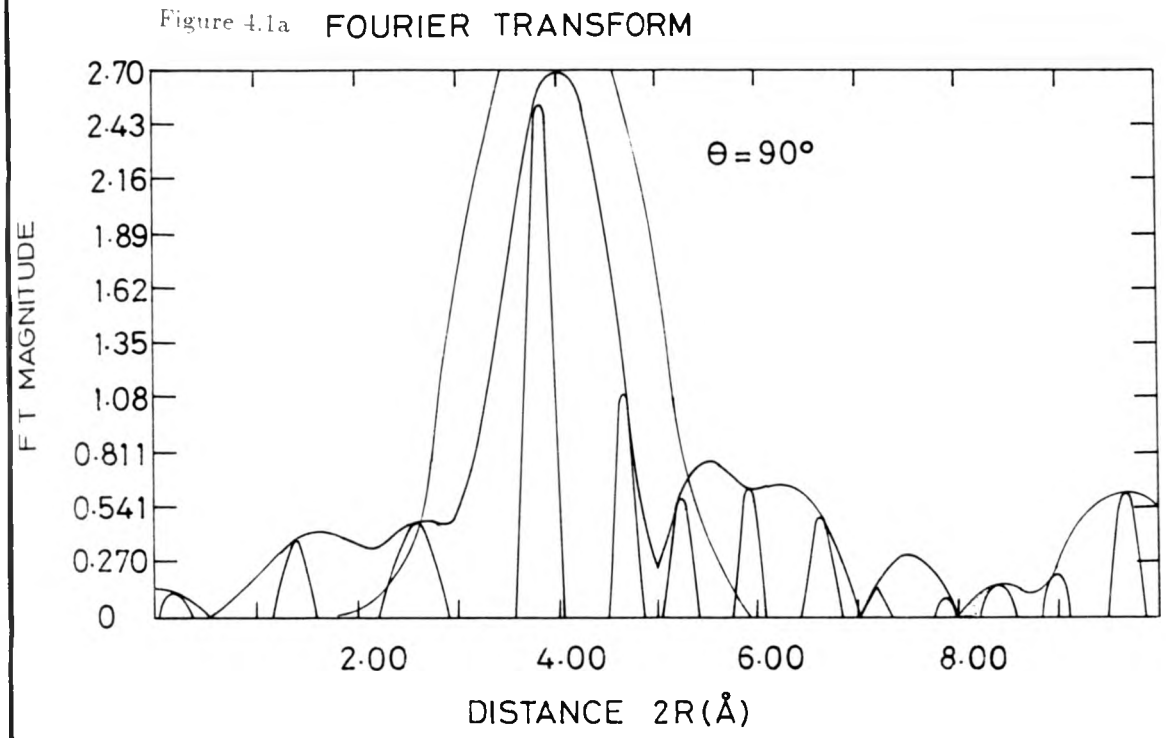

Figure 4.2a

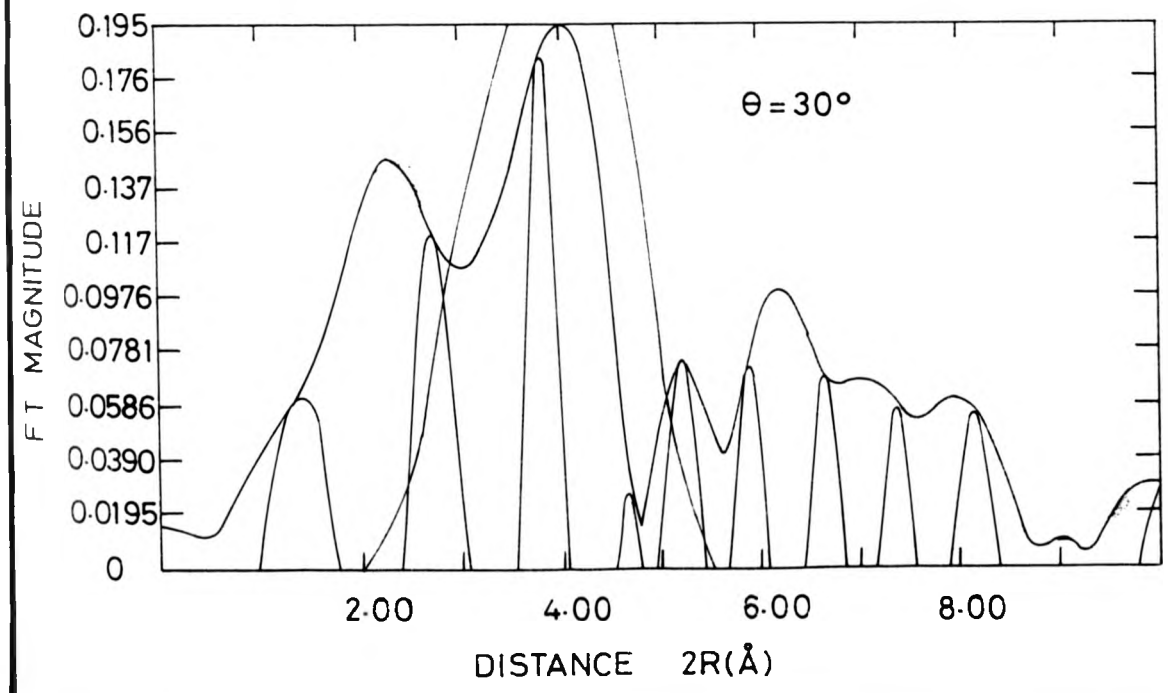

behaved and stable backgrounds. Analysis followed the routes suggested in chapter two. Background removal and normalization was straightforward for both angles of incidence. Fourier transformation from k space into real space (Figures 2a and 2b) revealed that the data was dominated by a single distance and that the Fourier filtering single shell analysis, gave acceptable bondlength determinations for the nearest neighbour Cu-S distance. The dominance of the first nearest neighbour shell is particularly evident for the normal incidence data , for the case of the off normal data, however, a low K peak is visible. This is attributable to C-S scattering within the mercaptide group. This C-S shell was analysable using the EXCURVE programs [5] and taking the results of both single and multishell analyses it was apparent that no appreciable interference occurred between the Cu-S and the C-S shells.

The result of single shell analysis for both angles of incidence gave a nearest neighbour Cu-S bondlength of 2.38Å $\pm$ 0.03Å. This analysis used a CuCl model compound rather than CuS. The reason for this was that the bulk structure of CuCl is better characterized than it is for CuS [6] and the principle of phase shift transferability appeared to hold between S and Cl as a shift of only a few eV was necessary to describe the S/Cu scattering adequately. In order to validate this transferability further some NiS phase shifts were employed in the multishell analysis (see later)- these had been used in a recent SEXAFS study of the adsorption of S on Ni(111)[7] and these phase shifts as well as theoretically calculated CuS phaseshifts provided results within the error limits we obtained with the CuCl model compound phaseshift.

The results of Fourier back transformation of the windowed Fourier transforms are shown superimposed on the background subtracted fine structure

functions and the dominance of the scattering by a single shell is clearly evidenced (see figures 3).

4.2.1 Multishell Analysis

More detailed results are obtained using the more sophisticated EXCURVE multishell analysis package [5]. This program used the same phase shifts as those used in the single shell analysis for the Cu-S scattering as well as some calculated Cu-S phaseshifts and some experimentally derived NiS phaseshifts [7] , these provided the same result and thus phase shift transferability between the model compound and the experimental system was adequately demonstrated. A theoretically calculated carbon phase shift was used to describe the C-S scattering. This phase shift was not optimised to a model compound and hence the accuracy of the C-S bondlength obtained (which was 1.88Å) cannot readily be ascertained, however, comparison with the Cu-S bondlength in the free mercaptan molecule which is 1.81Å indicates that the value of 1.88Å is plausible when considering that the error bar on this C-S bondlength is likely to be larger than for the Cu-S shell.

The contribution of the C shell at 60^0 off normal incidence is evidenced by the differences at low K between these data and the normal incidence data ($3Å^{-1}$ to $4Å^{-1}$ see figures 4a and b) and the incorporation of a carbon shell provides a good fit to the additional structure between 3 and $4Å^{-1}$ in the off normal incidence data.

The amplitude analysis of the carbon sulphur scattering allows a determination of the absorber to scatterer angle, β, relative to the surface normal. If the angle of incidence of the X radiation polarization vector relative to the surface normal is θ then the amplitude of the SEXAFS contributed by a given

Figure 4.3a FINE STRUCTURE FUNCTIONS SUPERIMPOSED ON FOURIER BACKTRANSFORM

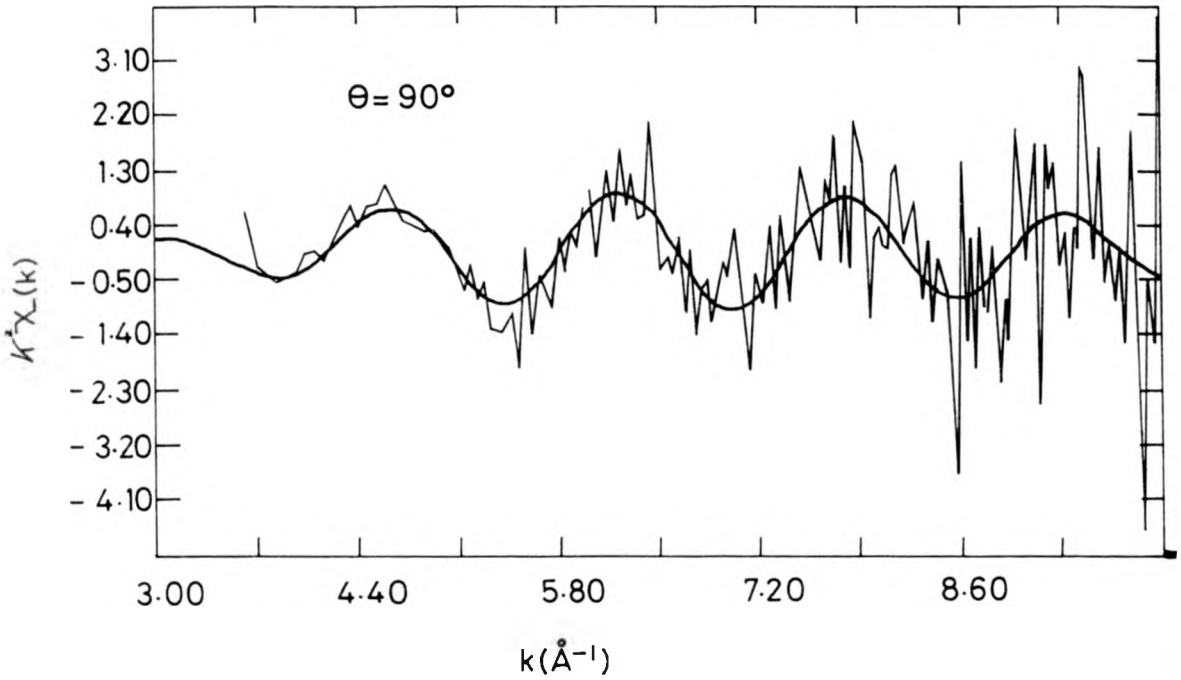

Figure 4.3b

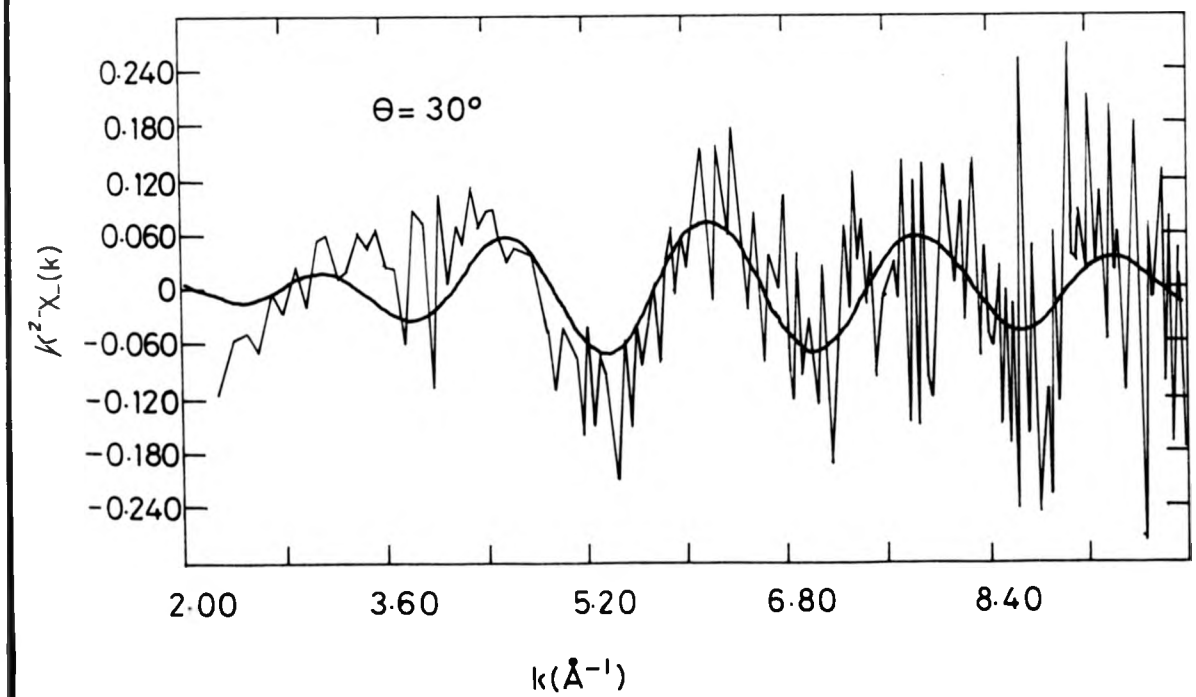

scatterer (or set of symmetrically equivalent scatterers) is given by

$$N_j^* = 3N_j(cos^2\theta\ cos^2\beta + 0.5sin^2\theta\ sin^2\beta)$$

thus the observed absence here of any C-S scattering at $\theta = 90^0$ indicates that $\beta = 0^\circ \pm 15^\circ$. This means that the mercaptide group is bonded perpendicularly to the surface. This conclusion is in agreement with a previous photoelectron diffraction study of the methoxy (CH_3O) group bonding behaviour on the Cu(100) surface [8], but not with simple interpretations of Near Edge X ray Absorption Fine Structure data (NEXAFS) for this same mercaptide system [9], but the discrepancy with this NEXAFS study is believed to be attributable to inadequacies of the interpretation of the NEXAFS data.

Data from both angles of incidence gave evidence of the role of S-S scattering at a separation of 3.4 ± 0.15Å. The amplitude of this scattering is greater at normal incidence than for 30^0 incidence by a factor of fourteen to one. Analysis of this polarization dependence (using the equation above) gave a value of β of 80 ± 10^0. These two observations would correspond to a 0.7ML coverage of S in a coplanar layer above the copper surface - (if this phase covered the entire surface.)

The reliability of these conclusions about the C-S and S-S shells is reduced by the fact that S-S and C-S scattering is very weak to the dominating Cu-S scattering in the data. Nevertheless they constitute useful secondary information.

The bondlength obtained for the nearest neighbour Cu-S scattering is identical to that given by the single shell analysis which was 2.38 ± 0.03Å. Studies of the dependence of this shells EXAFS amplitude on the X ray polarization

Figure 4.4 A multishell simulation of the normal incidence CH_3S on Cu(111)

data

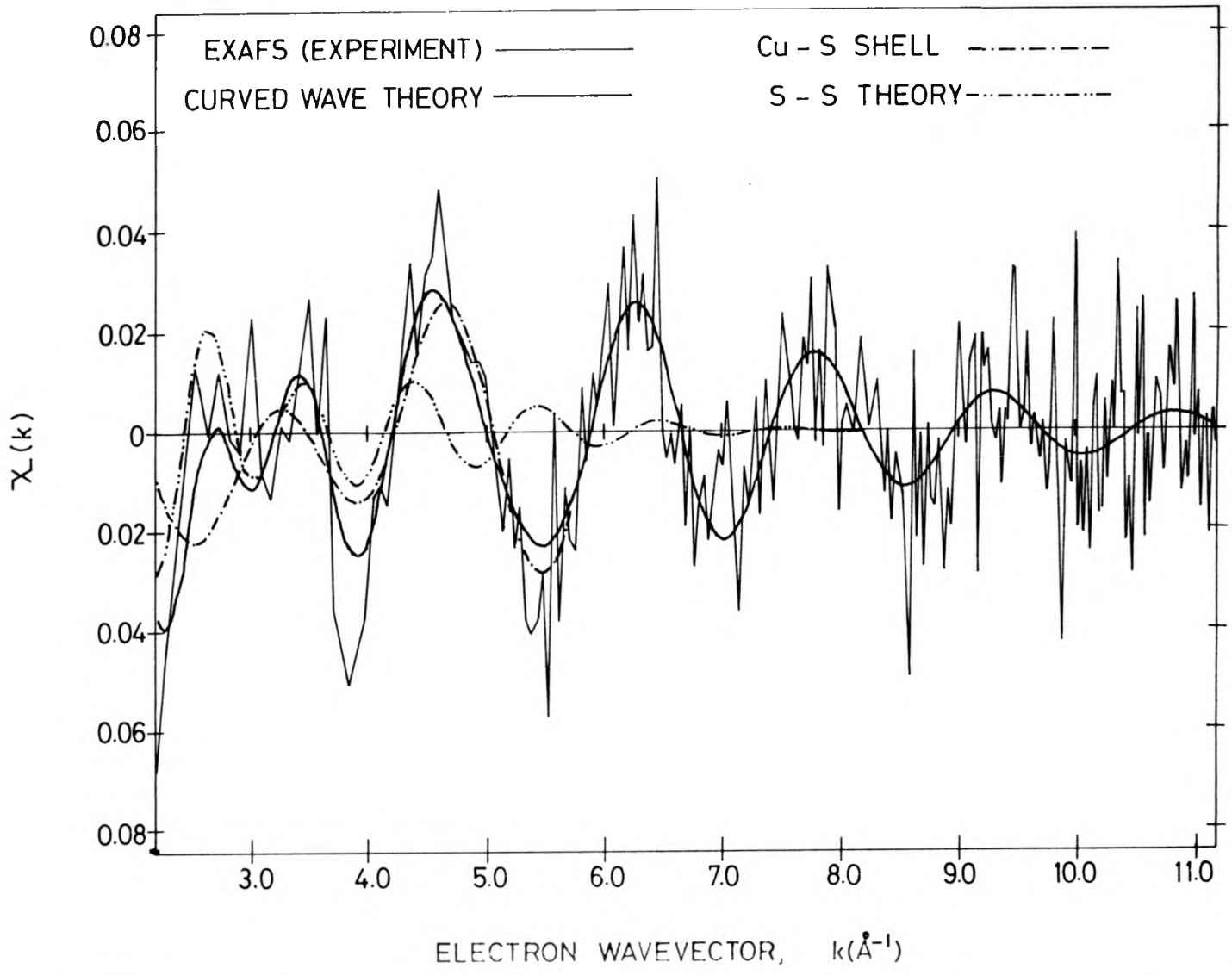

Figure 4.5 A multishell simulation of the off normal incidence CH_3S on Cu(111) data

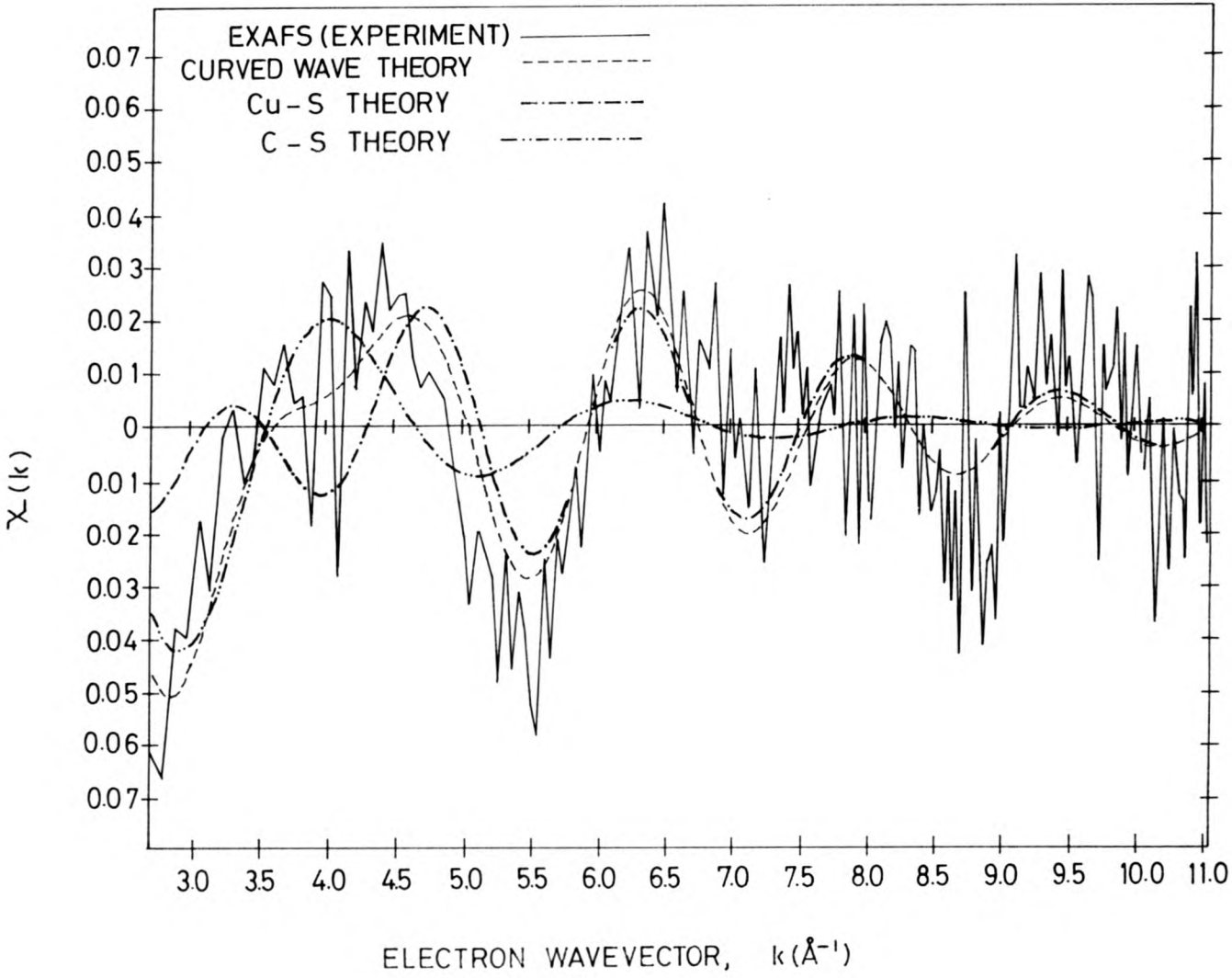

gave a β value 60 $\pm$ 5^0. This angle is greater than the 'magic' angle of 54.7^0 - at this bond angle the scattering shell shows no dependence of it's amplitude on X ray polarization. For bond angles below 54.7^0 the scattering shell shows stronger EXAFS for X ray beams angles closer to grazing incidence and for bond angles greater (ie values of β) than 54.7^0 the scattering shell would show stronger EXAFS modulations for X ray beams closer to normal incidence on the sample surface. For most systems involving simple overlayer chemisorption into well defined high symmetry sites of the surface with no distortion of the substrate, the first nearest neighbour bond angle (β) is usually considerably less than 54.7^0 and hence stronger EXAFS is usually seen at more grazing incidence. In fact all values of β which would be found for simple overlayer chemisorption of the S atom in the mercaptide group into high symmetry sites at an undistorted Cu(111) surface fall between 0^0 (for the atop site) and 38^0 (for the three fold hollow) and hence the bond angle found here by SEXAFS is inconsistent with simple overlayer chemisorption. (These values of β have been calculated assuming the measured Cu-S bond length from an undistorted lattice.)

Taking the bondlength of 2.38 $\pm$ 0.03Å and the bondangle of 60^0 together gives a vertical distance of 1.2 $\pm$ 0.1Å for the sulphur overlayer formed by the adsorption of the mercaptide group. Referring to the polarization dependence of the S-S scattering (which gave a β value of 80 $\pm$ 10^0) it is believed that this S overlayer is not appreciably buckled. This observation is borne out by the NISXW data shown in figure five.

Figure five shows normal incidence standing X ray wave data (NISXW) for the CH_3S on Cu(111) system with theoretical simulations superimposed.

Figure 4.6 NISXW data for the CH_3S on Cu(111) system

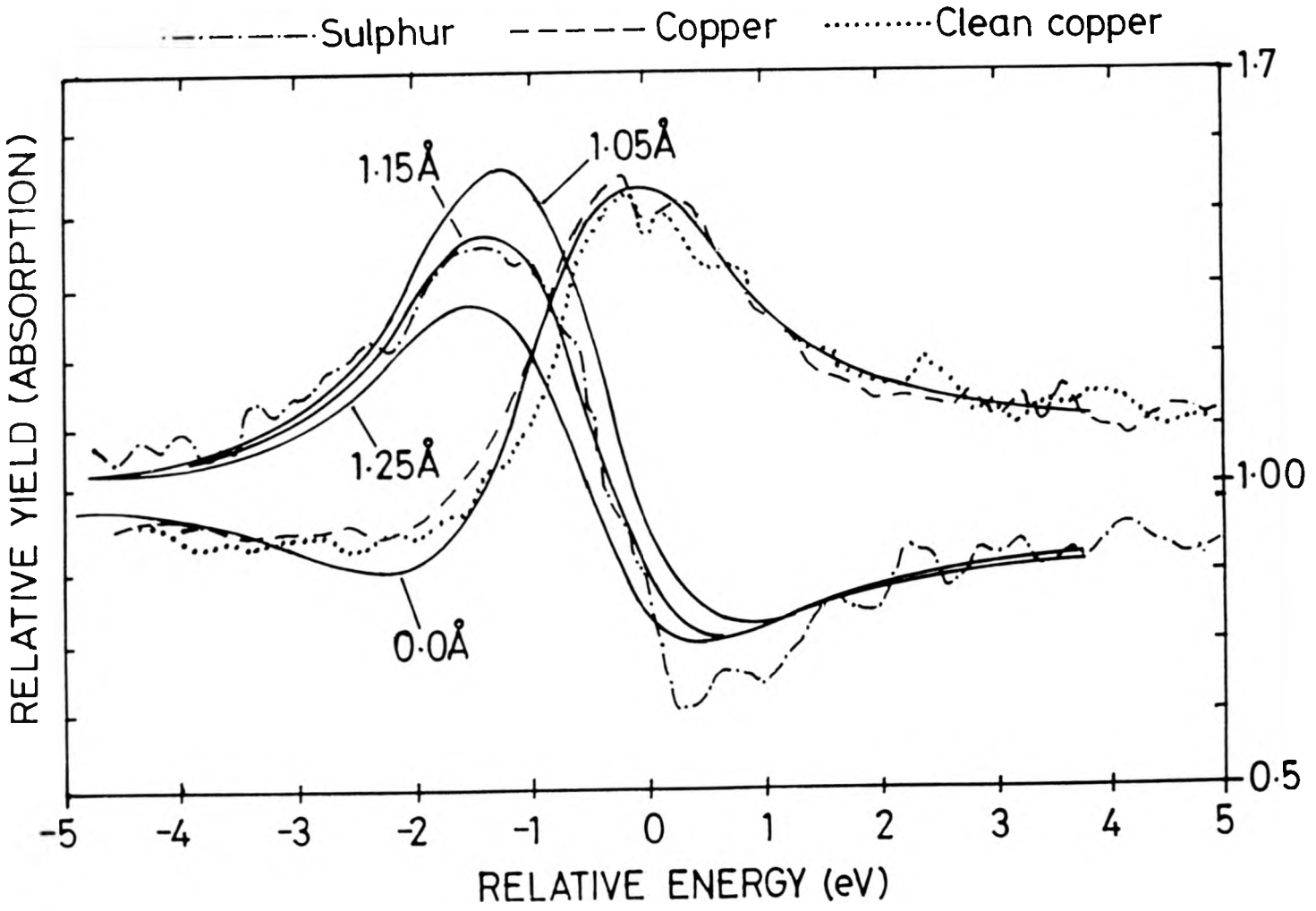

Analysis of the amplitude, shape, and energy position of this modulation is consistent with an adsorbate substrate layer spacing of 1.15 $\pm$ 0.05Å which corroborates the layer spacing suggested by SEXAFS. The value of the coherent fraction for this system is 0.85 (ie 85% of the sulphur atoms are at this location (1.15 $\pm$ 0.05Å) - a result which is consistent with the sulphur- sulphur bond angle determined by SEXAFS.

Taking these results together effectively rules out the possibility of simple chemisorption as the layer spacings corresponding to all the simple overlayer chemisorption bond angles would all fall between 1.88Å and 2.38Å and so all these sites are clearly incompatible with the data from either experimental technique.

As the possibility of simple overlayer chemisorption is ruled out it is necessary to consider a model for the surface structure which involves a substantial structural rearrangement of the substrate by the mercaptide group. Possibilities which were investigated involved the partial penetration of the Cu surface by the adsorbed sulphur atom. In this case it is proposed that the sulphur atom forces it's way down into surface opening up a three fold hollow as it does so. The exact nature of this opening up of a three fold hollow is elucidated by taking the Cu-S bondlength of 2.38 $\pm$ 0.03Å and layer spacing of 1.15 $\pm$ 0.05Å and assuming that the S atom is sited directly above the centre of a three fold hollow. This implies that the projection of this bond parallel to the surface would be 2.05Å as opposed to 1.47Å which would be the case for simple overlayer chemisorption - ie no distortion of the substrate. Hence a movement of the surface copper atoms of 0.6Å parallel to the surface would occur, this movement would, of course, redefine the Cu-Cu spacing on the top

layer of the copper surface which would change from 2.55Å to become 3.58Å. It is of interest to note that this distance is close to the S-S distance which was implied by the SEXAFS data (3.40 ±0.15Å). The opening up of the three fold hollow is, of course, a rather dramatic alteration of the surface structure but there is no evidence for long range order in this system (LEED experiments having led to the breaking of the C-S bond to give the $(\sqrt{7} X \sqrt{7})$ R 19.1°-S pattern which provide no information on the mercaptide group's periodicity) and hence the distortion may be purely local. This idea of a local distortion need not conflict with the fact that a resolvable S-S distance emerges in the SEXAFS analysis as it is possible that this distance is defined only over small regions of the surface.

The structural effects of adsorption into the hexagonal close packed as well as the face centred cubic three fold hollow site are shown schematically in figs 6a and 6b. The f.c.c. site is directly above a copper atom in the third metal layer below the surface and the h.c.p. site is above a copper atom in the second layer below the surface. For the case of adsorption into the f.c.c hollow the Cu atoms in the top distorted atomic layer are forced toward atop sites with respect to the second atomic layer of copper. If we assume a hard spheres in contact model of the surface structure then this would mean that atoms in the top layer of the substrate would ride up over the atoms in the second layer such that there would be an expansion of the distance between the first and second layers of copper by 0.30Å. For the case of adsorption into the h.c.p. three fold hollow, however, the atoms in the top copper layer would be forced into bridge sites with respect to the second copper layer below the surface and in this case the outer layer expansion would be 0.12Å. A reason for favouring the h.c.p.

Figure 4.7 Diagram illustrating possible adsorbate-substrate registries for mercaptide on copper and the difference between the layer spacings measured by NISXW and SEXAFS

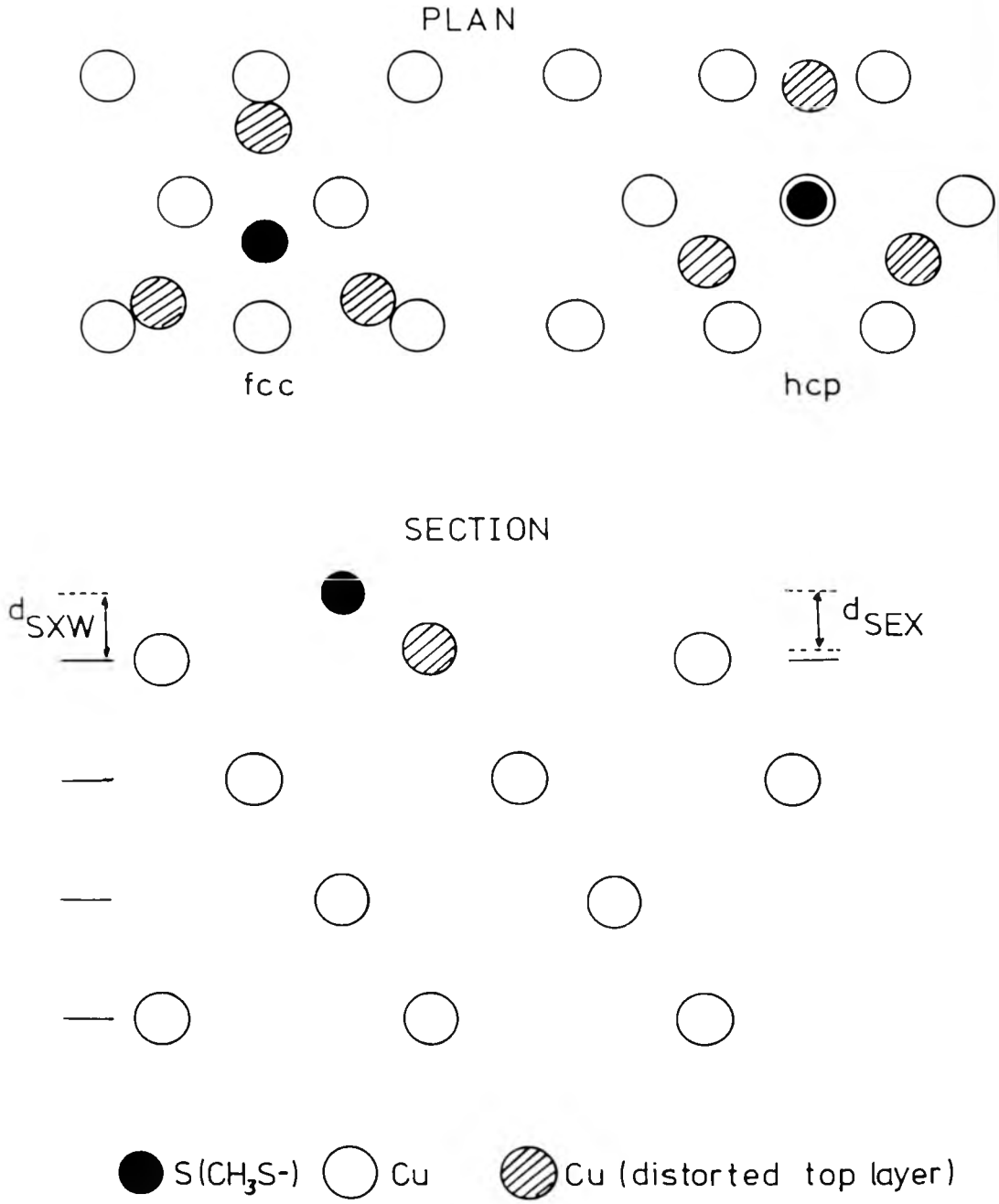

hollow site is now apparent. This can be seen by considering the fact that there is no significant difference between the layer spacings given by SEXAFS and NISXW. The SEXAFS value of 1.2Å is the true local value of the layer spacing as the SEXAFS technique is essentially a local probe of structural environment, whereas the NISXW field is built up over many lattice planes and it's periodicity is therefore defined by the bulk copper copper layer spacing and thus the Cu-S layer spacing is measured as if no outward expansion of the top layer of the substrate had occurred (see fig. 7). Thus the standing X ray wave technique will exceed the layer spacing by an amount corresponding to any outward relaxation of the top atomic layer. Therefore the close agreement between the NISXW layer spacing of 1.15 $\pm$ 0.05Å and the SEXAFS layer spacing of 1.2 $\pm$ 0.1Å indicate the relaxation of the outer layer is rather slight and therefore the data are best accommodated by assuming the h.c.p hollow as the favourite site. Adsorption into, and the subsequent distortion of, other high symmetry sites of the Cu(111) surface were also considered but these would lead to greater outward relaxations of the top layer which would not be consistent with our data. It is important to note that the 3.58Å overlayer if it covered the whole surface would be incommensurate and so the arguments above about particular adsorption sites would start to break down. X ray stimulated Auger spectra indicate a coverage of about one third of a monolayer and so some pseudo ordering is inevitable but there may be extensive defects in the overlayer periodicity which would leave some plausibility in the arguments above.

This result raises some interesting questions such as: what is the driving force for such a large disturbance of the substrate and in what way is the

surface morphology of the crystal altered, if it all, in order to accommodate the sizeable in surface movements of the substrate atoms.

In answering the first question it is obvious that the driving force must be brought about about by the process of the chemisorption as the clean Cu(111) surface of copper which has been cleaned and prepared in U.H.V. is stable. Certainly it is the case that no lateral movements of the copper atoms in the surface have been observed. One LEED study, however, has found evidence for a contraction of the distance between the first and second atomic layers of copper of 0.08Å $\pm$ 0.02A, in a direction perpendicular to the surface. However, a later study on the same surface involving a larger database and updated analysis procedures has found no such contraction and puts a value of 0.006Å $\pm$ 0.02Å on the relaxation which could , of course, be indicative of no deviation from the bulk interlayer spacing at the Cu(111) surface.[10,11]

In view of this stability of the Cu(111) surface it is necessary to attribute the driving force for reconstruction to either; a process of local chemical bond formation at the surface or to changes in the local surface electronic structure which are brought about by chemisorption.

Exploring the latter mechanism further, some literature has been published on some rather large scale reconstructions which are induced either by surface formation or by the process of chemisorption, and, it has been proposed [12,13] that these reconstructions may be accounted for by long range electronic effects [14].

Specific examples of these reconstructions are the Au, Pt, and Ir(110) surfaces which when cleaned and annealed in ultra high vacuum spontaneously reconstruct to form (1 X 2) LEED patterns and also the Ag(110) and Cu(110)

surfaces which although they do not spontaneously reconstruct are known to do so after the adsorption of small amounts of alkali metals (less than 0.25ML) such as Li,K, and Cs. It is also reported that the (1 X 2) reconstruction of Ag(110)Cs may be lifted upon the adsorption of oxygen and that subsequent dosing with yet more Cs will restore the (1 X 2) LEED pattern. It is also found that this process can be repeated in a cyclic fashion. Another observation indicating a similar effect is that the adsorption of electronegative adsorbates such as CO, NO, and Cl can lift the spontaneous reconstruction of the clean Pt(110) surface [15].

Hence it appears that processes of charge transfer to and from the surface can induce or destroy surface reconstructions. The electronic theory which attempts to account for this range of effects [14] hinges around the idea that the formation of a surface defines a radically different electronic environment for the new surface atoms and that this may either define new equilibrium positions for the surface atoms or leave behind a very delicate balance of electronic forces at the surface which may be readily and pathologically altered by the presence thereon of foreign atoms which arrive during the process of chemisorption. This model points out that the nature of the reconstructions produced by the redefinition of electronic environment are very strongly dependent on local geometry and this may explain the similar behaviour exhibited by a range of (110) surfaces.

A surface structural model, found by SEXAFS, which has been offered for the Ag(110) (1 X 2)-Cs surface suggests that every second row in the (001) direction is missing. A similar LEED pattern has been found for the adsorption of oxygen on Cu(110) and SEXAFS and ion scattering studies of this (2

X 1) surface have also found that a missing row reconstruction accounts for the Cu(110) - (2 X 1) - O data [16,17]. These results, however, do not fit in with the idea that the Cu(110) (2 X 1) O reconstruction is induced by the same mechanism as the alkali metal induced reconstructions of Ag(110) and Cu(110). Firstly note that the direction of the unit cell doubling is perpendicular to that which is observed for the Ag(110)(1 X 2)Cs surface and also note that previously the adsorption of oxygen on Ag(110)Cs was found to lift the (1 X 2) reconstruction. Electronegative adsorbates such as CO, NO, and Cl have also been found to lift the spontaneous (1 X 2) reconstruction of the clean Pt(110) surface. So it appears that the Cu(110) surface when dosed with oxygen is not sensitive to electron donors and acceptors in the same way as the alkali metal reconstructed surfaces or the spontaneous (1 X 2) clean surfaces of Au(110), Pt(110), and Ir(110). Hence it is necessary to attribute the driving force for the Cu(110)(2 X 1)-O reconstruction to some other mechanism - possibly a process of local chemical bond formation involving the incorporation of oxygen into the surface to form an oxide layer at the surface . Structural models of this surface suggest that a missing row is involved here but, of course, in a direction perpendicular to the ones seen for Ag(110)Cs and Cu(110)Cs [16,17]. It is interesting to note, however, that a more recent ion scattering ion scattering study does not support the missing row model of the Cu(110)(2 X 1)-O surface (M J Ashwin unpublished) and that another IS study for the adsorption of N on the Cu(110) surface gives a (2 X 3) LEED pattern which is attributed to the reconstructive local chemical bond formation of a surface nitride [18]. Thus the suggestion is that electronegative adsorption on clean Cu(110) surfaces leads to reconstructive

local chemical bond formation rather than an electronic destabilisation of the surface structure.

For the case of alkali metal adsorption on Ag(110) and Cu(110), however, it is very probable that reconstruction is due to long range electronic effects as these reconstructions are seen for Li, K and Cs adsorption and, as these atoms have a large range of ionic sizes (0.6 to 1.9Å) it is expected that local chemical bond formation would lead to a similar diversity of surface structures which is, of course, not the case.

Moving to (111) surfaces it is known that while Au(110) is unstable, the Au(111) surface is even more unstable to lateral distortions of it's surface, this surface displays (22 X 1) and (23 X 1) LEED patterns. This is surprising in view of the fact that the (111) surface is more close packed than the (110) and hence may be expected to be more stable to lateral distortions of the unit cell [19].

The Cu(111) surface, however, does appear to be more stable than the Cu(110), nevertheless, significant distortions of this surface upon adsorption are not unheard of and reported cases of reconstruction are found for the adsorption of tellerium, oxygen and sulphur. In all these cases local chemical bond formation appears to be the most probable cause of substrate distortion.

For the case of tellerium on copper, a SEXAFS study, [20] finds that tellerium penetrates the top substrate layer by substitution with copper atoms in the surface - in this case it is believed that no lateral distortion of the remaining unsubstituted copper atoms in the surface - which suggests that a highly localised process is producing the substrate reconstruction in this case. The evidence for this incorporation of Te into the surface is rather strong and is

based on studies of the polarization dependence of the scattering between tellerium and the first nearest neighbour copper shell. In common with the study reported here it is found that the SEXAFS is stronger at normal incidence than it is at grazing incidence thus implying that the Te-Cu first nearest neighbour bond angle is larger than 54.7^0 as is the case for the Cu-S first nearest bond angle reported here for the mercaptide species on Cu(111).

This bonding geometry cannot be accommodated by the simple unreconstructed surface and so the substitutional model for Te on Cu(111) has been proposed. The inadequacies of this model are that it does not correctly predict the observed LEED patterns for the structure. The model is based on the substitutional displacement of one third of a monolayer of the surface copper atoms and this would predict a simple $(\sqrt{3}X\sqrt{3})$R 30^0 LEED pattern rather than the observed $(2\sqrt{3}X\sqrt{3})$R 30^0 pattern. This paper suggest that this discrepancy may be accounted for by (i) Te dimerization, or (ii) surface or subsurface buckling or finally, (iii) that it may be due to decoration of the surface by those copper atoms which were previously displaced by Te. The paper also reports that the data cannot distinguish between these possibilities, which raises the question of exactly how these large scale reconstructions are accommodated by surfaces.

Returning to the Au(111) surface, an electron microscopy study of this surface has found that in plane expansions of this surface are accommodated by the formation of hill and valley surface morphologies which would provide space for lateral expansions. Hill heights of up to five or six atomic layers were found to develop during the etching processes (by water) of the Au(111) surface under study [21]. This paper also suggests that expansive stresses in

the plane of the surface when coupled with the constraint for surface atoms to sit in register with the layers below can lead to displacements of the top layer in a direction perpendicular to the surface. Displacements of this type have in fact been found for a large range of surfaces by techniques like LEED and ion scattering. Particular cases are the Cu(110) and Ni(110) surfaces. For Cu(110) two ion scattering studies indicate top layer contractions of the clean surface of 5.3 $\pm$ 1.6 % and 10% of the bulk interlayer spacing respectively [22,23] For the case of Ni(110) a 4% contraction of the bulk interlayer spacing is found and this gives way to a 1% expansion after the adsorption of oxygen [24,25].

A more radical disturbance has been found for the Cu(111)-O surface [26]. Ion scattering results and work function measurements for this surface suggest the displacement of surface copper atoms by 0.3Å and that oxygen is incorporated into the surface layer. The evidence for this incorporation arises from the fact that the work function change of the surface after adsorption is not significant hence suggesting the absence of a measurable surface dipole which would give rise to a work function change. A SEXAFS study of the adsorption of atomic S on Cu(111) also finds evidence for adsorbate incorporation into the surface (see chapter 5). This evidence, like that for the Te and mercaptide on the same Cu(111) surface, is also derived from the polarization dependence of the SEXAFS amplitudes.

Thus it can be seen that there is a sizeable database for the adsorption structures of electronegative adsorbates on transition metal surfaces and Cu(111) in particular, for which results are available for O, Te and S adsorption. These results which have been acquired by more than one technique have all suggested reconstruction of the substrate which involves a mixed layer of

adsorbate and substrate atoms. Thus it is presumed that these adsorbates, all in the same group of the periodic table give rise to local chemical bond formation at the surface of Cu(111).

The CH_3S, mercaptide species, has been found to behave in a similar way on this surface, however, it is necessary to point out a few essential differences . Firstly all the above cases of reconstruction are found for the case of atomic adsorption and so far few or maybe zero cases of molecular adsorbate induced reconstruction have been reported. This may be due to the fact that surface to molecule bonding is often weak compared to atom to surface bonding, this is apparently not the case for for mercaptide as heating or electron bombardment leads to the breaking of the C-S bond rather than the Cu-S bond. Nevertheless, despite the weakness of the C-S bonding the methyl group does play an important role in the determination of the adsorption structure of CH_3S on Cu(111) as the adsorption structure of atomic S on Cu(111) is quite different to that found for mercaptide. This is the second important difference between mercaptide adsorption and that found for other electronegative adsorbates.

4.3 Conclusion

It has been found that the dosing of the Cu(111) surface with CH_3S leads to the adsorption of the mercaptide group's S atom into the hexagonal close packed three fold hollow. This gives rise to a subsequent distortion of the hollow which involves 0.6Å movements of the surface copper atoms. This movement is principally in the plane of the surface which represents a large, though not unprecedented, distortion of the Cu(111) surface. The manner in which the surface accommodates this distortion is beyond the scope of this study. It is

possible, however, that the distortion is purely local but, of course, this cannot be proved by this data and so further studies by electron or scanning tunneling microscopy would possibly be better suited to the investigation of this issue.

4.4 References

1. M C Tsai, U Seip, I C Bassignana, M Küppers and G Ertl, Surf. Sci. 155 (1985) p387-399
2. P H Citrin, D R Hamann, L F Mattheis, and J E Rowe, Phys. Rev. Letts. 49 (1982) 1712
3. D A Outka, R J Madix, and J Stöhr Surf. Sci. 164 (1985) p235-239
4. M D Crapper and D P Woodruff, Phys. Rev. Letts. 54 2250-2252 (1985) and Surf. Sci. 171 1-12 (1986)
5. S J Gurman, N Binsted and I Ross J. Phys. C. 17 (1984) p143
6. M M Kazinets, Soviet Crystallography 14, (1970) p599
7. D R Warburton, D Norman, C H Richardson, F M Quinn, and R McGrath, Vacuum 38 (1988) 241
8. Th Lindner, J Somers, A M Bradshaw, A L D Kilcoyne and D P Woodruff Surf. Sci. 203 (1988) 333
9. D L Seymour, S Bao, C F McConville, M D Crapper, D P Woodruff, and R G Jones Surf. Sci. 189/190 (1987) p529
10. P R Watson, F R Shephard, D C Frost, and K A R Mitchell, Surf. Sci. 72 (1978) p562
11. S P Tear, K Röll, and M Prutton, J. Phys. C. 3297 (1981)
12. B E Hayden, K C Prince, P J Davie, G Paolucci and A M Bradshaw, Solid State Communications Vol 48 No4 p325-327 (1983)
13. J W M Frenken, R L Krans, E Holub Krappe, and K Horn, Phys. Rev. Letts. Vol 59 No 20 (1987)

14. V Heine and L D Marks, Surf. Sci. 165 (1986) p65-82

15. H P Bonzel and S Ferrer, Surf. Sci. 118 L263 (1982)

16. J Yarmoff, D M Cyr, J H Huang, Sehun Kim, and R S Williams Phys. Rev. B Vol 133 No 6

17. M Bader, A Puschmann, C Ocal and J Haase Phys. Rev. Letts. Vol 57 No 26 p3273

18. D Heskett, A Baddorf and E W Plummer, Surf. Sci. 195 (1988) p94-102

19. U Harten, A M Lahee, J P Toennies and C H Wöll Phys. Rev. Letts. 54 (1985) p2619

20. F Comin, P H Citrin, P Eisenberger and J E Rowe Phys. Rev. B Vol 26 No 12 (1982) p7060

21. L D Marks and D J Smith, Surf. Sci. 143 (1984) p495-508

22. I Stensgaard, R Feidenhans'l and J E Sorenson Surf. Sci. 128 (1983) p281-293

23. J Yarmoff and R S Williams, J. Vac. Sci. and Technol. A4(3) May/Jun 1986 p1274

24. J F Van der Veen, R G Smeenk, R M Tromp and F W Saris, Surf. Sci. 79 (1979) 212-218

25. J F Van der Veen, R G Smeenk, R M Tromp and F W Saris, Surf. Sci. 79 (1979) 219-230

26. H Niehus Surf. Sci. 130 (1983) p41-49

Chapter 5

S on Cu(111)

5.1 Introduction

When a foreign atom chemisorbs onto the surface of a well ordered, stable, single crystal, one of two types of behaviour may be observed. Either the atom may adsorb (typically into high symmetry sites) at the surface and cause little or no structural rearrangement of the substrate (other than slight displacements of the top atomic layers in a direction perpendicular to the surface see for example [1,2,3]) or the surface may reconstruct as the atoms therein adjust to new equilibrium positions which are defined by the change in environment engendered by chemisorption. Several influences have been suggested as the driving force for these reconstructions, such as,long range electronic forces or local chemical bond formation for instance.

In the last chapter cases of reconstruction which were believed to be induced by local chemical bond formation were discussed, specifically, these involved the chemisorption of chalcogens and a chalcogen containing molecule on Cu(111) (O,Te, and,CH_3S).

Similar behaviour has been reported for the adsorption of halogens on Ni(100) and Cu(100) [4,5] more work on these substrates involving the ad-

sorption of C, N, and O has indicated that due to strong bonding between these adsorbates and substrates perturbations to the surface structure and properties result, comprising the formation of surface nitrides,carbides and oxygen induced surface phonon softening.

The evidence for this behaviour is based on LEED ,SEXAFS and surface phonon dispersion measurements. Cases of particular interest are the Ni(100)(2 x 2)N and the Ni(100)(2 x 2)C systems for which LEED and SEXAFS results indicate definite reconstructions. [6,7]

A theoretical analysis of the (2 x 2) carbon and oxygen overlayers on Ni(100) has presented the results of lattice dynamical and total energy calculations. These results led the authors to suggest that the carbon induced reconstruction and the oxygen induced phonon softening were due to adsorbate induced charge redistribution at the surface and that this redistribution arises due to strong adatom to nickel bonding which removes charge from the weaker inter metal bonds in the substrate. This leads to incomplete screening of the nickel nuclei thus giving rise to unbalanced forces in the substrate surface which in turn leads to the surface reconstruction for the carbon overlayer and phonon softening for the Oxygen overlayer. The carbon induced reconstruction involves the rotation of the surface nickel atoms about the C atoms to which they are bonded, this form of substrate distortion is also observed experimentally for the Ni(100)(2 x 2)N system.[8,9] The results of surface structural studies for the oxygen overlayers have been conflicting and controversial [10,11,12]

It is difficult to think of how this type of reconstruction could be accommodated in only a local fashion and hence it appears to be long range effect.

All this suggests that for carbon and nitrogen adsorption on Ni(100) the argument as to whether these reconstructions are caused by long or short range electronic effects is likely to be controversial (see later).

Another interesting point concerning these adsorbates is that due to their small sizes compared to the substrate atom sizes [covalent radii are oxygen = 0.66 Å nitrogen = 0.70 Å carbon = 0.77 Å] it would be impossible for them to adsorb into the sites at the surface which an atom of the next layer of the substrate would occupy (If such a layer were to be grown epitaxially at the surface) and still obtain significant overlap of the bonding orbitals. Hence they can get very close to the surface and possibly even bury themselves in the hollows of the surfaces on which they adsorb thus making them likely candidates to induce substrate distortions. In the cases of nitrogen and carbon adsorption on Ni(100) LEED and SEXAFS studies have suggested adsorbate substrate layer spacings of 0.1Å for the C overlayer and the same value for the nitrogen overlayer.[7,10]. For the case of oxygen on Cu(100) the results of recent work are as yet unpublished but they indicate definite substrate reconstruction involving surface oxide formation. This would certainly be consistent with the strong indications of adsorbate induced reconstructions for O on Cu(110) and Cu(111).[1,13]

The c(2 x 2) overlayer of Cl on Ag(100) was also believed to be coplanar with the top layer of the Ag(100) substrate. This is the structure which would be expected for an epitaxial layer of silver chloride. However after closer assessment of the theoretical calculations, which originally suggested the mixed layer model, it was found that a simple overlayer model gave a better interpretation of apparently conflicting angle resolved photoemission and LEED

results. The reason for the apparent contradiction between these results was found to be due to the usage of an unrealistic bulk value of the surface AgCl bondlength as an input to the electronic structure calculations [5] which were originally compared to the ARPS data. The usage of a more realistic, SEXAFS determined, bondlength of 2.53 Å rather than 2.77 Å yielded much better agreement between the ARPS data and theory provided that a simple overlayer model was assumed for the surface structure. Thus the contradiction between LEED (which had always suggested a simple overlayer) and ARPS was resolved and the mixed layer model was discarded in favour of the simple overlayer model. [14]

The adsorption of the larger halogen iodine on Ni(100), however, has been confirmed as forming a bulk like surface iodide, via a strong chemical interaction between the adsorbate and substrate. The evidence for this comes from a range of experimental results such as; LEED and Auger electron spectroscopy (AES) and valence band photoemission which provides the most convincing support. Due to the fact that the NiI_2 surface iodide is a layer compound it's bandstructure is little effected by any periodicity in the direction perpendicular to the layers and hence this surface iodide even though it was found to consist of only one layer (by AES), still showed the bandstructure of bulk NiI_2. This was evidenced by a comparison with previously calculated bandstructures of $NiCl_2$ and $NiBr_2$ [15].

The structure of this surface iodide was obtained by SEXAFS from the iodine L_3 edge, it was proposed to involve a hexagonal layer of iodine sandwiched between two nickel layers, with a layer of nickel uppermost at the surface [4]. A structure of this type means that investigation of the SEXAFS polarization

dependences in order to distinguish between simple and strongly interactive chemisorption may be less effective than it is for other cases, such as Te and CH_3S on Cu(111) for instance. Couple this with the fact that the EXAFS polarization dependence is weaker for L_2 or L_3 edges than it is for K edges and it is easy to see how the distinction between simple chemisorption and reconstruction may be difficult to observe in this system.

Results of exhaustive, combined SEXAFS and NISXW studies have indicated that the kind of geometry found for the surface iodide may have features in common with a surface sulphide formed by the interaction of H_2S with the Cu(111) surface. (ie complete penetration of the surface by S) but in this case the SEXAFS data were collected from a K edge rather than an L edge and so here the SEXAFS polarization dependence showed clear evidence for the formation of a surface sulphide. Also the NISXW studies indicated occupation of at least two distinct adsorbate-substrate layer spacings which so far can only be rationalized in terms of the formation of a surface sulphide phase which must involve complete penetration of the surface by sulphur atoms.

The suggestion that the adsorption of S can lead to surface sulphide formation on Cu(111) has long been recognised [16]. Another observation supportive of this idea is that the two dimensional sulphides have been found to be thermodynamically more stable than their bulk analogues, [17] and hence it is with some confidence that these studies conclude that the interaction of atomic sulphur with Cu(111) does not lead to simple chemisorption but forms a sulphide involving a mixed layer of Cu and S.

A complete and unambiguous surface structure determination, however, has not been possible, even after two experimental runs (one NISXW alone

and one SEXAFS/NISXW together). The reasons for this are that LEED and NISXW data both strongly suggest the occupation, by sulphur, of at least two different sites which are symmetrically non equivalent. SEXAFS is expected to average out the information for these sites and hence limit the incisiveness of the structure determination . Another complication was that the relative occupancy of the NISXW layer spacings was seen to vary as well as the data quality (caused by monochromator broadening which led to larger error bars for the results of the later run.) Despite these variations the NISXW gave essentially the same values for the layer spacings for both runs and a mutually supportive interpretation of the results of both techniques has been found.

5.2 Results

SEXAFS data for Cu(111)($\sqrt{7}$ x $\sqrt{7}$)R19.1°-S has been collected at normal incidence and at 36^0. (ie 54^0 away from normal). The raw data sets are shown in figures 1a and 1b. In common with the data taken for the CH_3S on Cu(111) system these spectra were recorded by collecting S KLL Auger electrons (2106eV). The incident photon energy range used to excite these electrons was from 2450eV to 2950eV which covered the S K edge at 2472eV. No single shell analysis was attempted here because despite the frequently observed reliability of Fourier filtering single shell analysis this method of data analysis is not so effective in cases where multiple shells contribute to the data, especially when the signal to noise characteristics of the data are poor. Therefore, the analysis of this data has been carried out using the EXCURVE programs at Daresbury laboratory [Ref 20]. The phase shifts used in this analysis were the same as those used for analysing the CH_3S and were derived from a CuCl model com-

Figure 5.1a Raw normal incidence data for the ($\sqrt{7} \times \sqrt{7}$)R-19.1°-S Cu(111) system

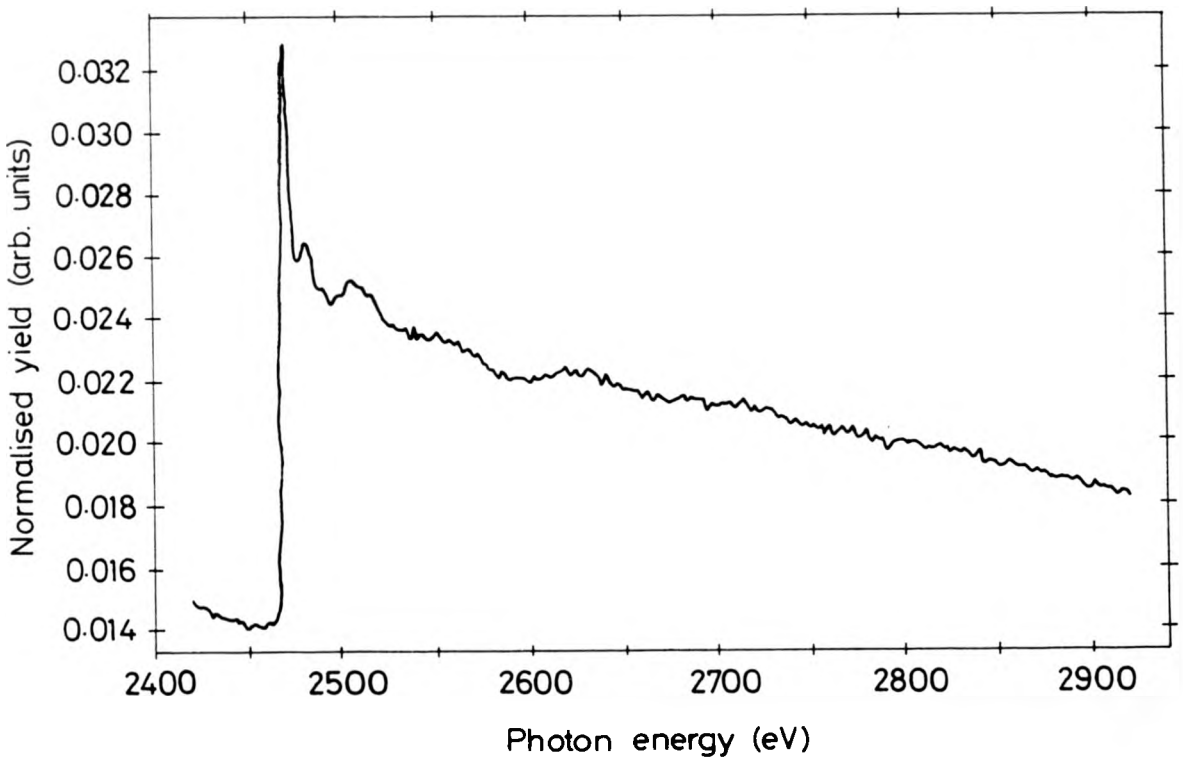

Figure 5.1b Raw off normal incidence data for the ($\sqrt{7} \times \sqrt{7}$) R-19.1°-S Cu(111) system

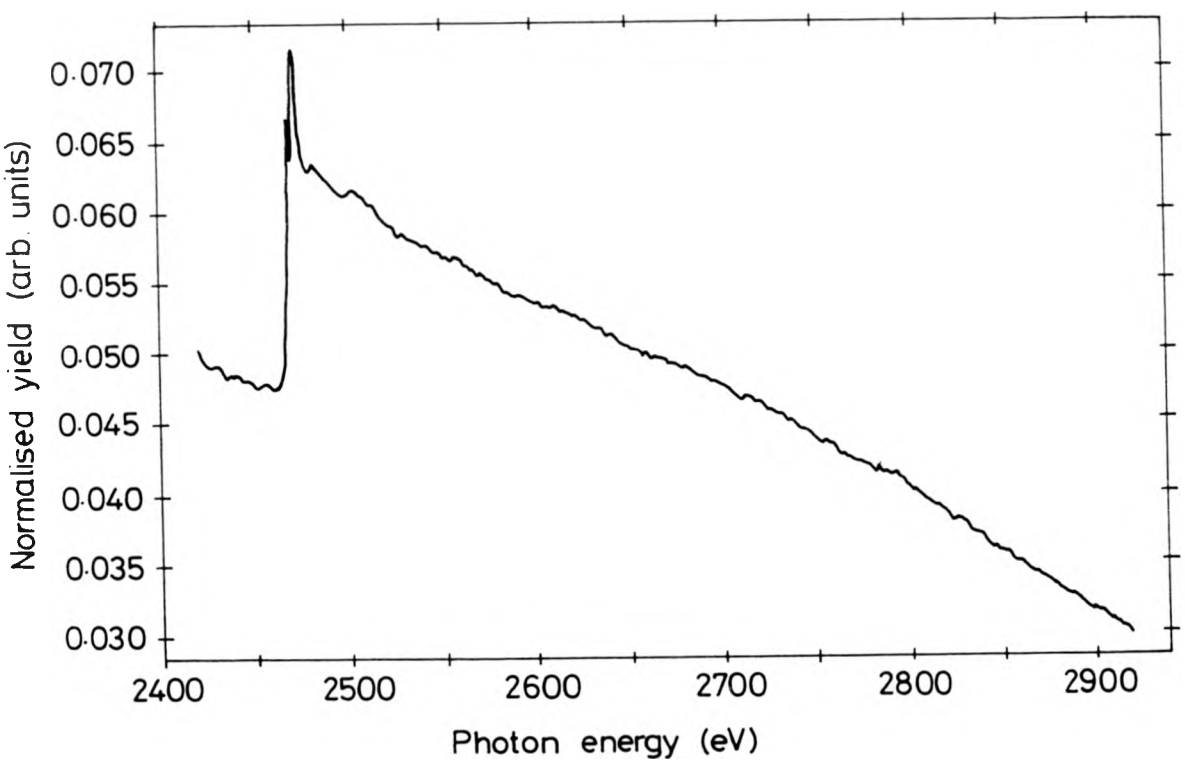

pound. The EXCURVE programs performed both background subtractions and multishell simulations of the data (see figures 1c,d,e,f). The first nearest neighbour bondlengths obtained were 2.30 ± 0.03 Å for normal incidence and 2.34 ± 0.03 Å for 54^0 off normal. A simple analysis of the polarization dependence of this first nearest neighbour shell SEXAFS amplitude indicates that the SEXAFS is stronger for normal incidence than off normal by a factor of 1.7 ± 0.3 . This would give a β value of 67 ± 5^0 (angle between adsorbate-substrate vector and the surface normal).

NISXW data are presented in figures 2a,2b,2c,3a,3b and 3c. These data are the results of the two experimental runs, both of which collected S KLL (2106eV) and Cu LVV (920eV) Auger electrons in the vicinity of the Cu(111) Bragg reflection at 2975eV. The data from both of these runs have been analysed in the way described in Chapter 2. Data from the first experimental run is given in figures 2a and 2b, these represent the best visually assessed fits to the data plus further model curves for the sulphur signal in order to demonstrate the likely size of the error bars. No fit could be achieved with a single layer spacing and therefore as two layer spacings are involved here it has been necessary to show the effect of variation of one layer spacing at a time on the fit (see figs 2a and 2b). The best fit suggests a mixture of two layer spacings at 0.85 ± 0.10Å and 1.77 ± 0.05 Å, with an 80% occupation of the 1.77Å spacing. The 1.77Å spacing has a smaller error bar due to it's being the majority position. Figure 2c plots the same experimental curves but this time the relative occupancies have been varied in order to demonstrate the sensitivity of the fit to this parameter and hence produce error bars for this part of the analysis. The relative occupancy is clearly within 5% of the stated

Figures 5.1c,d,e,f EXCURVE simulations of the ($\sqrt{7} \times \sqrt{7}$)R19.1° -S on Cu(111) system

Figure 5.1c

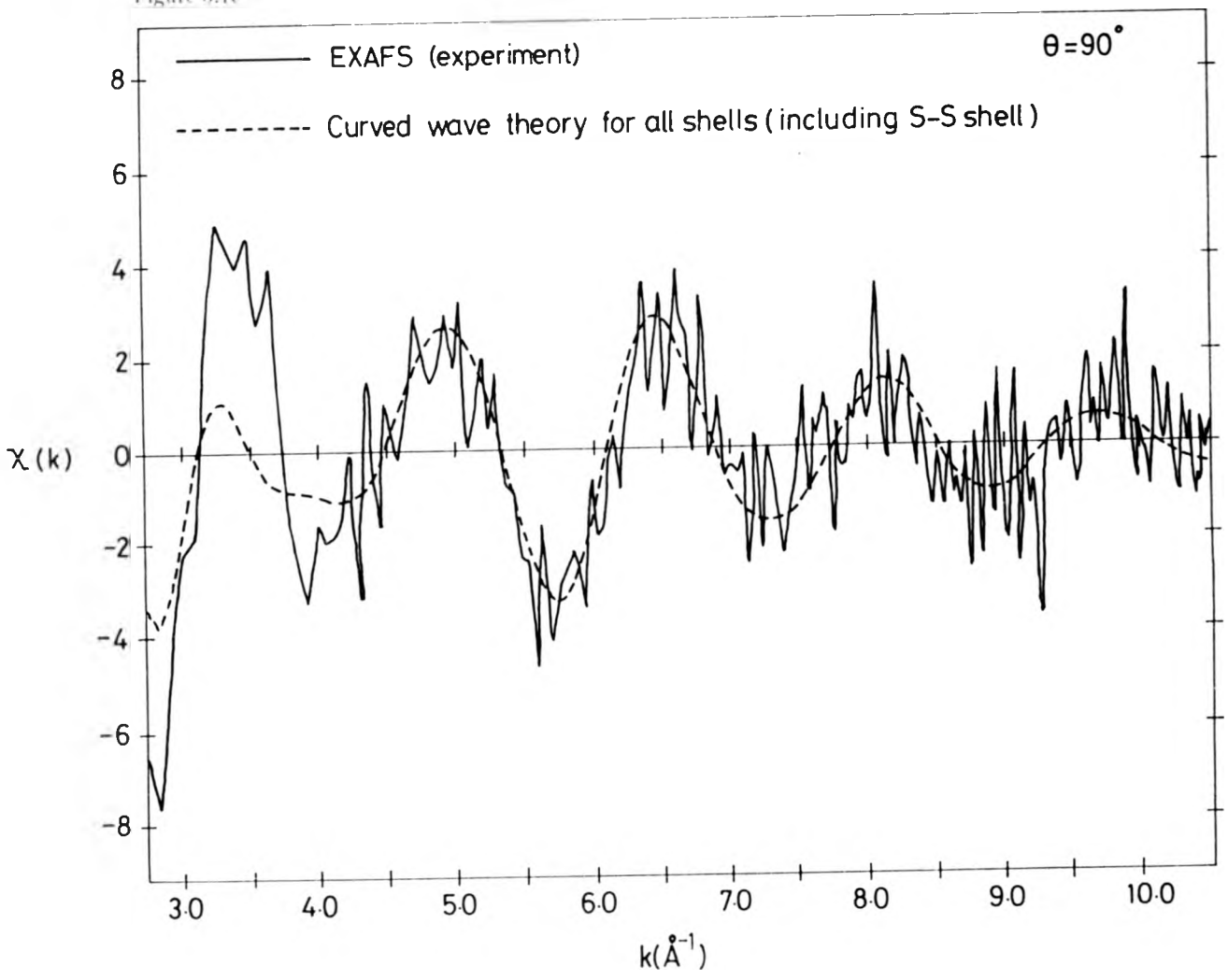

Figure 5.1d

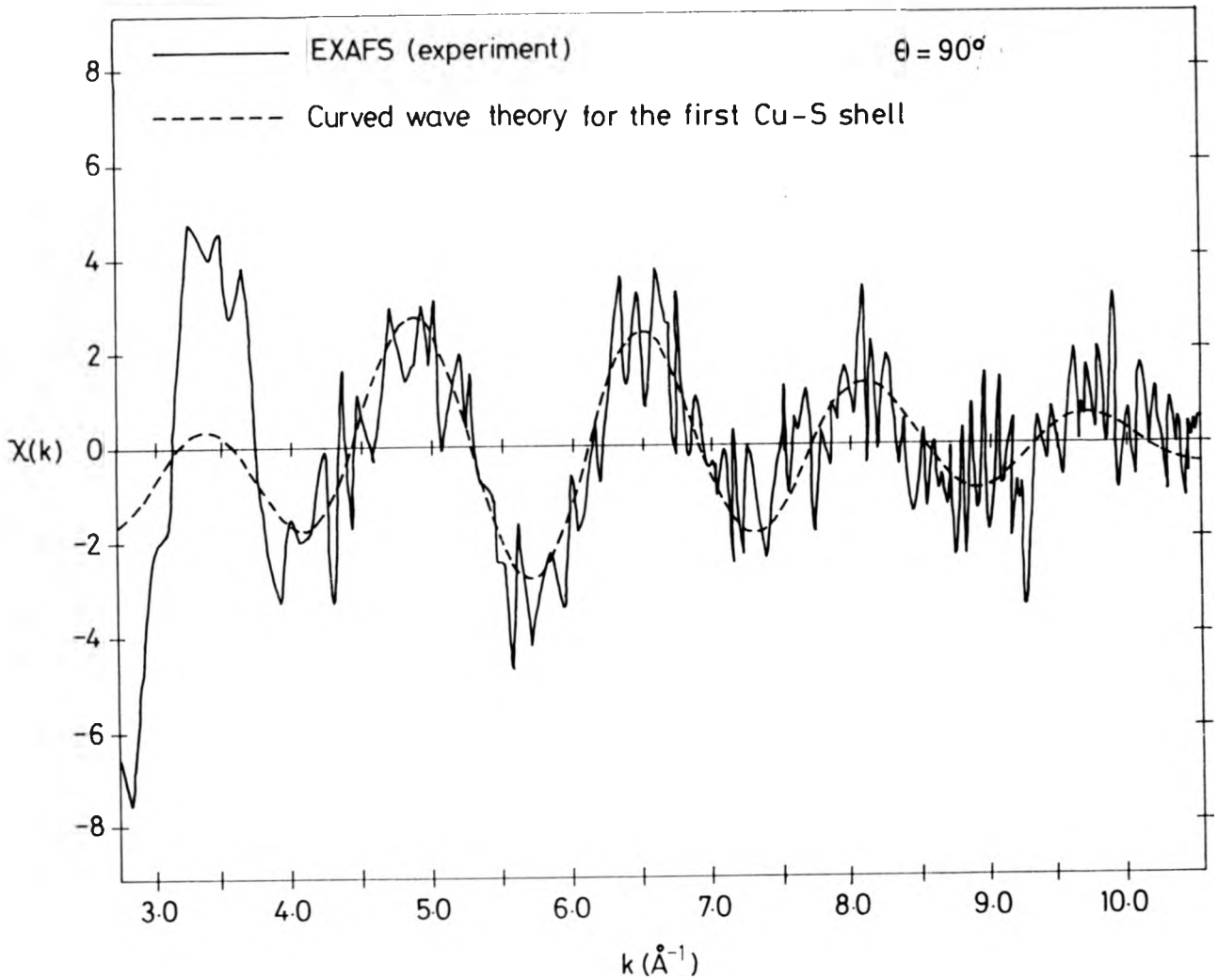
EXAFS (experiment)
θ = 90°
Curved wave theory for the first Cu-S shell
χ(k)
8
6
4
2
0
-2
-4
-6
-8
3·0
4·0
5·0
6·0
7·0
8·0
9·0
10·0
k (Å⁻¹)

Figure 5.1e

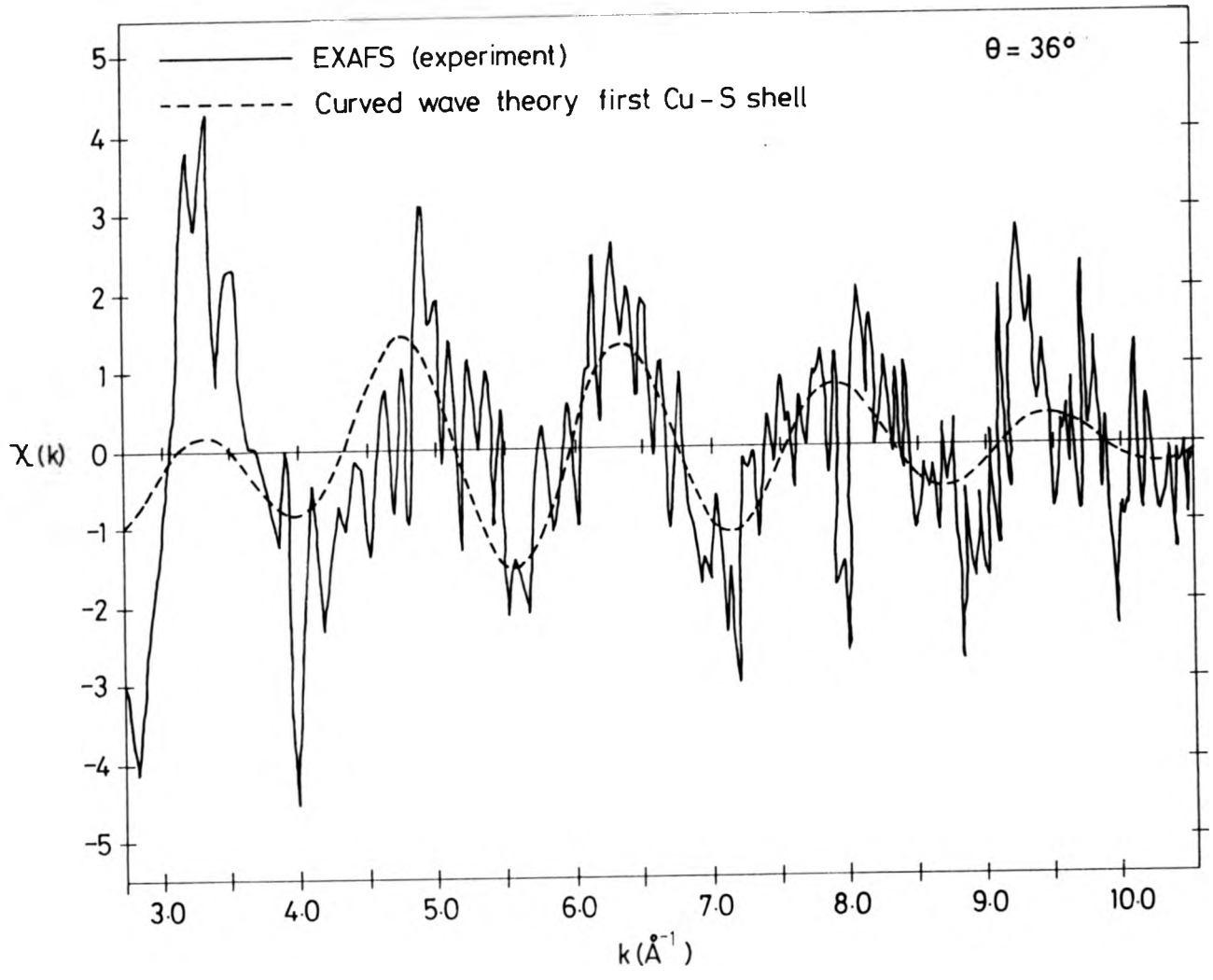
EXAFS (experiment)
Curved wave theory first Cu – S shell
θ = 36°
χ(k)
5
4
3
2
1
0
-1
-2
-3
-4
-5
3·0
4·0
5·0
6·0
7·0
8·0
9·0
10·0
k (Å⁻¹)

Figure 5.11f

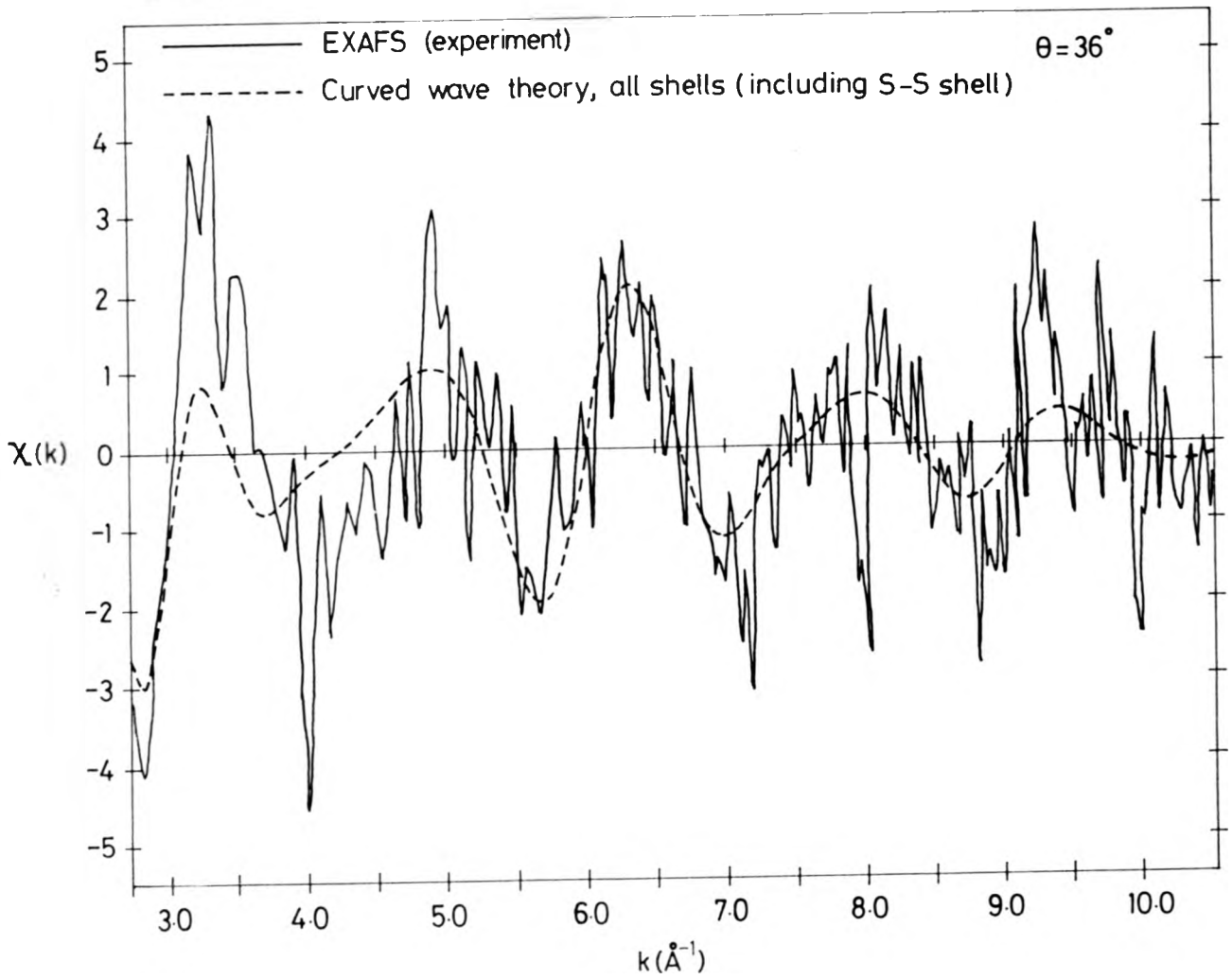
EXAFS (experiment)
Curved wave theory, all shells (including S-S shell)
θ=36°
χ(k)
5
4
3
2
1
0
-1
-2
-3
-4
-5
3·0
4·0
5·0
6·0
7·0
8·0
9·0
10·0
k(Å⁻¹)

Figures 5.2a,b,c Experiment theory comparisons for NISXW data from the $(\sqrt{7} \times \sqrt{7})$R19.1°S on Cu(111) system

Figure 5.2a

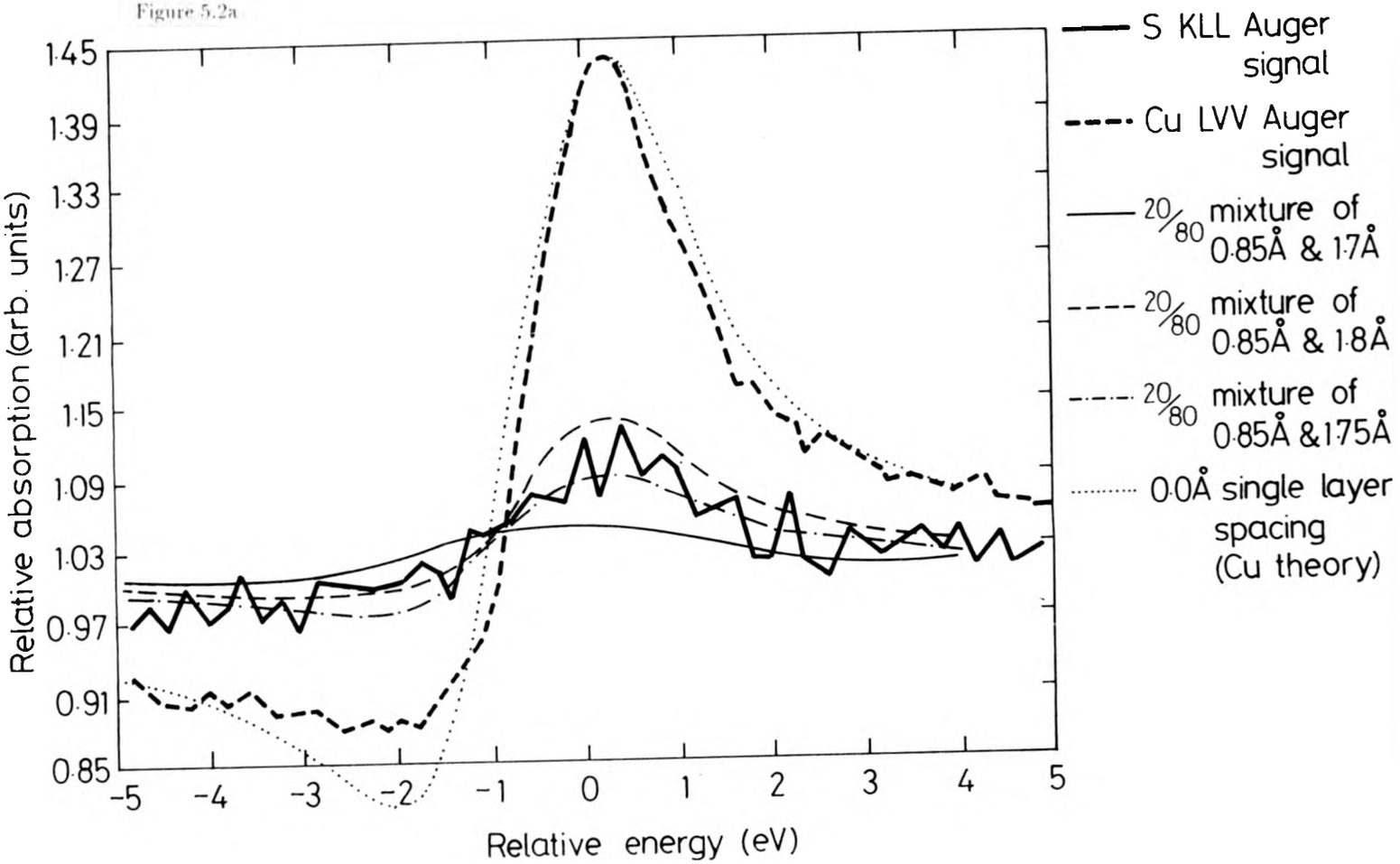

Figure 5.2b

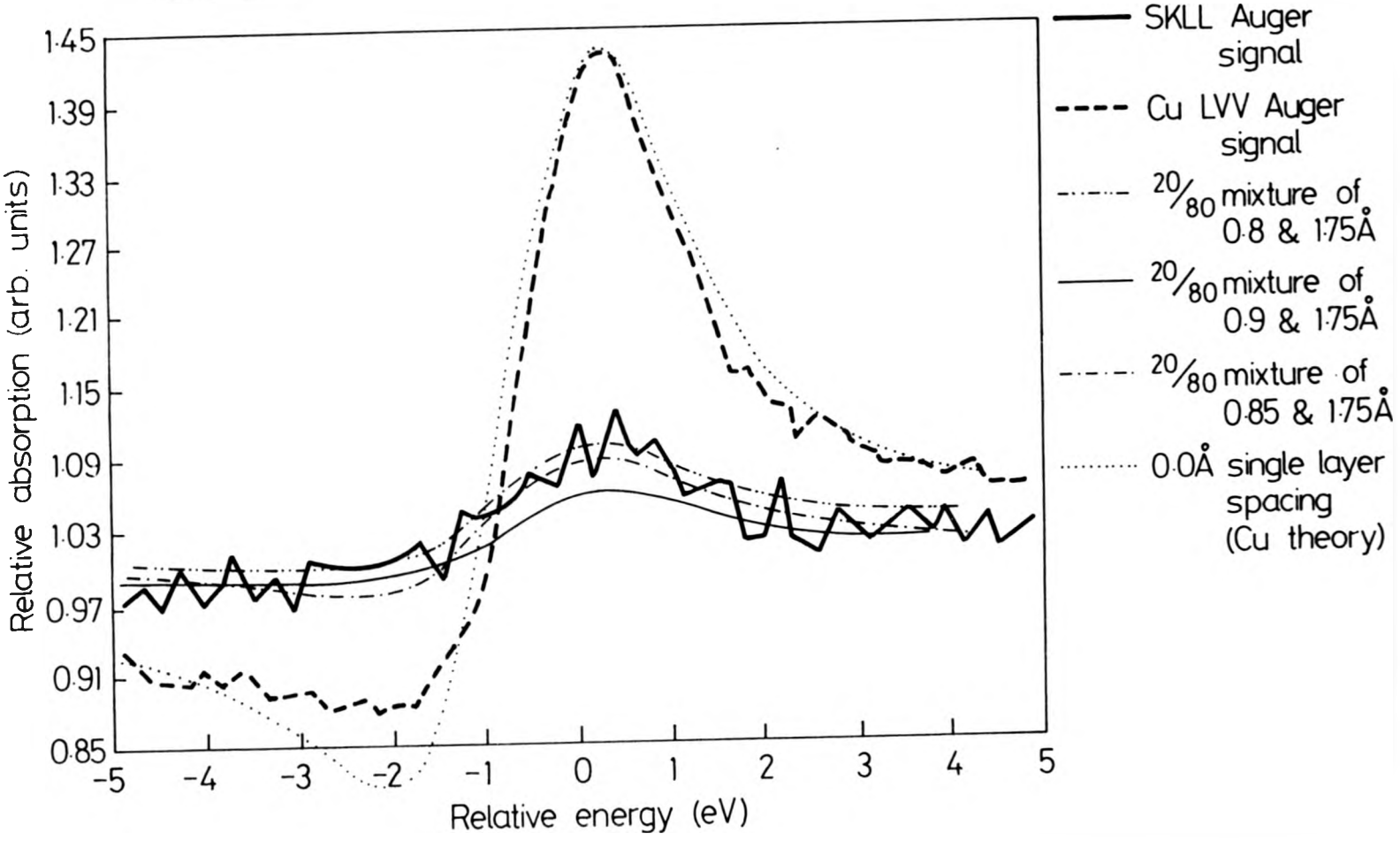
1·45
1·39
1·33
1·27
1·21
1·15
1·09
1·03
0·97
0·91
0·85
Relative absorption (arb. units)
-5
-4
-3
-2
-1
0
1
2
3
4
5
Relative energy (eV)
SKLL Auger signal
Cu LVV Auger signal
20/80 mixture of 0·8 & 1·75Å
20/80 mixture of 0·9 & 1·75Å
20/80 mixture of 0·85 & 1·75Å
0·0Å single layer spacing (Cu theory)

Figure 5.2c

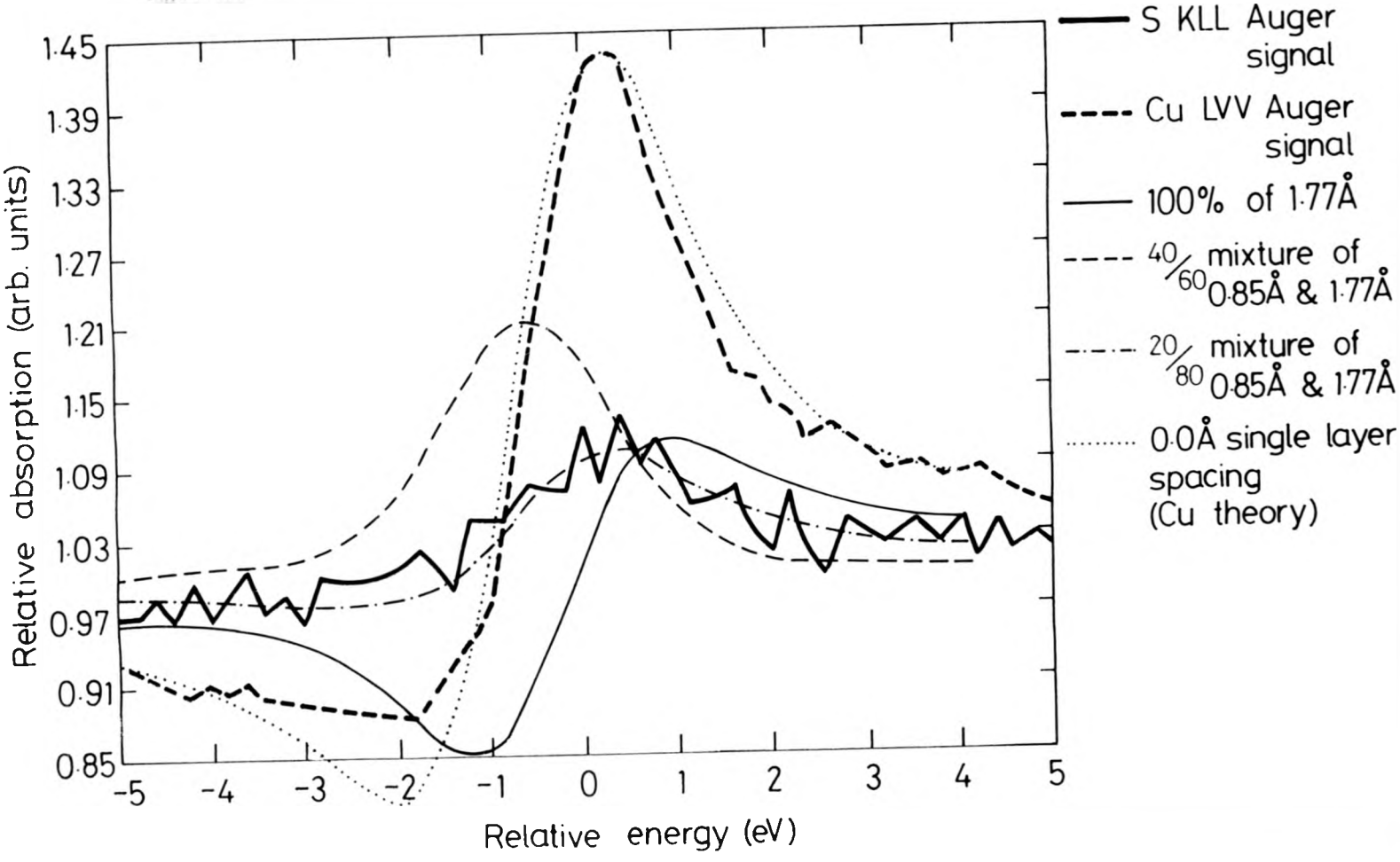
Relative absorption (arb. units)
1·45
1·39
1·33
1·27
1·21
1·15
1·09
1·03
0·97
0·91
0·85
-5
-4
-3
-2
-1
0
1
2
3
4
5
Relative energy (eV)
S KLL Auger signal
Cu LVV Auger signal
100% of 1·77Å
40/60 mixture of 0·85Å & 1·77Å
20/80 mixture of 0·85Å & 1·77Å
0·0Å single layer spacing (Cu theory)

value

The Cu LVV profile was fitted to a layer spacing of 0.0 Å, the shape of this modulation indicated a value of 0.85 for the coherent fraction of the surface atoms (ie 85% of the surface copper atoms sit in a 0.0 Å layer)

Figures 3a,3b and 3c display NISXW data for a later experimental run. (This run also involved the SEXAFS measurements referred to earlier). This surface displayed the same ($\sqrt{7} \times \sqrt{7}$)R19.1-S LEED pattern as was obtained for all previous surface formations, nevertheless some obvious differences are observable are between these data and those found for the earlier run. One difference is that the energy range is twice as large for these spectra - this was used because of a discernible broadening of the monochromator output which was observed between January and November 1988. This broadening has given rise to an obvious worsening of the signal to noise ratio for the Cu LVV profile. (It is of course not sensible to make the same comparison for the sulphur signals - due to variations in the form and size of the signals indicating that there is a variation in the relative occupancy of sites which arose in this later run). Also notice that for these data it is not possible to assign the values of the layer spacings with the same accuracy as before. Figures 3a and 3b show the effect of the variation of the layer spacings and figure 3c shows the effect of different relative occupancies. Once again the analysis suggests the occupation of two distinct layer spacings but this time these fall between 0.5Å and 0.85Å for one spacing and between 1.8Å and 1.95Å for the other layer. The relative occupancy of these was found to be 60% to 40% in favour of the larger layer spacing, with an error bar of the order of 10%.

Figures 5.3a,b,c Experiment theory comparisons for a later NISXW run on the $(\sqrt{7} \times \sqrt{7})$R19.1°S on Cu(111) system

Figure 5.3a

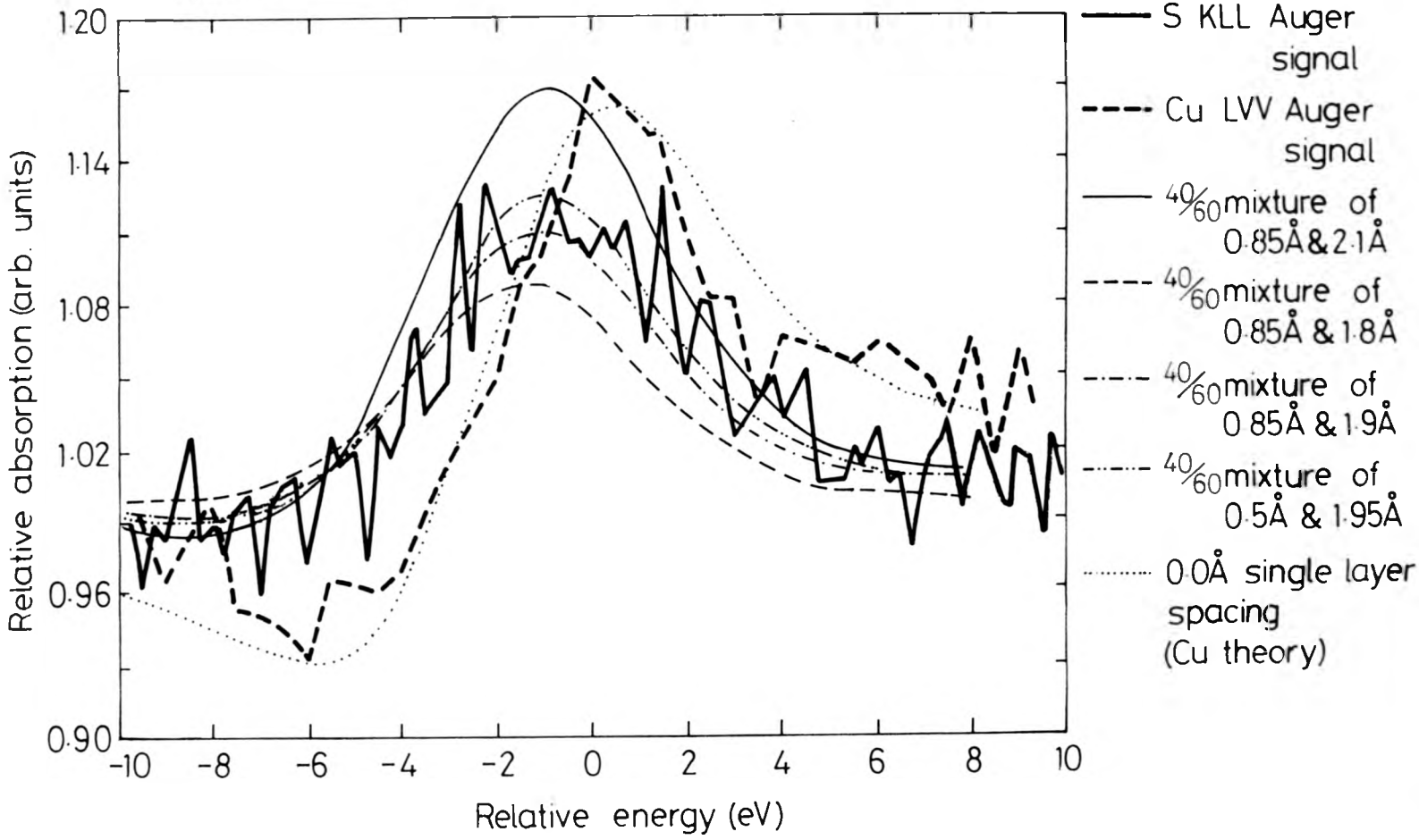

Figure 5.3b

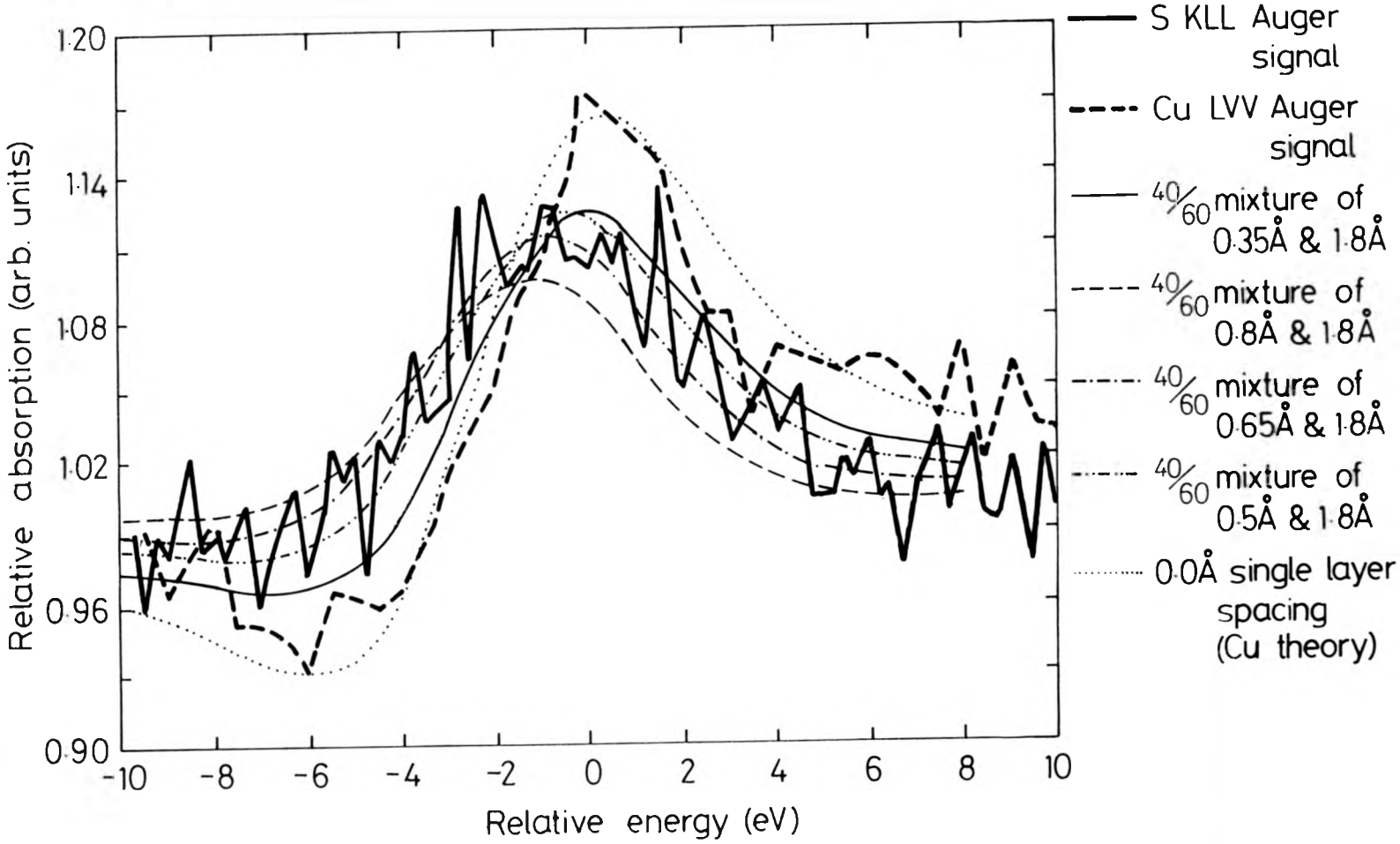
1·20
1·14
1·08
1·02
0·96
0·90
Relative absorption (arb. units)
-10
-8
-6
-4
-2
0
2
4
6
8
10
Relative energy (eV)
S KLL Auger signal
Cu LVV Auger signal
40/60 mixture of 0·35Å & 1·8Å
40/60 mixture of 0·8Å & 1·8Å
40/60 mixture of 0·65Å & 1·8Å
40/60 mixture of 0·5Å & 1·8Å
0·0Å single layer spacing (Cu theory)

Figure 5.3c

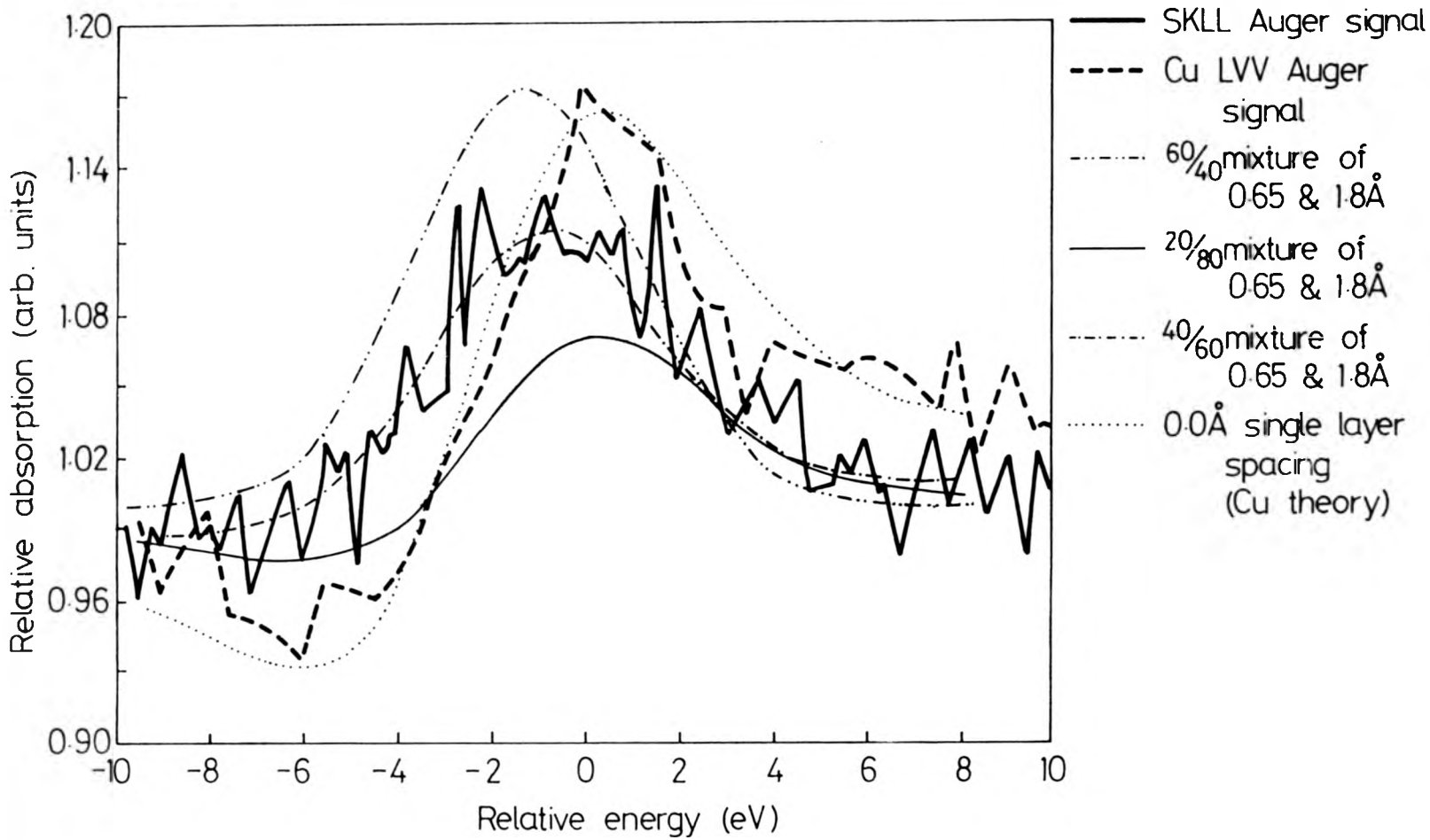
1·20
1·14
1·08
1·02
0·96
0·90
Relative absorption (arb. units)
-10
-8
-6
-4
-2
0
2
4
6
8
10
Relative energy (eV)
SKLL Auger signal
Cu LVV Auger signal
60/40 mixture of 0·65 & 1·8Å
20/80 mixture of 0·65 & 1·8Å
40/60 mixture of 0·65 & 1·8Å
0·0Å single layer spacing (Cu theory)

5.3 Discussion

Neither the NISXW or the SEXAFS results are consistent with simple chemisorption on the ($\sqrt{7}$ x $\sqrt{7}$)R 19.1-S surface. Taking the SEXAFS data first we can see that the polarization dependence of the first nearest SEXAFS gives a bond angle β of 67 ± 5^0 which is outside the range of angles expected for adsorption into high symmetry sites with no distortion of the substrate. These sites would give bond angles between 0^0 (for the atop site) and 39^0 (for the three fold hollow). Other lower symmetry sites were also considered such as; off bridge, off hollow and near atop (see figure 4) but these all give angles in the range given above.

The reason for the consideration of these sites was derived from the LEED data. This pattern consists of two separate orientations of the ($\sqrt{7}$ x $\sqrt{7}$)R19.1-S mesh which are rotated in opposite directions about a substrate lattice vector. This results in the pattern photographed in Chapter 3 and shown schematically in fig 5. The unit cell dimension of this structure would indicate a 3.37Å S-S spacing for a close packed 4/7 monolayer of sulphur or a 3.90Å spacing for a 3/7 monolayer. This SEXAFS data finds evidence for a S-S spacing of 3.90 ± 0.2Å which is derived from analysis of S-S scattering. This assignment must be regarded as secondary information due to the weakness off the S-S scattering shell when compared to the dominant Cu-S scattering. More reliable evidence for the 3/7 monolayer is drawn from radioactive tracer measurements of S_{35} on Cu(111) which favour the 3/7 monolayer [16]. It is also important to note that the 4/7 monolayer of sulphur would not correspond to a surface sulphide and would be more consistent with simple chemisorption, which has of course been ruled out above.

Figure 5.4 Diagram showing various S overlayer sites which were considered in the modelling of the NISXW and SEXAFS data for the ($\sqrt{7} \times \sqrt{7}$)R 19.1°-S on Cu(111) system

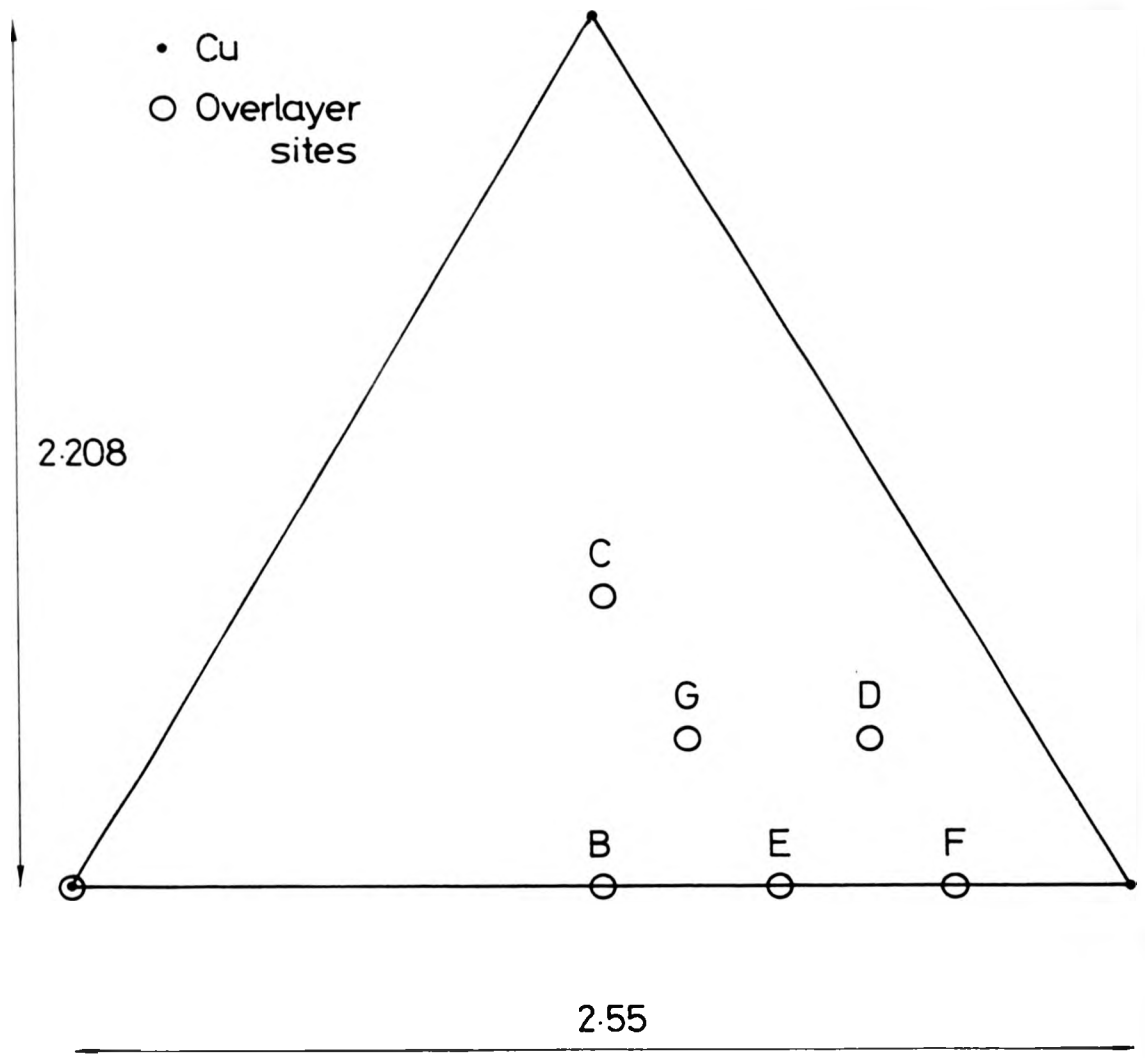

Figure 5.5 A schematic diagram of the Cu(111)-($\sqrt{7} \times \sqrt{7}$)R19.1°-S LEED pattern showing both orientations of the $\sqrt{7}$ mesh.

· overlayer spot superimposed on a substrate spot ·

• one orientation

the other orientation

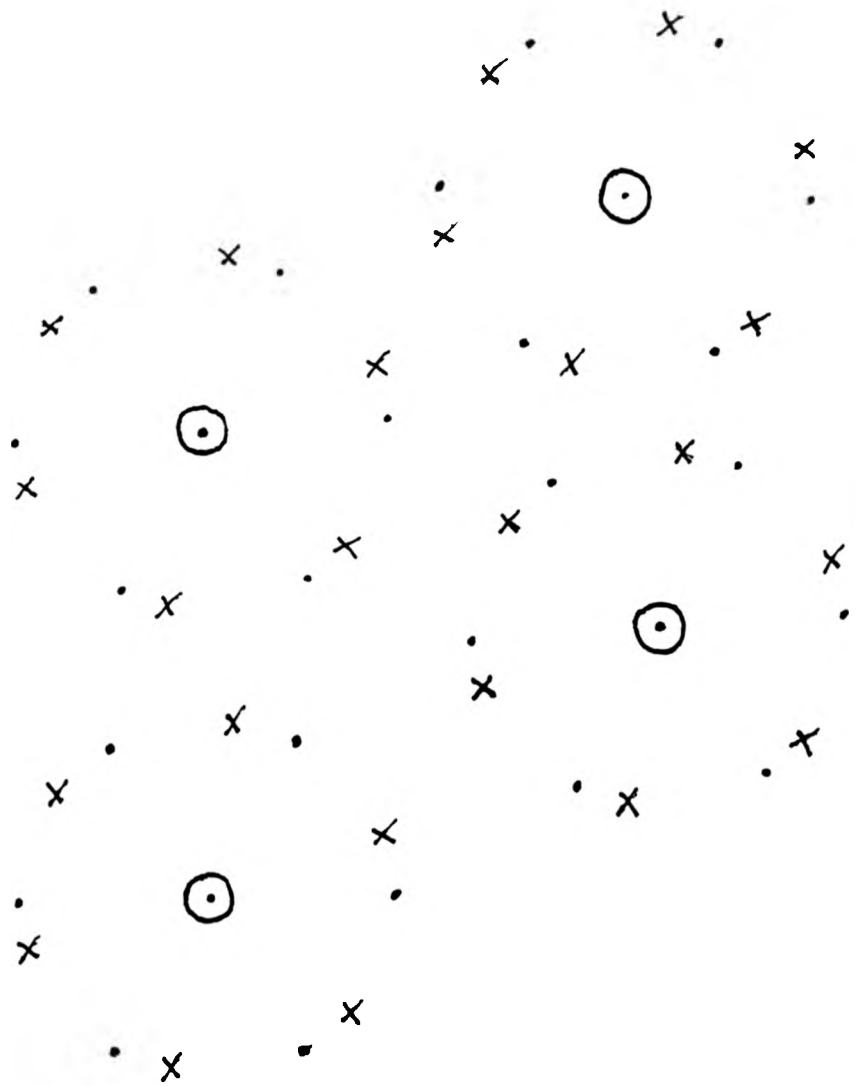

Thus it has been assumed that a 3/7 monolayer sulphide phase has been formed and that this phase must involve sulphur atoms which are nearly coplanar with the substrate atoms in order to explain the bond angle found by SEXAFS. The bulk copper sulphide which would be the closest analogue of this surface sulphide appears to be the tetrahedrally bonded zincblende structure. This involves Cu-Cu and S-S spacings of 3.93Å, and a Cu-S spacing of 2.30Å. [refs 18,19] In order to calculate specific model structures to explain the NISXW and SEXAFS data this tetrahedral structure has been overlaid on an undisturbed Cu(111) substrate. Two orientations of a single layer of this structure (involving 3/7 of a monolayer each of S and Cu) were considered, one in which the S atoms in the sulphide were uppermost at the surface and one which the copper atoms were uppermost (ie a layer of sulphur is sandwiched between two layers of copper). This procedure leads to the range of prospective sites given in figure 4.

In order to obtain a commensurate overlayer this surface sulphide must have Cu-Cu and S-S spacings which are 3.90Å rather than the bulk value of 3.93 Å this means that the tetrahedra are slightly distorted and the tetrahedral bond angle is 103^0 (ie $\beta = 77^0$) rather than the normal value of 108.27^0 ($\beta = 72.33^0$). The overlaying of this distorted tetrahedral structure produces the structures (i) to (iv) which occupy the sites given in table 1. These are the sites occupied if the copper atoms are uppermost in the sulphide layer. The occupancies for uppermost S atoms are found by interchanging the Cu and S sites (see table 2).

Assuming these structures gives rise to the shell radii given in table 3 for the copper atoms uppermost and the radii in table 4 are for the case of uppermost

Table 1 Possible adlayer-substrate site combinations considered for a sulphide overlayer comprising 3/7 monolayer S and 3/7 monolayer Cu. Individual sites are as shown on fig. 4. Relative site occupancy is in atoms per overlayer unit mesh. Here the Cu layer is uppermost at the surface

	S sites	Cu sites
i)	2 in C (hollow), 1 in A (atop)	3 in E
ii)	2 in D 1 in B (bridge)	1 in F, 2 in G
iii)	3 in E	2 in C (hollow), 1 in A (atop)
iv)	2 in G, 1 in F	2 in D, 1 in B (bridge)

Table 2 Possible adlayer-substrate site combinations considered for a sulphide overlayer comprising 3/7 monolayer S and 3/7 monolayer Cu. Individual sites are as shown on fig. 4. Relative site occupancy is in atoms per overlayer unit mesh. Here the S layer is uppermost at the surface

	Cu sites	S sites
(i)	2 in C (hollow), 1 in A (atop)	3 in E
(ii)	2 in D 1 in B (bridge)	1 in F, 2 in G
(iii)	3 in E	2 in C (hollow), 1 in A (atop)
(iv)	2 in G, 1 in F	2 in D, 1 in B (bridge)

Table 3 Shell structures for possible sulphide adlayer structures as shown in table 1 with the Cu adlayer above the S adlayer. Nomenclature as in table 1.

	Structure (i)	(ii)	(iii)	(iv)
Cu	2.30 (4.4,4.3)	2.30(3.3,3.2)	2.30(2.8,3.0)	2.30(2.8,3.1)
Cu				2.53(0.9,0.4)
Cu			2.71(1.4,0.5)	
Cu				2.74(0.9,0.5)
Cu		2.93(2.5,1.5)		
Cu			3.11(2.4,1.6)	3.11(0.4,0.2)
Cu				3.28(1.5,1.2)
Cu	3.44(4,3.7)	3.44(1.5,1.2)		
Cu				3.59(1.4,0.3)
Cu			3.74(2.0,2.0)	3.74(0.4,1.3)
Cu	3.88(1.3,0.01)	3.88(2.5,2.8)		3.88(0.6,0.7)
S	3.90(2.4,8.0)	3.90(2.4,8.0)	3.90(2.4,8.0)	3.90(2.4,8.0)

Table 4 Shell structures for possible sulphide adlayer structures as shown in table 2 but with the Cu adlayer below the S adlayer. Nomenclature as in table 1.

	Structure (i)	(ii)	(iii)	(iv)
Cu	2.30(1.1,2.8)	2.30(1.1,2.8)	2.30(1.1,2.8)	2.30(1.1,2.8)
Cu			2.77(1.8,0.2)	
Cu	2.86(0..7,0.01)			2.84(0.6,0.01)
Cu		2.90(1.2,0.06)		
Cu				3.02(1.2,0.1)
Cu		3.07(1.1,0.2)		3.06(1.1,0.2)
Cu	3.22(2.6,0.6)		3.14(1.5,0.45)	
Cu				3.36(1.0,0.3)
Cu		3.42(2,0.6)	3.47(2.7,1.3)	
Cu				3.52(0.5,0.2)
Cu		3.57(0.9,0.4)		
Cu				3.67(0.9,0.4)
Cu		3.86(0.9,0.9)		3.82(0.9,0.5)
S	3.90(2.4,8.0)	3.90(2.4,8.0)	3.90(2.4,8.0)	3.90(2.4,8.0)

Table 5 Layer spacings of S atoms (in Å) relative to the top substrate atom layer and, in parentheses, relative to the nearest extended lattice layer, for the sulphide phase structures of table 3 and 4. CuS indicates copper atoms below S on the surface (table 4). SCu indicates that these layers are inverted (table 5).

CuS(i)	2.86	(0.78)
CuS(ii)	2.81	(0.73)
CuS(iii)	2.64	(0.56)
CuS(iv)	2.81	(0.73)
SCu(i)	2 @ 1.77 + 1 @ 2.30	(0.22)
SCu(ii)	2 @ 2.18 (0.10) + 1 @ 1.93	
SCu(iii)	2.14 (0.06)	
SCu(iv)	2 @ 2.02 + 1 @ 2.27 (0.19)	

sulphur atoms. The polarization dependences of these shells are also indicated in these tables. In table 5 the expected layer spacings of the sulphur layers are given for the structures (i) to (iv). For the case of copper atoms being uppermost in the sulphide layer a mixture of layer spacings is obtained -(see table 5 , the SCu layers) because these are spaced rather closely the modeling procedure has assumed them to approximate to a single layer. In the case of sulphur atoms being uppermost a single layer spacing is expected (see table 5, the CuS layers.)

Comparing these tables to the NISXW data for the first run seems to suggest that 20% occupancy of the structure (i) for an uppermost sulphur layer in the sulphide and an 80% for an uppermost copper layer would best fit the data. This assignment would also reasonably approach the observed SEXAFS polarization dependence (see tables 3 and 4) as it would give 0.8 x 1.04 + 0.2 x 2.66 = 1.36 for the $N^{\bullet}_{90}/N^{\bullet}_{36}$ which is just outside the error bar of the measured value which is 1.7± 0.3. Of course no SEXAFS data were measured during this first NISXW run and this is the most likely reason for the discrepancy in these polarization dependences . Notice that even this smaller value still suggests a bond angle β which is well outside the range expected for simple chemisorption.

Comparing the tables to the second set of NISXW results leads to less clear conclusions and here it is apparent that a 60/40 mixture of any of the structures (i) to (iv) will provide a reasonable fit to the data. However, a closer analysis of the SEXAFS data yields two higher copper shells at 3.25Å± 0.04Å and 3.41Å± 0.04Å, these would be expected for the mixture of the structures (i). Also the fact that the structures (i) were favoured for the

earlier NISXW run leads to a preference for the structures (i) here also. This mixture of 60% copper layer uppermost and 40% sulphur layer uppermost in the sulphide would lead to a polarization dependence of 0.4 x 2.66 + 0.6 x 1.04 = 1.62 for the first nearest neighbour SEXAFS which is well inside the error bar of the measured value for the SEXAFS taken for this later NISXW run (1.7 $\pm$ 0.3).

One possible conclusion of all this is that the interaction of atomic sulphur with Cu(111) leads, via a strong chemical interaction, to the formation of a surface sulphide with two phases involving two orientations of a slightly distorted tetrahedral overlayer. These must have very similar energies of formation and therefore a very delicate balance of energy at the surface determines the relative occupancy of these phases.

Another interpretation of these results which does not rely on a cumbersome two phases model is best illustrated by examination of figure six which depicts a model of structure (i). Sulphur atoms are shown in grey , note that two out of every three of these lie in three fold hollow sites (site c in fig 4) and the other lies in the atop site (site a in fig 4) and that the three copper atoms (black) that constitute the rest of the unit cell of this overlayer lie in the E sites. (Between the bridge and atop sites). It is possible that the two sulphur atoms in the three fold hollow sites lie below the level of the copper atoms but that the atop S atom, which rides higher on the substrate, may be forced up to form a local inversion of the tetrahedral structure. Thus the atop S atom is forced above the three neighbouring copper atoms into the 0.85Å (2.93Å) layer spacing found by the NISXW technique. (The value in parentheses is the actual value of the layer spacing but due to the translational periodicity

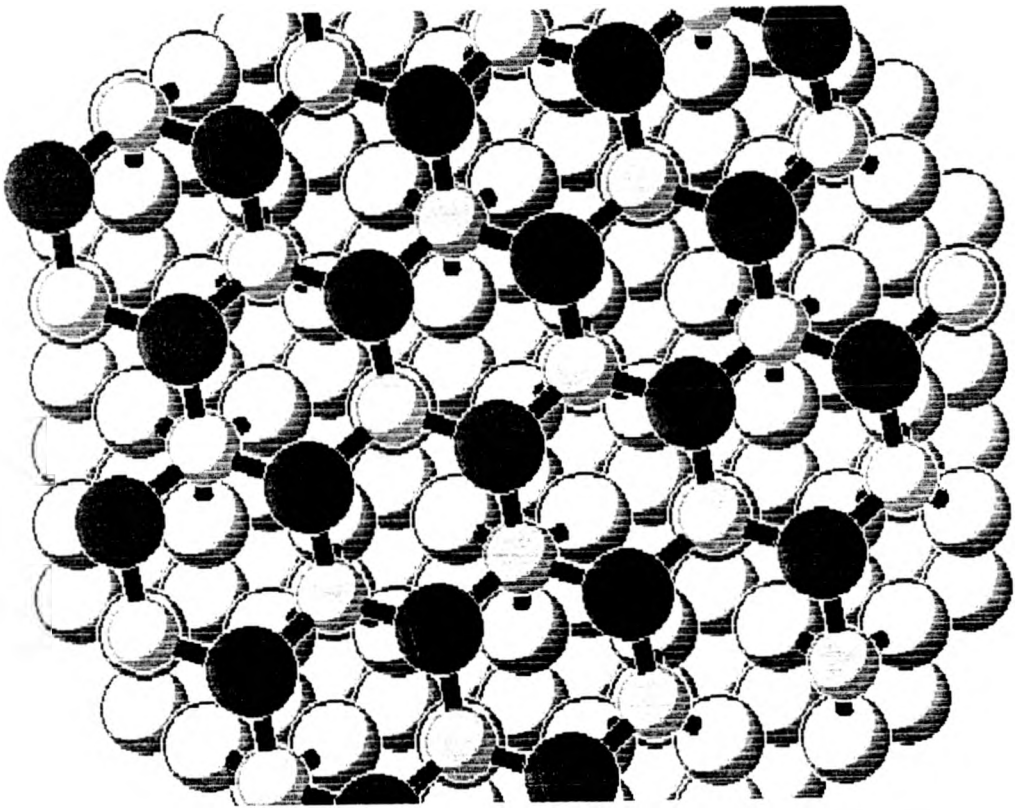

Figure 5.6 A schematic diagram of the proposed structure of the $(\sqrt{7} X \sqrt{7})$R19.1°-S on Cu(111) system

of the SXW field, the SXW technique measures this value - the bulk Cu(111) layer spacing of 2.084Å). This periodic inversion of the tetrahedral structure would therefore give rise to a buckled, mixed layer of Cu and S which would involve occupation , by sulphur, of 66% of a 1.78Å layer spacing and 33% occupation of a 0.85Å layer spacing. This would fit the observed 60/40 mixture quite well. This sulphide overlayer involves a mixture of adsorption sites as well as bond angles and hence SEXAFS will be expected to average out these pieces of information. This does seem to be borne out by the fact that the SEXAFS produces an estimate of the bond angle β (67 ± 5^0) which is in between that expected for the distorted tetrahedron (77^0) and the three fold hollow site of 39^0. The presence of two bonding angles would also explain the observed polarization dependence of first nearest neighbour bondlength found by SEXAFS (2.30Å$\pm$ 0.04Å for normal incidence and 2.35Å $\pm$ 0.04Å for 54^0 off normal) as the normal incidence spectra would be more influenced by the scattering for the larger bond angle and the off normal data would be more sensitive to the smaller bond angle.

5.4 Conclusion

This study concludes that the interaction of H_2S with Cu(111) is a strong chemical reaction which results in the formation of a bulk like, distorted, tetrahedral sulphide overlayer on Cu(111). NISXW and LEED have both indicated that the S atoms in this system must involve at least two distinct adsorbate-substrate registries. This is evidenced by the fact that SEXAFS recorded above the S K edge has produced averaged data which in itself is difficult or impossible to interpret such that a complete structure determination avails.

Combined NISXW and SEXAFS, however, has been more successful. In particular the NISXW layer spacings have been rationalized with the polarization dependence found for the first nearest neighbour SEXAFS. Some uncertainties however remain due to the non ideality of the data which exhibited steadily degrading signal to noise characteristics throughout the duration of these studies and it is also important to realize that structures of this complicated form are at the very limit of what is analysable by any existing surface structure determination techniques.

5.5 References

1. J A Yarmoff, D M Cyr, J H Huang, Sehun Kim, and R S Williams Phys Rev B Vol 33 No 6 p 3856-3868

2. J F Van der Veen, R G Smeenk, R M Tromp, F W Saris Surf. Sci. 79 (1979) 212-218

3. J F Van der Veen, R G Smeenk, R M Tromp, F W Saris Surf. Sci. 79 (1979) 219-230

4. R G Jones, S Ainsworth, M D Crapper, C Somerton, D P Woodruff, R S Brooks, J C Campuzano, D A King, G M Lamble, and M Prutton Surf. Sci. 152/153 (1985) 443-442

5. H S Greenside and D R Hamann Phys Rev B Vol 23 No 10 (1981) p4879

6. J H Onuferko, D P Woodruff, and B W Holland Surf. Sci. 87 (1979) 357-374

7. L Wenzel, D Arvanitis, W Daum, H H Rotermund, J Stohr, K Babershcke and H Ibach Phys Rev B Vol 36 No 14 (1987) p7689

8. W Daum, S Lehwald, and H Ibach Surf. Sci. 178 (1986) 528-536

9. J E Muller, M Wuttig and H Ibach Phys Rev Letts Vol 56 No 15 (1986) p1583

10. J H Onurferko and D P Woodruff Surf. Sci. 95 (1980) 555-570

11. S Kono, S M Goldberg, N F T Hall, and C S Fadley Phys Rev Letts Vol 41 (1978) 1831

12. U Döbler, K Babershcke, J Stohr and D A Outka Phys Rev B Vol 31 No 4 p2352

13. H Niehus Surf. Sci. 130 (1983) 41-49

14. P H Citrin, D R Hamann, L F Mattheis and J E Rowe Phys Rev Letts Vol 49 No 23 (1982) p1712

15. S Antoci and L Mihich Phys Rev B (1978) 5768

16. L Domange and J Oudar Surf. Sci. 11 (1968) 124-142

17. J Bernard, J Oudar, N Barbouth, E Margot, and Y Berthier Surf. Sci. 88 (1979) L35-L41

18. M M Kazinets, Soviet Phys. -Crystallography 14 (1970) 599

19. R W G Wyckoff, Crystal Structures, Vol 1 (Interscience, London, 1948) p332

20. S J Gurman, N Binsted and I Ross J Phys. C. 17 (1984) 143

Chapter 6

Hg on Ni(100)

6.1 Introduction

The adsorption of mercury has been studied on a range of surfaces including Ag(100), W(100), Fe(100), Cu(100) and $Cu_3Au(100)$ [1, 2, 3, 4] as well as the Ni(100) surface. All these systems involve weak chemisorption. For instance a 1.4eV bond is found for Hg on Ni(100). This compares with bond energies of typically 10eV for systems involving strong chemisorption. Thus the balance between adsorbate- adsorbate and adsorbate substrate interactions may be very delicate for these systems. In certain cases the adsorbate - adsorbate interaction has dominated the adsorption behaviour. The nature of these interactions is seen to be quite strongly dependent on the Hg overlayer mesh size. For example the lattice parameter of Fe is 2.87Å which being smaller than the atomic radius of Hg (3Å) means that the (1x1) overlayer of mercury which forms on Ni(100) is compressed relative to bulk mercury and here evidence is found for repulsive lateral interactions between Hg atoms at the surface. This type of compression is also observed (3 to 4 percent) for the Ag(100) surface, and here the dominating influence of adsorbate-adsorbate interactions on adsorption behaviour is evidenced by the fact that adsorption is only possible

below room temperature. For the cases of W(100) and Cu(100), however, the lattice parameters are 3.14Å and 3.61Å respectively and therefore these (1x1)Hg overlayers are expanded relative to the bulk by 5% and 20% respectively; here the adsorbate adsorbate interactions are attractive. Correlations between the mesh size and the electronic structure of the mercury overlayers have also been noted [4].

The nature of the adsorbate-adsorbate interactions of mercury overlayers on Ni(100) has been shown to be more complicated than may be inferred from the observations above. Even though this surface has a lattice parameter of 3.52Å, thus allowing a 17% expansion of the bulk Hg-Hg spacing, it is still found that there is a coverage dependent transition in the sign of the adsorbate-adsorbate interactions and that these interactions are in fact repulsive for the c(2x2) overlayer which involves an Hg-Hg spacing of 3.52Å. This shows that for this surface at least the Hg-Hg interaction is not just a simple through space effect and must be mediated by the surface.

A through surface effect has been observed for iodine on Ni(100). For this system a series of rectangular meshes is exhibited during the thermal desorption of iodine from the surface, these range from a highest coverage c(2x2) overlayer and pass through a range of structures involving a continuously variable rectangular mesh, until long range order is lost at a coverage of a third of a monolayer. (Forming this surface at elevated temperature and subsequently cooling causes the formation of the surface iodide referred to in the last chapter). During this heating process [5] the mesh size increases and leads to a reduction of the I-I repulsion. This repulsion appears to be active over a separation range of 3.52Å (c(2x2) phase) all the way to 4.84Å which is a sur-

prisingly long range for what is expected to be a short range, hard, repulsion (the iodine nickel bond is not ionic). This has been attributed to a weakening of the iodine to metal bond which gives rise to less valence shell filling of iodine thus allowing an increase of the I-I overlap. This is termed a through metal interaction and an effect of this type may explain the complex behaviour of the Hg overlayers which form on Ni(100) and particularly the fact that this surface exhibits a higher coverage phase with a complex LEED pattern as well as the already repulsive c(2x2) phase.

Therefore for systems involving only weak chemisorption, (like Hg on Ni(100)) involving high coverages or small unit celled substrates, strong adsorbate-adsorbate forces may be expected to dominate over adsorbate-substrate bonding,(which may be weakened by through metal interactions) possibly to such an extent that incommensurate overlayers may be formed. For the case of larger substrate meshes or lower coverages, however, commensurate phases are more likely to form.

These systems are an attractive area for study as their geometrical structure can be varied in a controlled manner by either choosing a range of substrate cell sizes or by altering coverages and therefore the impact on electronic structure and bonding may be carefully analysed as a function of the Hg lattice parameter. This approach has been adopted by previous studies but none of these has set out to obtain detailed surface structural information on these metallic overlayers. This is a surprising observation, particularly for the case of Hg on Ni(100), because the coverage dependent transitions which are observed between the different meshs of mercury on Ni(100) may be expected to reveal changes in bonding and adsorption site. This type of behaviour would

be ideal for study by SEXAFS. For this reason we have attempted to study the Ni(100)c(2x2)Hg surface using the SEXAFS and NISXW combination.

6.2 Results

The lack of success of this SEXAFS study is evidenced in Figure 1. This study attempted to record SEXAFS data from the Mv edge at 2295eV by collecting Hg M_VNN Auger electrons of energy 2073eV. Figure 1 shows the yield of these electrons in the vicinity of the Hg M_V and M_{IV} edges , the expected energies of which are marked. In both cases the effect of delayed onset due to the centrifugal barrier which is characteristic of photoemission from states of high angular momentum is apparent [6]. Also the delayed onset is followed by a resonance in the 3d-f excitation channel and therefore it is concluded that atomic effects are too strong to permit SEXAFS measurements in the energy range between the Mv and Miv edges, which is only 90eV. Measurements from the M_{III}, M_{II} or the M_I edges were not attempted as here the cross sections are smaller, also no measurements were taken from the deeper L edges as these were not accessible to the energy range of the monochromator.

The NISXW experiments were more successful, these data were recorded by monitoring the yields of the Ni L_{III}VV (848eV) and the Hg M_VNN (2073eV) Augers in the vicinity of the Ni(200) Bragg reflection at 3522eV. The Ni(100) reflection is, of course, a forbidden reflection. The strength of the Hg M_VNN yield proportional to the M_V (weak) photoionisation cross section and for this reason these data have a weaker signal than that obtained for the previously measured sulphur containing systems [7]. This factor coupled with the increased monochromator broadening engendered in moving from 2975eV

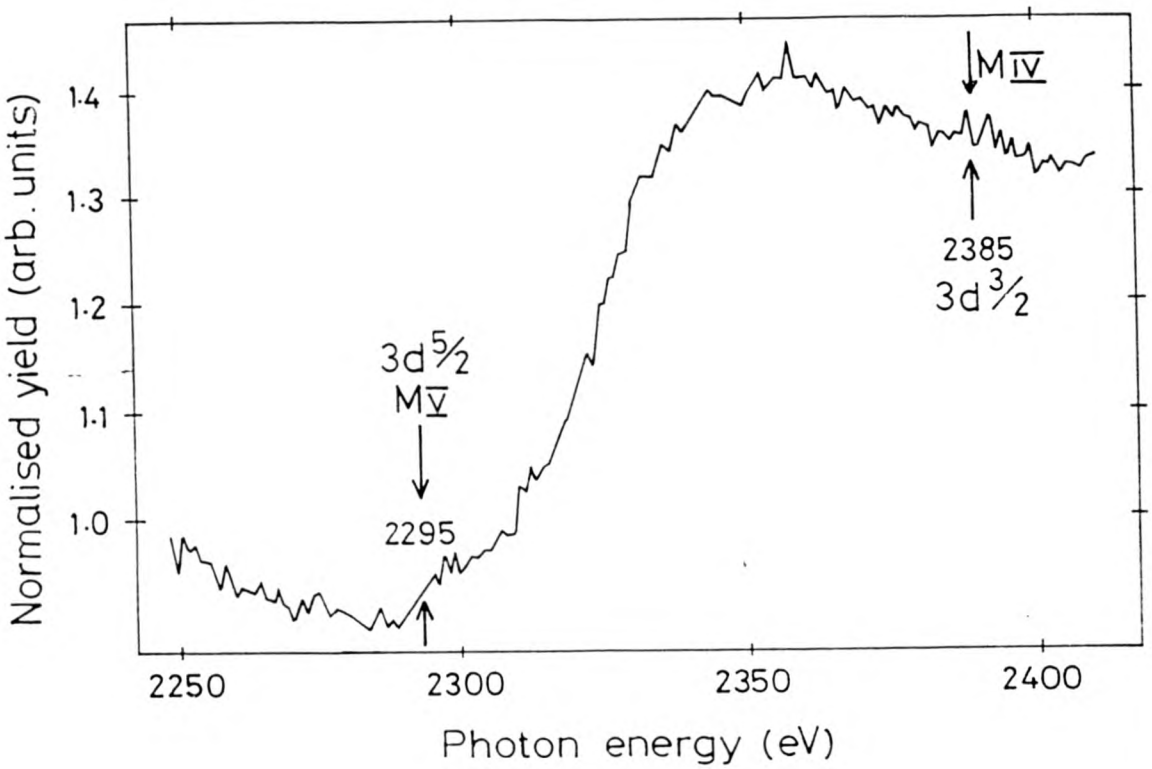

Figure 6.1 A SEXAFS data set measured on the Ni(100) c(2 X 2)Hg system, this data was recorded above the M_V edge at 2295eV.

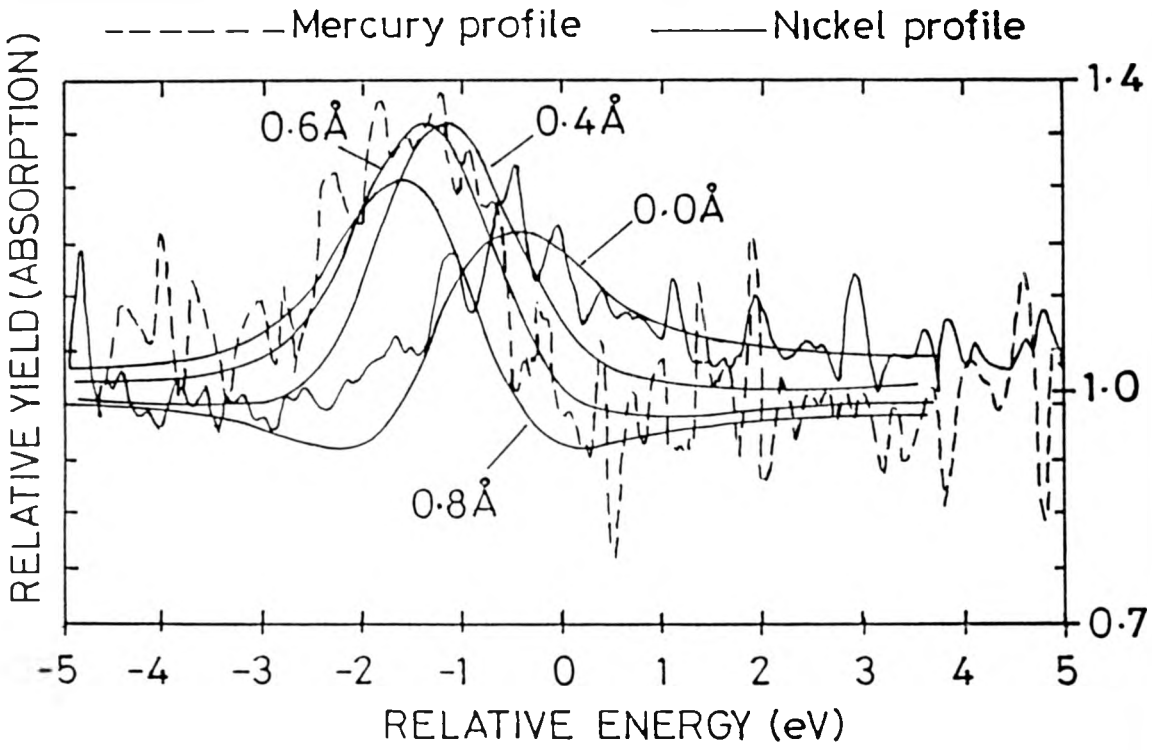

Figure 6.2 NISXW data for the Ni(100) c(2 X 2)Hg system. this spectrum was collected around the Ni(200) Bragg reflection at 3522eV.

(The Cu(111) Bragg reflection) to 3522eV results in the larger error bars and worsened signal to noise ratio seen in Figure 2. The data analysis once again followed the procedures described in chapter 2 and a result of 0.6 Å ± 0.1 Åwas obtained for the Ni-Hg adsorbate to substrate layer spacing. This of course corresponds to an adlayer height of (1.76+0.6)± 0.1Å =2.36± 0.1Å(1.76Å = Ni(200) spacing).

Due to the failure of SEXAFS to provide a value for the Ni-Hg first nearest neighbour bondlength it was necessary to take the Hg-Ni distance found in the compound NiHg, 2.63Å [8], as an estimate. Using this value to calculate the adlayer heights of the mercury overlayer for the high symmetry adsorption sites yields: 1.95Å (0.19Å) for the four fold hollow , 2.31Å (0.55Å) for the bridge site and 2.63Å (0.87Å) for the atop site. The values in parentheses are those which would be obtained in the NISXW analysis, which are actual local values of the layer spacing minus the Ni(200) spacing of 1.76Å. The reason for this is that the NISXW field has the periodicity of the substrate layer spacing and extends far above the surface, this means that due to the translational symmetry of the NISXW field, the value of layer spacing given by NISXW is referenced to the continuation of the lattice periodicity.

The experimental result of 0.6Å would appear to suggest that mercury adsorbs into bridge sites, this would be a surprising result as this overlayer would be expected to involve non directional metallic bonding which would favour the highest available co-ordination site. This would suggest the four fold hollow site rather than the two fold co-ordinated bridge site.

It is important to note at this point that the SXW result standing alone is not sufficient to determine the surface structure completely. The reason for this

is, as stated in previous chapters, that the SXW technique determines layer spacings with respect to the underlying bulk periodicity of the substrate and therefore these values will be susceptible to any relaxations of the topmost substrate layers which occur in a direction perpendicular to the surface. [ie if the top layer relaxes outward to produce an enlarged value of the distance between the first and second atomic layers of the substrate, then the SXW technique will overestimate the true local value of the layer spacing by an amount corresponding to this relaxation and the opposite effect occurs for substrate layer contractions.] The fact that these relaxations are generally never observed to be more than a few percent of the bulk interlayer spacing and noting that an outer layer expansion of greater than 20% is required to reconcile the result of this study with four fold site occupation, seems to suggest that this effect alone cannot be giving rise to a false site determination. It is interesting to note, however , that an adsorbate induced surface layer relaxation of this size has been reported for the adsorption of oxygen on Cu(110)[9].

Another way to account for this surprising result is that the bondlength of 2.63 Å which was obtained for NiHg may have been inappropriate. Other values could have been obtained by using (i) the metallic radius of β mercury (1.41Å) (a body centered tetragonal structure) or (ii) the metallic radius of α Hg (1.49Å) (a rhombohedral phase) together with the metallic radius of Ni, these lead to NiHg bondlengths of 2.66Å and 2.74Å which would both still suggest bridge site adsorption. Another pair of bondlengths for α and β Hg are found by using the Zachariasen radii [10]. These are calculated by averaging the bondlengths over the first shell of near neighbours. Metals such as Hg pack into structures where a few neighbours are very close and

the remainder of the first shell have considerably longer bondlengths and thus the averaging procedure produces rather large metallic radii for Hg. These are 1.62Å and 1.58Å for α and β Hg respectively giving values of 2.87Å and 2.83Å for the NiHg bondlengths which in turn give rise to layer spacings of 2.27Å and 2.22Å respectively. One of these would be within the error bar of result for the case of four fold co-ordination.

One reference [11] suggests that the Zachariasen radius is the most appropriate value but, the preference of this reference, arises from measurements of the adsorbate-adsorbate spacings in a large range of metallic overlayers which are commensurate with their substrates and thus the influence of these substrates on these lengths might be expected to be give large values of the metallic radius. For this reason we prefer to use the known NiHg amalgam bondlength of 2.63Å and so bridge site adsorption is favoured by these results.

6.3 Conclusion

This study adopts a straightforward interpretation of the NISXW result. This suggests that mercury adsorbs into the bridge sites of Ni(100) to form a c(2x2) LEED pattern. Nevertheless the possibility of four fold co-ordination is not ruled out due to the likelihood of (i) an inaccurate value of the NiHg bondlength being used in the calculation of the expected layer spacing and (ii) a local substrate layer expansion at the surface or (iii) a combination of these effects. The reason for these doubts is that for this system the application of the normally incisive combination of SEXAFS and NISXW was not possible due to the special difficulties of recording SEXAFS data above absorption edges of high angular momentum.

6.4 References

1. M Onellion, J L Erskine, Y J Kime, Shikha Varma, and P A Dowben Phys Rev B Vol 33 No 12 p8833
2. R G Jones, and D L Perry Vacuum 31 p493- p498
3. R G Jones, and D L Perry Surf Sci 71 (1978) p59 p71
4. M Onellion, Y J Kime, P A Dowben, and N Tache J Phys C Solid State Phys 20 (1987) L633 L640
5. C Somerton, C F McConville, D P Woodruff, and Robert G Jones Surf Sci 136 (1984) p23-p40
6. U Fano, and J W Cooper Rev Mod Phys 40, (1968),441
7. S T Manson, and J W Cooper Phys Rev 165 (1968) p126-p138
8. M Puselj, and Z Ban Zeit. fur Naturf B32, 479
9. J A Yarmoff, D M Cyr, J H Huang, Sehun Kim, and R S Williams Phys Rev B Vol 33 No 6 p3856-p3868
10. W H Zachariasen J. Inorg Nucl. Chem 35, 3487
11. C T Campbell Surf. Sci. 167 (1986) L181-L186

Chapter 7

General Conclusions

7.1 Introduction

The combined use of SEXAFS and NISXW has been applied to the study of atomic and molecular adsorption on transitional metal surfaces. These adsorption systems were widely different in terms of the strength of bonding between the adsorbate and substrate and this has led to two extremes of adsorbate - substrate interaction. One extreme was where adsorbate bonded to the surface causing little or no structural rearrangement of the substrate and the other involved dramatic surface reconstruction. Both spectroscopic techniques were shown capable of giving complementary and detailed information on surface structure and the newer technique of NISXW has been shown to have a much wider range of applicability than it showed prior to these studies.

7.2 CH_3S on Cu(111)

SEXAFS data analysis for this system revealed a Cu-S bondlength of 2.38 $\pm$ 0.03Å for the nearest neighbour shell, and that the data was dominated by scattering from this shell. Some weak intramolecular C-S scattering was also analysable. This gave a C-S bondlength of 1.88Å . S-S scattering also made a contribution

to the SEXAFS and a S-S separation of 3.4 ± 0.15Å was found. Analysis of the SEXAFS polarization dependences for all these shells gave a bond angle β of 80 ± 10^0 for the S-S bond, 0^0 for the C-S bond and 60 ± 5^0 for the nearest neighbour Cu-S bond. This Cu-S angle is much larger than would have been expected for simple chemisorption.

Also NISXW data for this same experimental geometry gave an adsorbate - substrate layer spacing which was wholly inconsistent with simple, non substrate distortive, chemisorption into any high symmetry site at the Cu(111) surface. This was 1.15 ± 0.05Å . Taking the SEXAFS bondlength and bondangle and calculating the expected adlayer spacings produced by adsorption into distorted high symmetry sites of the surface revealed that the best fit to both sets of experimental data was provided by assuming adsorption of the mercaptide group's S atom into a distorted three fold hollow site. Of both three fold hollows the H.C.P. site was found to be the most likely. Bonding into this site at this layer spacing would involve the large scale distortion of the three fold hollow. 0.6Å movements of the surface copper atoms in a direction parallel to the surface would be necessary to accommodate such a distortion. Such movements would produce a surface layer of copper which is incommensurate with the atomic layers below but due to the non applicability of LEED to this system this is impossible to confirm. However,it is suspected that the structure forms in clusters leading to only local distortions of the substrate.

7.3 S on Cu(111)

The interaction of H_2S with Cu(111) leads to the formation of a $(\sqrt{7} X \sqrt{7})$R 19.1^0-S LEED pattern which is most likely to involve a 3/7 monolayer of sulphur.

SEXAFS analysis gives a value of 2.30 ± 0.03Å for normal incidence and 2.34 ± 0.03Å for off normal (54^0) incidence. Amplitude analysis of this nearest SEXAFS gave a bond angle β of 67 ± 5^0. In common with the mercaptide system this data is dominated by a first shell and the bond angle of the atoms in this shell is inconsistent with simple chemisorption. NISXW data was not analysable in terms of the occupation of a single Cu-S adlayer spacing and this, like the SEXAFS data for this system, is similarly inconsistent with the idea of simple chemisorption in this system.

The only corroborative interpretation of both NISXW and SEXAFS data was that a strong chemical interaction between H_2S and Cu(111) leads to the formation of a bulk like sulphide at the surface. The closest bulk analogue of this sulphide is one which is tetrahedrally co-ordinated - the surface sulphide is a slightly distorted arrangement of this type which involves a mixed layer of copper and sulphur. This system produces a mixture of S sites at the surface as well as a mixture of Cu-S bond angles and the fact that SEXAFS averages the structural information from these sites leads to a less incisiveness structure determination than those found for single site adsorption. The combination of NISXW and SEXAFS however allows for firmer conclusions thus highlighting the need for the application of complementary techniques in surface structure determination.

7.4 Hg on Ni(100)

An attempt has also been made at the application of the NISXW and SEXAFS combination to the Ni(100)c(2 X 2)Hg surface. SEXAFS data for this system showed no observable SEXAFS oscillations. This was believed to be due to the

combined effects of delayed onset and strong structure in the photoionisation cross section. Such effects are typical of X ray absorption studies of electronic states of high angular momentum. (This SEXAFS data was recorded above the Hg M_V edge at 2295eV). The fact that previous work on this system indicates that this Hg overlayer is only weakly adsorbed indicates that there may be a high value of the Debye-Waller type factor for this NiHg shell. This would lead to an attenuation of the NiHg SEXAFS which may also be responsible for the lack of clearly observable SEXAFS oscillations for this system.

NISXW data, however, was attainable from this system, this put a value of 0.6 ± 0.1Å on the Ni-Hg adlayer spacing. Assuming simple, non reconstructive, chemisorption for this system, and taking various estimates of the NiHg bondlength (of which 2.63Å was the favourite) suggests that this adlayer spacing is suggestive bridge site adsorption by mercury. For what is expected to be strongly directional, metallic, bonding between adsorbate and substrate this is a somewhat surprising bonding site. The assignment of bridge adsorption site for mercury is, however, not firm due to the lack of corroborative SEXAFS data on this system and the less surprising conclusion of adsorption into the four fold hollow of the Ni(100) can be reconciled with our result if (i) a surface relaxation of the top layers of the Ni(100) substrate is assumed or (ii) if the NiHg amalgam bondlength assumed for the surface structure was not representative of the actual surface bondlength, or (iii) a combination of these effects. Once again the need for complementary surface structure determination is highlighted.